

PART I - LOWER LIMIT OF THE TOTAL ENERGY OF
EARTHQUAKES AND PARTITIONING OF
ENERGY AMONG SEISMIC WAVES

PART II - REFLECTED WAVES AND CRUSTAL STRUCTURES

Thesis by

Francis Taming Wu

In Partial Fulfillment of the Requirements

For the Degree of

Doctor of Philosophy

California Institute of Technology

Pasadena, California

1966

(Submitted May 10, 1966)

PART I

LOWER LIMIT OF THE TOTAL ENERGY OF EARTHQUAKES
AND PARTITIONING OF ENERGY AMONG SEISMIC WAVES

Acknowledgements

The author is indebted to Professor D. L. Anderson for his support and guidance throughout this study. Helpful comments and encouragements from Professors C. F. Richter, S. W. Smith, and J. N. Brune are gratefully acknowledged.

The author is grateful to Drs. A. Ben-Menahem and James Hannon for their assistance and encouragements. Valuable discussions were held with Mr. T. L. Teng and L. R. Johnson.

Mr. Laszlo Lenches prepared the figures; Mrs. Barbara Sloan typed the manuscript; their assistance is gratefully acknowledged.

The research was supported by the Advanced Research Projects Agency and was monitored by the Air Force Office of Scientific Research under Contract AF 49(638)-1337.

Abstract

The basic formulae for estimating the energy in the seismic waves are derived. The formulae take into account the radiation pattern of the source, the compensation for the non-elastic absorption of the waves, the velocity-density structure of the earth, the effects of the crustal structure under the receiver and the response of the recording instruments. Operations are performed in the frequency domain.

Estimation of the seismic energy of an earthquake is closely related to the determination of the source mechanism and the radiation pattern of the source. We have determined the surface wave radiation pattern of a shallow shock and the P wave radiation pattern of an intermediate shock to show the correspondence between the fault-plane solutions and the fault mechanisms derived from radiation pattern.

We have obtained the energies of the two earthquakes mentioned above as well as 7 other earthquakes with known fault-plane solutions and/or radiation patterns. The "total" seismic energies for these earthquakes (magnitudes between $6\frac{1}{2}$ and $7\frac{1}{2}$) using the present procedures are at least an order of magnitude higher than those arrived at from the current magnitude-energy formula. The S wave energies are approximately an order higher than that of the P waves. The surface wave energies for the shallow shocks are three orders of magnitude less than the body wave energies. Thus, the S wave seems to be the main seismic wave energy carrier.

Energies in the lower order spheroidal oscillations ($\ell = 2, 15$) for the 1964 Alaskan earthquake have been calculated from Isabella strain data and Berkeley ultra-long period pendulum seismometer data. The sum of the energies is 10^{23} ergs.

Table of Contents

	<u>Page</u>
Introduction.....	1
Basic Formulae.....	7
Body Wave Energy.....	9
Surface Wave Energy.....	13
Discussion.....	17
Integration for Energy in Practice.....	19
Spatial Integration.....	19
Frequency Integration.....	23
The Partitioning of Seismic Energy from a Surface Fault.....	25
Data and Data Analysis.....	34
Total Energy and Partitioning of Energy for a Shallow Earthquake.....	41
Introduction.....	41
Radiation Pattern of Surface Waves and Source Mechanisms of 1 September 1962, Iran Earthquake.....	43
Reduction of Body Waves.....	50
Integration for Energy.....	54
Energy Content of P and S Waves for an Intermediate and a Deep Earthquake.....	55
Calculation of Energy for Earthquakes with Known Fault Mechanisms.....	65
Free Oscillation Energy.....	68
Free Oscillation Energy of Alaskan Earthquake.....	78

Table of Contents (Continued)

	<u>Page</u>
Energy Estimates of Jeffreys, Gutenberg and Richter and Others.....	84
Energy Budget of Earthquakes.....	95
Conclusion.....	99
References.....	101
List of Tables.....	110
Tables.....	111
Figure Captions.....	127
Figures.....	129
Appendices.....	147
Attenuation of Body Waves.....	147
Integration of Body Wave Radiation Pattern.....	149
Method of Integration for the Integral (7.4).....	152
Variation of Angle of Incidence of Oceanic Rayleigh Wave.....	160

Introduction

The problems of the total elastic energy emission during an earthquake and the partitioning of this energy among various seismic waves, mainly the P and S body waves and fundamental-mode Rayleigh and Love surface waves, have been of interest to seismologists for many years. The total elastic energy is closely related to the strain energy released at the source in the case of fracture type earthquakes, or to chemical-physical energy released when the earthquake results from a phase change of the mineral assemblage in the upper mantle. Although it is not clear how much energy is being dissipated near the source through non-linear wave propagation or fracturing of the ground, the energy contained in the elastic waves may still give an order of magnitude estimate of the total energy released at the source. The partitioning of the total energy among seismic waves, on the other hand, is characteristic of the source that emits the waves and also of the property of the material in which the source is located.

Energy estimation in the past had mostly been in the direction of determining one parameter from the seismograms, the Richter magnitude, for a number of earthquakes, then independently estimating the energy of each earthquake, establishing the functional relation between energy and the magnitude, and using this relationship

subsequently to determine the energy whenever the Richter magnitude of that event was given. This procedure would be perfectly legitimate if, on one hand, the Richter magnitude is the parameter that completely describes the energy of the earthquake, and on the other hand, the independent estimation of energy is properly done. The efficacy of the Richter magnitude in earthquake statistics studies to define the seismicity of a region has long been recognized. But the fact that independent magnitude determinations for one single earthquake can differ by 1, roughly two orders of magnitude for energy, indicates that the magnitude scale does not uniquely describe an earthquake. Besides, owing to the non-uniformity and scarcity of instruments, and the lack of high-speed computing facilities, the direct energy estimate was done under several simplifying assumptions; in light of present knowledge regarding the nature of the earth's interior and wave propagation, a number of improvements can be made.

The validity of the magnitude-energy formula is especially uncertain when the P or S wave is no longer a well defined pulse. Perusal of seismograms shows evidence that many of the large shallow earthquakes (e.g. the Chilean earthquake of 1960, the Alaskan earthquake of 1964, and the Aleutian earthquake of February, 1965) consist of not one but a series of shocks separated in space (of the order of tens of kilometers) and in time (of the order of a few seconds). As a consequence, the magnitude is underestimated, if body waves are used, as only one of the many shocks in the series is measured. And due to

the fact that quite a large portion of the energy would go into long period oscillations, surface waves as well as "free vibrations," instead of being contained in the individual P or S wave, a large portion of the energy would be neglected.

Now that we have made advances in other fields of geophysics, e.g., the knowledge of heat flow, we wish to correlate earthquake energy with other energies, and we have a need to refine the energy estimation. With the establishment of world-wide standardized seismometers and availability of efficient computers, we have the means to put the energy estimation procedure on a physical basis.

In the present work, attempts were made to employ as much as possible the present knowledge regarding the velocity-density structure in the Earth, the attenuation of seismic waves, the radiation pattern of the source and the influence of crustal structure at the receiver, so that each single determination of the earthquake energy would be significant, and that we can have a closer estimate of the total energy involved.

The velocity-density structure determines the path of the body waves and the displacement-depth function for the surface waves. Data reduction under the assumption of a homogeneous mantle or a heterogeneous mantle yields noticeably different results; however, if we disregard data near the travel time cusps, the current earth models give results well within the experimental error. For convenience we have used Jeffereys' model for the body waves and

CIT11 model for surface waves.

Attenuation of seismic waves can account for a factor of 3 to 10 in amplitudes for P waves in the period range considered, and considerably more for S waves. For surface waves, the amplitude attenuation can be very severe if we consider waves that have travelled around the earth several times. Attenuation coefficients for surface waves are better known than that for body waves. Surface wave Q, the dimensionless loss factor, has been given by Ben-Menahem (1965) for periods between 50 and 300 seconds, and by Alsop et al (1961) at free oscillation periods. Anderson and Archambeau (1964) formulated a theory for inversion of Q data and obtained Q as a function of depth, which was subsequently employed by Anderson and Julian (1965) and Teng (1965) to compute the body wave attenuation as function of epicentral distance and frequency.

Unequal azimuthal radiation of the source was noticed by many earlier workers (Gutenberg, 1955; Bath, 1959), but the lack of uniform instruments prevented a thorough investigation. We have experimentally obtained the surface wave radiation patterns of a shallow shock and the body wave radiation patterns of an intermediate shock and included this factor in the spatial integration for energy. It is now quite well established (see also Teng and Ben-Menahem, 1965) that the theoretical radiation pattern (Ben-Menahem et al, 1965) calculated by using the fault elements derived from "fault-plane solutions" fits quite closely the observed radiation pattern at least for

surface waves (additional evidence can be found in Chander and Brune, 1965) and body waves from intermediate or deep earthquakes. It is possible to calculate the energy of an earthquake by integrating the P and S waves on three-component seismograms from one station, when the "fault-plane solution" of the earthquake is given.

The crust at the receiver acts like a band-pass filter. Although the long-period responses are not very much different for crustal models having different layerings, the short-period responses are quite distinctive from one another. Therefore when considering the energy in short period waves, the choice of the correct crustal model is very critical.

Any disturbance in a finite body can be represented as the superposition of the free modes of the body. As a consequence we have two possible interpretations of a seismic record: as a sum of free oscillations of the Earth or as waves travelling outward from a localized source with their ensuing reflections at boundaries and interfaces. It is a matter of practicality, insofar as the estimation of energy is concerned, which interpretation we use. Extraction of low frequency signals requires the recording of information long after the initiation of the disturbance; a time interval in which the waves have travelled a few times around the Earth and therefore "know" that they are in a finite body. Body waves and surface waves for relatively high frequency (corresponds to periods shorter than 300 seconds, say) are more easily processed as travelling waves. Under

the assumption of linear elasticity we can obtain the total seismic energy by adding up the energy content in different frequency bands, since no energy transfer among different frequencies is possible.

There are certain intrinsic difficulties involved in energy measurement, arising mainly from our inability to record the complete seismic signal. Several factors prevent us from doing so. First, the instrument response is inevitably band-limited; in order to recover a wider spectrum we have to use a series of instruments with different frequency characteristics: for example, a strain seismometer, and pendulum seismometer with different pendulum-galvanometer combinations. In the present work we use mainly WWNSS long-period instruments supplemented by strain seismometers and ultra-long period pendulums for free oscillation energy measurement. Secondly, scattering of high frequency seismic waves, when the wavelength becomes comparable to the dimensions of the inhomogeneities in the crust, increases as the fourth power of frequency; this effect tends to reduce high frequency waves to the noise level before they reach the seismometer. Since the energy content of the high frequency part of the spectrum is relatively high compared to that of low frequency waves, we are prone to underestimate the total seismic energy if the source does generate considerable high frequency energy. Thus, our estimate is at most a lower limit of the total elastic energy generated by the source.

Basic Formulae

Consider a region R, occupied by the elastic solid, and bounded by a "geometric surface" (not a boundary or any "physical surface") S. Both R and S are fixed in space and time. The energy E contained in the region S consists of the kinetic energy of particle motion and the elastic potential energy

$$E = \iiint_V \left[\frac{1}{2} \rho \left(\frac{\partial \vec{s}}{\partial t} \right)^2 + \frac{1}{2} |\boldsymbol{\chi} \cdot \boldsymbol{\epsilon}| \right] dv$$

where \vec{s} is the displacement field, ρ the density, $\boldsymbol{\chi}$ the stress dyadic and $\boldsymbol{\epsilon}$ the strain dyadic. Then the flow of energy out of the surface is

$$\begin{aligned} \frac{\partial E}{\partial t} &= \iiint_V \left[\rho \left(\frac{\partial \vec{s}}{\partial t} \right) \cdot \left(\frac{\partial^2 \vec{s}}{\partial t^2} \right) + |\boldsymbol{\chi} \cdot \frac{\partial \boldsymbol{\epsilon}}{\partial t}| \right] dv \\ &= \iint_S \left[\left(\frac{\partial \vec{s}}{\partial t} \right) \cdot \boldsymbol{\chi} \right] \cdot d\vec{A} \end{aligned}$$

(Morse and Feshbach, 1953).

This formula can be integrated with respect to time from t_0 to t_f to obtain the total energy, if at t_0 , all the energy we are

interested in is contained in the volume and at t_f the energy has been transported across S . However, to use this formula we need to have both strain measurement and displacement measurement at points on the closed surface S .

If we have the displacement fields only, we can consider an alternative expression for kinetic energy

$$\frac{\partial E}{\partial t} = \frac{1}{2} \iint_S \rho \left(\frac{\partial \vec{s}}{\partial t} \right)^2 \vec{v} \cdot d\vec{A}$$

which is a direct consequence of conservation of energy. Using this formula we can obtain the total kinetic energy in the volume and with the knowledge that potential energy equals kinetic energy in the average we can multiply the time integral by 2 and obtain the total energy, i.e.,

$$E = \int \frac{\partial E}{\partial t} dt = \int_{t_0}^{t_f} \iint_S \rho \left(\frac{\partial \vec{s}}{\partial t} \right)^2 \vec{v} \cdot d\vec{s} dt$$

The significance of this formula is that if we are given the time behavior of the displacement on a closed surface in the vicinity of the source, which is bounded also in time, we can integrate with respect to space coordinates and the time to obtain the total energy. In practice we observe seismic waves at a distance from the source; we have to equalize the waves back to the source before we can perform

the integration. In what follows, we will discuss the body wave energy integration and surface wave energy integration separately since the method of equalization and the surface of integration are slightly different. Implied in this treatment is the assumption that we are dealing with waves at large distances compared with the wave length, so that the waves are separated into different phases, and can be deemed as signals bounded in time. The equalization process, of course, recovers only the elastic field of the source. The energy that is dissipated around the source as heat is not our concern here.

Body Wave energy

For body waves P and S we use a spherical surface to enclose the source, and spherical coordinates are chosen for convenience. The kinetic energy density at time t is

$$\psi_p = \frac{1}{2}\rho v^2 = \frac{1}{2}\rho(r_s) \left(\frac{\partial \vec{s}_p}{\partial t}(\theta, \phi, t) \right)^2$$

where $\rho(r_s)$ = density of material at the source, and $s_p(\theta, \phi, t)$ = particle displacement, then the total kinetic energy in the P wave

$$E_p = \frac{v_p(r_s)}{2} \int \int \int r^2 \rho(r_s) \left(\frac{\partial \vec{s}_p}{\partial t}(\theta, \phi, t) \right)^2 \sin\theta \, d\theta \, d\phi \, dt$$

where

$v_p(r_s)$ = velocity of P wave at the source.

Similar expressions can be written for S waves.

Let

$$\tilde{V}(\theta, \phi, \omega) = \int_{-\infty}^{\infty} e^{-i\omega t} \frac{\partial \vec{s}}{\partial t}(\theta, \phi, t) dt$$

we have, by Parseval's theorem,

$$\int_{-\infty}^{\infty} \left(\frac{\partial \vec{s}}{\partial t}(\theta, \phi, t) \right)^2 dt = \frac{1}{2\pi} \int_{-\infty}^{\infty} \left[\tilde{V}(\theta, \phi, \omega) \right]^2 d\omega$$

$\tilde{V}(\theta, \phi, \omega)$ is the velocity spectrum density. This can be derived from displacement spectrum density:

$$\tilde{V}(\theta, \phi, \omega) = i\omega \tilde{s}(\theta, \phi, \omega)$$

$\tilde{s}(\theta, \phi, \omega)$ = displacement spectrum density.

The spatial dependence can be separated from the frequency dependent part, assuming a frequency independent radiation pattern (Ben-Menahem et al, 1965):

$$\tilde{s}(\theta, \phi, \omega) = \tilde{s}(\theta_o, \phi_o, \omega) R(\theta, \phi)/R(\theta_o, \phi_o)$$

$\tilde{s}(\theta_o, \phi_o, \omega)$ is the source spectrum observed at (θ_o, ϕ_o) , a point on the focal sphere. $R(\theta, \phi)$ is the radiation pattern of the source; it is discussed in detail in a paper by Ben-Menahem et al, (1965).

There are several ways of obtaining it. 1) With sufficient stations around the source an actual radiation pattern can be worked out, 2) a theoretical pattern from a double couple or single couple source (Ben-Menahem et al, 1965), can be fit to the available data points, 3) the surface wave radiation pattern (Wu and Ben-Menahem, 1965) or first motion method can be used to deduce the parameters and calculate the radiation pattern.

Since we invariably observe seismic waves at a distance from the source, these waves must be equalized back to the focal sphere* by compensating for the effect of geometrical spreading and absorption. Let $F(\omega)$ be the observed spectrum at some station then

$$\tilde{s}(\theta_o, \phi_o, \omega) = r_o F(\omega) [T(\omega) I(\omega)]^{-1} \left| \frac{d\Delta}{di_s} \right|^{\frac{1}{2}} \left| \frac{\sin \Delta \cos i_o}{\sin i_s} \right|^{\frac{1}{2}} e^{-\int \gamma(\omega, \Delta) d\Delta}$$

where

i_s = take-off angle at the source.

i_o = angle of incidence at the station

Δ = epicentral distance

r_o = radius of the earth

$\gamma(\omega)$ = attenuation coefficients

$T(\omega)$ = crustal transfer function

$I(\omega)$ = instrumental response

* The operation here only recovers the far field part of the elastic displacement.

The crustal transfer function was discussed by Haskell (1960, 1962), Phinney (1964), Hannon (1964) and Ben-Menahem et al (1965). It is sensitive to the layer parameters of crust under the instrument and the incidence angle; hence it has to be separately computed for each station. The attenuation factor $\gamma(\omega)$ has been investigated by Anderson and Julian (1965) and Teng (1965). (See Appendix I)

One complication arises in practice. In the discussion above we assumed that the P or S waves we observed are uncontaminated by other arrivals, which is more or less true for a P wave from earthquakes at a depth of 150 km or more, but for large shallower shocks the P pulses that usually persists for a duration of more than 20 seconds become entangled with the reflection from the crust above the source. The S wave, with its longer dominant period, is isolated for earthquakes at depth 300 km or more at suitable distances. In order to extract the energy for the primary signal, when P and pP or S and sS are superposed, we have to divide the observed spectrum by the transfer function of the system consisting of the crust above the source in addition to the operations discussed above. We will discuss the isolation for P for a shallow earthquake in a later section.

The total kinetic energy can therefore be obtained by combining the expressions above

$$E_p = \frac{r_o^2 v_p(r_s) \rho(r_s)}{2\pi} \int_0^{2\pi} \int_0^\pi R^2(\theta, \phi) \sin\theta \, d\theta \, d\phi$$

$$\cdot \int_0^\infty \frac{\omega^2 F^2(\omega)}{R^2(\theta_o, \phi_o)} \left[T(\omega) I(\omega) \right]^{-2} \left| \frac{d\Delta}{di_s} \right| \left| \frac{\sin\Delta \cos i_o}{\sin i_s} \right| e^{\int 2\gamma(\omega, \Delta) d\Delta} \, d\omega$$

where r has been taken to be unity.

Surface Wave Energy

For surface waves we use a semi-infinite cylindrical surface. Since no energy flows upward or downward only radial transport is involved.

$$\frac{dE}{dt} = \int_0^\infty \int_0^{2\pi} \psi(\theta, z, t) \, r \, v_r \, d\theta \, dz$$

$$v_r = \begin{cases} v_R & \text{in case of Rayleigh wave} \\ v_L & \text{in case of Love wave} \end{cases}$$

For a dispersive medium v_r is the group velocity, the velocity at which energy is being transported. As the frequency content of the wave is a function of time $v_r(\omega)$ is a function of time through frequency. This implies that we have to know the source time function, but this is unknown. To circumvent this difficulty we sum up energies

contained in narrow frequency band over which the group velocity is nearly constant:

$$\frac{dE}{dt} = \sum_{n=0}^{\infty} \int_0^{2\pi} r d\theta \int_0^{\infty} dz \left(\frac{\partial s_n}{\partial t} (\theta, z, t) \right)^2 \rho(z) \cdot v_{rn}$$

where s_n is the displacement and v_{rn} the group velocity for the frequency band $n \cdot \Delta\omega \rightarrow (n+1) \cdot \Delta\omega$, $\Delta\omega$ being the bandwidth. The total kinetic energy is

$$E = \sum_{n=0}^{\infty} \int_0^{2\pi} r d\theta \int_0^{\infty} dz \rho(z) \cdot v_{rn} \int_{-\infty}^{\infty} \left(\frac{\partial s_n}{\partial t} (\theta, z, t) \right)^2 dt$$

Again, using Parseval's theorem

$$\int_{-\infty}^{\infty} \left(\frac{\partial s_n}{\partial t} (\theta, z, t) \right)^2 dt = \frac{1}{2\pi} \int_{n \cdot \Delta\omega}^{(n+1) \cdot \Delta\omega} \tilde{s}_n^2(\theta, z, \omega) d\omega$$

where

$$\begin{aligned} \tilde{s}_n(\theta, z, \omega) &= \int_{-\infty}^{\infty} \frac{\partial s_n}{\partial t} (\theta, z, t) e^{-i\omega t} dt \\ &= -i\omega S_n(\theta, z, \omega) \end{aligned}$$

$S_n(\theta, z, \omega)$ being the displacement spectrum density at the vicinity of the source. To equalize the observed spectrum $G_n(\omega)$ at some azimuthal angle θ_0 and a distance Δ away from the epicenter and on the surface we do the following operation

$$S_n(\theta, z, \omega) = r_0^{1/2} G_n(\omega) \frac{R(\theta, \omega)}{R(\theta_0, \omega)} \left[I(\omega) \right]^{-1} |\sin \Delta|^{1/2} \cdot e^{\gamma(\omega)\Delta} \cdot H(z, \omega)$$

$R(\theta_0, \omega)$ is the radiation pattern which can be derived from observed spectrum around the source (Wu and Ben-Menahem, 1965). $H(z, \omega)$ is the normalized (to surface displacement) displacement - depth function. This can be determined by using Haskell's matrix method once the layer constants are given. The integral

$$J(\omega) = \frac{1}{2} \omega^2 \int_0^{\infty} \rho(z) H^2(z, \omega) dz$$

is numerically computed and plotted in figures 1 - 3 separately for Rayleigh wave, vertical and horizontal components, and Love wave, for the CIT II structure (Anderson and Toksöz, 1963). The expression for the energy can, therefore, be written as

$$E = \frac{r_0}{\pi} \sum_{n=0}^{n=\infty} \int_0^{\infty} d\theta v_{rn} \int_{n \cdot \Delta\omega}^{(n+1) \cdot \Delta\omega} G_n^2(\omega) \left[\frac{R(\theta, \omega)}{R(\theta_0, \omega)} \right]^2 \left[I(\omega) \right]^{-2} \cdot e^{2\gamma(\omega)\Delta} J(\omega) d\omega$$

The plots of $J(\omega)$ all demonstrate the fact that as period decreases $J(\omega)$ increases. We can show here that for Rayleigh wave in a half space $J(\omega)$ indeed approaches ∞ as $\omega \rightarrow \infty$, and approaches 0 as $\omega \rightarrow 0$. In a half-space $H(z)$ of Rayleigh wave can be written as

$$\exp\left(-\sqrt{1 - c_r^2/\beta^2} z\right)$$

or

$$\exp\left(-\sqrt{1 - c_r^2/\alpha^2} z\right)$$

where $z \rightarrow 0$. We then have

$$J(\omega) = \frac{1}{2}\omega^2\rho \int_0^\infty e^{-2\eta\omega z} = -\frac{1}{4}\frac{\omega\rho}{\eta} e^{-2\eta\omega z} \Big|_0^\infty = \frac{1}{4} \frac{\omega\rho}{\eta}$$

where

$$\eta = 1/c_r \sqrt{1 - c_r^2/\beta^2} \quad \text{or} \quad 1/c_r \sqrt{1 - c_r^2/\alpha^2}$$

Therefore $J(\omega) \rightarrow \infty$ as $\omega \rightarrow \infty$, and $J(\omega) \rightarrow 0$ as $\omega \rightarrow 0$.

Thus energy would become quite large if the source spectrum does have finite amplitude at very high frequency. Since we do not expect nature to yield unreasonably large amounts of energy in earthquakes, a source frequency spectrum should not contain very high frequency components. Further discussion of spectral energy density $J(\omega)$ can be found in a paper by Harkrider and Anderson (1966).

Discussion

In the formulation above, we assumed we can integrate over the whole frequency band from 0 to ∞ , but in practice, using the 30-100 WwNSS seismogram, for example, we are able to observe a band-limited seismic signal only. At the low frequency end of the spectrum it is possible to use auxiliary instruments such as strain seismometers, tiltmeters or the like to record fundamental and higher modes of free-oscillation (Kovach and Anderson, 1966). We will discuss this in a later chapter, and use Isabella strain data and Berkeley Pendulum seismometer data to estimate the long period energy for Alaska earthquake. At the high frequency end of the spectrum the attenuation is severe and the effect of the crust - scattering and diffracting - render it difficult to recover the signal accurately. As we have just shown that $J(\omega) \rightarrow \infty$ as $\omega \rightarrow \infty$, the amount of energy we neglect by using a band-limited instrument or measuring energy at distances such that the high frequency waves are already reduced to noise level, can be quite significant. In this sense, we are at best only measuring the lower limit of the total elastic wave energy released during the earthquake. In order to make clear the meaning of the numbers - energy in ergs in this case - it is always desirable to specify the band over which we integrate.

In some applications, for example, to relate magnitude to energy, it may be advisable to bypass the frequency integration and look at, say, surface wave spectrum density instead. A perusal of the

seismograms from earthquakes of various magnitudes reveals that longer waves are observed only for large earthquakes. It is perhaps possible to reduce the energy spectrum densities to a one parameter family and use the parameter to specify the magnitude.

The differences between the methods used by other authors to obtain the energy of earthquakes and the method presented here will be discussed in a later chapter, after we obtain some experimental values of the energy.

Integration for Energy in Practice

Spatial Integrations

It would be desirable to integrate over the spatial coordinates experimentally, so that the final energy obtained will be free from assumptions as to the nature of the source. However, the distribution of stations does not warrant such a procedure; a much higher density of seismometers around the world is required for the purpose.

Insofar as it has been demonstrated that the seismic source can be approximated by a double couple source (see e.g., Hodgeson and Stevens, 1964; Stauder, 1964; Wu and Ben-Menahem, 1965; Teng and Ben-Menahem, 1965) we shall use the theoretical radiation pattern for our spatial integration.

1. Body Waves

Ben-Menahem et al (1965) gave the body wave radiation patterns for both shear and tensile faults in an infinite medium. We have listed the P, SV and SH radiation patterns for shear faults in Table I. These radiation patterns will be used in a later section to obtain the source mechanism of an "intermediate" earthquake.

The integration

$$I = \int_0^{2\pi} \int_0^{\pi} R^2(\theta, \phi) \sin\theta \, d\theta \, d\phi$$

is carried out in Appendix II.

From the physics of the situation, we can see immediately that the P integral will be independent of the attitude of the motion vector, therefore, independent of δ and λ . In other words, the integral is a constant. But it is not so in the case of SH or SV wave, because SH and SV is defined only when a surface or a preferred orientation is involved in the problem (in an infinite medium the surface is a geometrical one), and the attitude of motion vector - specified by δ and λ - will determine how much energy will go into each type.

The results are

$$I_p = \frac{4}{15} \pi$$

$$I_{SH} = \frac{4}{3} \pi (\alpha_1^2 + 4 \alpha_2^2) + \frac{2}{3} \pi (\beta_1^2 + \beta_2^2)$$

$$I_{SV} = \frac{\pi}{15} (19 \alpha_1^2 + 16 \alpha_2^2) + \frac{14}{15} \pi (\beta_1^2 + \beta_2^2)$$

where

$$\alpha_1 = \frac{1}{2} \sin \lambda \sin 2\delta$$

$$\alpha_2 = \frac{1}{2} \sin \delta \cos \lambda$$

$$\beta_1 = \sin \lambda \cos 2\delta$$

$$\beta_2 = \cos \lambda \cos \delta$$

2. Surface Waves

The spatial integration of the surface wave energy can be separated into the θ and z integrations. We have already performed the z integration when we calculated the kinetic energy density curves for Rayleigh and Love waves in the previous section; they are independent of the source. The θ dependence is the radiation pattern of the source. It was shown by Haskell (1963) that the radiation pattern of Rayleigh wave in a homogeneous, isotropic half-space is a function of the depth of source and the attitude of the motion vector and the frequency of the wave. Ben-Menahem and Harkrider (1964) extended his result to Rayleigh and Love wave radiation from dipolar sources with arbitrary elements in a multilayered elastic medium; in which case the radiation pattern is a function of the same variables as in Haskell's results, although in a much more complicated way.

According to Ben-Menahem and Harkrider, the radiation pattern from a dipolar source, at some frequency ω_0 can be expressed as

$$\begin{aligned}\chi(\phi) = & d_0 + i(d_1 \sin \phi + d_2 \cos \phi) + d_3 \sin 2\phi \\ & + d_4 \cos 2\phi\end{aligned}$$

where d_i 's are functions of ω , δ , λ and h . (See Harkrider and Ben-Menahem for definitions of d_i 's). Evidently, this function includes both the amplitudes and the phase; in calculating the spatial integral, only the amplitude part is needed.

The amplitude of $\chi(\theta)$ is

$$|\chi(\phi)| = \sqrt{(d_0 + d_3 \sin 2\phi + d_4 \cos 2\phi)^2 + (d_1 \sin\phi + d_2 \cos\phi)^2}$$

and the integral we have to calculate is

$$\begin{aligned} & \int_0^{2\pi} |\chi(\phi)|^2 d\phi \\ = & \int_0^{2\pi} (d_0 + d_3 \sin 2\theta + d_4 \cos 2\theta)^2 + (d_1 \sin\theta + d_2 \cos\theta)^2 d\theta \\ = & \pi (2d_0^2 + d_3^2 + d_4^2 + d_1^2 + d_2^2) \end{aligned}$$

This has been incorporated in the computer program for calculating the radiation pattern of Rayleigh and Love waves in a multilayered medium.

The integral depends on frequency as well as the attitude of the motion vector. The frequency dependence can be obtained in the process of fitting the observed radiation pattern at various frequencies by interpolating between the discrete frequencies values.

Frequency Integration

The general form of the frequency integral is

$$\frac{1}{2\pi} \int \omega^2 R^2(\omega) S^2(\omega) d\omega$$

where $S^2(\omega)$ is the spectrum density, $R(\omega)$ is the frequency dependence of the radiation pattern.

For body waves, it is assumed that $R(\omega) = A$, the integration therefore is reduced to

$$\frac{1}{2\pi} \int \omega^2 S^2(\omega) d\omega$$

In case of surface waves, however, $R(\omega) \neq \text{constant}$, and the functional dependence can be obtained in the process of fitting the surface radiation pattern. A frequency dependent spatial integration

$$\int_0^{2\pi} \chi^2(\phi, \omega) d\phi$$

can be performed numerically when calculating theoretical radiation patterns. This is then used as a weighting function in the frequency integral.

Theoretically, the spectrum from one station would suffice for the frequency integration after the radiation pattern has been determined.

The actual spectral densities at various stations from one single earthquake are invariably different from each other. Many factors could contribute toward this diversification, for example the finiteness of the source, effects of a propagating rupture, effects of different propagation paths as well as the choice of velocity window, and numerical processing.

In practice, we can choose several spectra, preferably at the maxima of the radiation pattern, perform the integration on these spectra, and obtain thereby an error estimate.

The Partitioning of Seismic Energy from a Surface Fault

The problem of partitioning of the seismic wave energy among different phases at large distances from the source can be experimentally solved as we have demonstrated in the previous section. It is obvious that partitioning of energy in general would depend on the type of source that generates the elastic waves. For example, we would not expect to observe much S wave from an explosion if no release of tectonic strain is involved in the event, while for most earthquakes, S wave is much stronger than P wave. When surface waves are concerned we would expect the partitioning to depend also on the layering or the inhomogeneities of the media in which the source is located and the proximity of the source to the channel or the free surface (Harkrider and Anderson, 1966). Although the exact mechanism of earthquake generation is yet to be expounded, it has been verified experimentally that as far as the first motion of the body waves and the radiation pattern of the bodily waves as well as the surface waves are concerned, the source can be represented as a double couple, which is an equivalent force system only, saying nothing about the actual mechanism, be it a slip on a plane or a result of phase change. (For a summary on first-motion studies see Scheidegger, 1957; for radiation pattern of bodily waves see Teng and Ben-Menahem; for surface wave studies see Wu and Ben-Menahem, 1965 and Chander and Brune, 1965).

In this section we will investigate the partitioning of energy from double couple sources which arise from equivalent force representations of faulting in a homogeneous half-space, and in a later section we shall compare the results we obtain here to those for the Iran Earthquake of September 1, 1962. The method we use here is based on a paper by Burridge et al, (1964) in which the representation theories of Burridge and Knopoff (1964) was used to set up equivalent double couple sources for dip-slip and strike-slip on an arbitrarily dipping plane, which is shrunk to zero area. In the treatment it was proved that an arbitrary fault (with zero surface area) can be reduced to a linear combination of three elementary displacement-dislocations namely (a) Slip on a horizontal plane, (b) Strike slip on a vertical plane and (c) Dip-slip on a plane dipping at 45° .

In order to avoid repetition we shall start our discussion from the integrals given by Burridge et al, (1964) and use their numberings of the equations

$$\begin{pmatrix} u \\ v \\ w \end{pmatrix}_p = \frac{S}{(2\pi)^3} \int_{-\infty}^{\infty} \frac{d\omega}{i\omega} \int_{-\infty}^{\infty} d\xi \int_{-\infty}^{\infty} d\eta \frac{\xi\eta\zeta'}{\mathcal{R}} \begin{pmatrix} \xi \\ \eta \\ \zeta \end{pmatrix} e^{i(\omega t - \xi x - \eta y - \zeta z)}, \quad (7.4)$$

$$\begin{pmatrix} u \\ v \\ w \end{pmatrix}^{SV} = \frac{S}{(2\pi)^3} \int_{-\infty}^{\infty} \int_{-\infty}^{\infty} \frac{d\omega}{i\omega} \int_{-\infty}^{\infty} d\xi \int_{-\infty}^{\infty} d\eta \frac{\xi\eta}{2\beta^2 - \xi^2 - \eta^2} \begin{pmatrix} \xi\xi' \\ \eta\xi' \\ -\xi^2 - \eta^2 \end{pmatrix} e^{i(\omega t - \xi x - \eta y - \zeta' z)}, \quad (7.5)$$

$$\begin{pmatrix} u \\ v \\ w \end{pmatrix}^{SH} = \frac{S}{(2\pi)^3} \int_{-\infty}^{\infty} \int_{-\infty}^{\infty} \frac{d\omega}{i\omega} \int_{-\infty}^{\infty} d\xi \int_{-\infty}^{\infty} d\eta \frac{\xi^2 - \eta^2}{\xi'(\xi^2 + \eta^2)} \begin{pmatrix} -\eta \\ \xi \\ 0 \end{pmatrix} e^{i(\omega t - \xi x - \eta y - \zeta' z)}, \quad (7.6)$$

$$\begin{pmatrix} u \\ v \\ w \end{pmatrix}^P = \frac{-D}{(2\pi)^3} \int_{-\infty}^{\infty} \int_{-\infty}^{\infty} \frac{d\omega}{i\omega} \int_{-\infty}^{\infty} d\xi \int_{-\infty}^{\infty} d\eta \left\{ \frac{\lambda}{\lambda + 2\mu} (\xi^2 + \eta^2) + \eta^2 \right\} \begin{pmatrix} \xi \\ \eta \\ \zeta' \end{pmatrix} \frac{1}{2\mathcal{R}} e^{i(\omega t - \xi x - \eta y - \zeta z)}, \quad (8.3)$$

$$\begin{pmatrix} u \\ v \\ w \end{pmatrix}^{SV} = \frac{-D}{(2\pi)^3} \int_{-\infty}^{\infty} \frac{d\omega}{i\omega} \int_{-\infty}^{\infty} d\xi \int_{-\infty}^{\infty} d\eta$$

(8.4)

$$\left\{ \frac{\lambda}{\lambda + 2\mu} (\xi^2 + \eta^2) + \eta^2 \right\} \frac{\omega^2}{2\beta^2} \frac{-\xi^2 - \eta^2}{2\mathcal{R}(\xi^2 + \eta^2)} \begin{pmatrix} \xi \zeta' \\ \eta \zeta' \\ -\xi^2 - \eta^2 \end{pmatrix} e^{i(\omega t - \xi x - \eta y - \zeta' z)},$$

-28-

$$\begin{pmatrix} u \\ v \\ w \end{pmatrix}^{SH} = \frac{-D}{(2\pi)^3} \int_{-\infty}^{\infty} \frac{d\omega}{i\omega} \int_{-\infty}^{\infty} d\xi \int_{-\infty}^{\infty} d\eta \frac{1}{\zeta'} \frac{\xi \eta}{\xi^2 + \eta^2} \begin{pmatrix} -\eta \\ \xi \\ 0 \end{pmatrix} e^{i(\omega t - \xi x - \eta y - \zeta' z)},$$

(8.5)

$$\lim_{h \rightarrow 0} \frac{1}{h} \begin{pmatrix} u \\ v \\ w \end{pmatrix} = \frac{2i\beta^2}{\omega^2} \xi \zeta' \mathcal{R} \left[\left(\frac{\omega^2}{2\beta^2} - \xi^2 - \eta^2 \right)^2 + \zeta^2(\xi^2 + \eta^2) \right] \begin{pmatrix} \xi \\ \eta \\ \zeta \end{pmatrix} e^{i(\omega t - \xi x - \eta y - \zeta z)}$$

$$\lim_{h \rightarrow 0} \frac{1}{h} \begin{pmatrix} u \\ v \\ w \end{pmatrix} = \frac{2i\beta^2}{\omega^2} \frac{\frac{\omega^2}{2\beta^2} - \xi^2 - \eta^2}{\mathcal{R}} \left[\left(\frac{\omega^2}{2\beta^2} - \xi^2 - \eta^2 \right)^2 + \zeta^2(\xi^2 + \eta^2) \right] \begin{pmatrix} \xi \zeta' \\ \eta \zeta' \\ -\xi^2 - \eta^2 \end{pmatrix} e^{i(\omega t - \xi x - \eta y - \zeta' z)}$$

(II.2)

$$\lim_{h \rightarrow 0} \frac{1}{h} \begin{pmatrix} u \\ v \\ w \end{pmatrix} = \frac{-2i\zeta' \eta}{\xi^2 + \eta^2} \begin{pmatrix} -\eta \\ \xi \\ 0 \end{pmatrix} e^{i(\omega t - \xi x - \eta y - \zeta z')}$$

SH

In these expressions ξ and η are the horizontal wave numbers in the direction of x and y respectively, $\zeta^2 + \xi^2 + \eta^2 = \omega^2/\alpha^2$ and $\zeta'^2 + \xi^2 + \eta^2 = \omega^2/\beta^2$ with $\alpha = (\lambda + 2\mu/\rho)^{1/2}$ and $\beta = (\mu/\rho)^{1/2}$. \mathcal{R} is the half space Rayleigh factor :

$$\mathcal{R} = (\omega^2/2\beta^2 - \xi^2 - \eta^2) + \zeta\zeta' (\xi^2 + \eta^2),$$

A glance at these integrals will show that in the integrand for P and SV waves the denominators all have the factor \mathcal{R} , which when equated to zero is the homogeneous half-space Rayleigh equation; as expected, the SH integral does not have such a factor. Since the presence of singularities (the solutions of Rayleigh equation) implies the interference of waves and conversion of a wave to Rayleigh wave in the far field solution, the P and SV will contribute to the Rayleigh wave while the SH wave will not. Of course, if there is any inhomogeneity, for example, layering, there will be Love waves. One advantage of separately treating P and SV integrals is that we can isolate the contribution to Rayleigh waves from these primary waves.

The method of integration used is very similar to the one used in the paper by Burridge et al, (1964); strictly speaking their approximation neglected the contribution from the singularity which lies along the contour, and is therefore not complete. Insofar as the body waves are the main objective of their paper, the results are still correct. We adopted an integration procedure given in

Brekhovskikh (1960) with slight modifications. In Appendix III, we have treated the integrals (7.4) in some detail to show the location of singularities, the branch cuts and the deformation of the contour. The other integrals can be treated in the same way.

The results of the integration are tabulated in Table II. Since the method of integration used is valid for $kR \gg 1$, we are therefore neglecting a part of the signal for finite distances. However, since in practice we are recording at large distance (compared to wave lengths of interest) from the source and looking at a band-passed signal the condition $kR \gg 1$ may easily be satisfied. To obtain the kinetic energy we can apply the same type of formulas as in the previous section on Basic Formulae,

$$E = \frac{1}{2} \rho \int_S \int_{-\infty}^{\infty} |\dot{u}|^2 ds d\omega$$

where $\dot{u} = \dot{u}(\omega, x, y, z)$ and S is a closed surface surrounding the source. To find the partitioning of energy among the different phases, we need not carry out the ω integration. This is so because all the velocity spectra are of the same degree in ω ; for Rayleigh waves it is true after integrating on z . Thus it is clear that in a homogeneous half-space the total energy will be dependent on the source time function, but the partitioning of energy among different waves will not be. A word may be said here about the source spectrum. In order

to keep the total energy finite it is necessary that

$$S_o(\omega) \rightarrow \frac{1}{\omega^n} \quad \text{as } \omega \rightarrow 0 \quad n \leq 1$$

and

$$S_o(\omega) \rightarrow \frac{1}{\omega^n} \quad \text{as } \omega \rightarrow 0 \quad n \geq 1$$

Take E_p as 1 for source (b) and (c) we have calculated E_{sv}/E_p , E_{sh}/E_p , $(E_r/E_p)_p$ and $(E_r/E_p)_{sv}$ and $E_p/E_{sh} + E_{sv}$ and E_R/E_B , where the subscript B denotes body waves. They are tabulated in Table III.

Haskell (1964) used de Hoop's representation theorem (de Hoop, 1958) to calculate the partitioning of energy between P and S waves for a finite propagating fault in an infinite space. The final stage of his faulting is represented by a discontinuity of shear stress across a strip of length L and width W, the thickness of the fault region is small compared to the wavelength in question. The rupture starts at one end of the strip and moves to the other end with a velocity of V. The medium is unstressed prior to the rupture. The results he obtained for shear faults are:

Longitudinal shear fault

$$\frac{E_p}{E_s} = \begin{array}{ll} .03294 & \alpha T/L > a + 1 \quad \text{and} \quad \beta T/L > b + 1 \\ .01829 & \alpha T/L < a - 1 \quad \text{and} \quad \beta T/L < b - 1 \end{array}$$

Transverse shear fault

$$\frac{E_p}{E_s} = \begin{array}{ll} .03652 & \alpha T/L > a + 1 \quad \text{and} \quad \beta T/L > b + 1 \\ .02557 & \alpha T/L < a - 1 \quad \text{and} \quad \beta T/L < b - 1 \end{array}$$

where

$$\frac{E_p}{E_s} = \frac{\text{LONGITUDINAL WAVE ENERGY}}{\text{SHEAR WAVE ENERGY}}$$

α = P wave velocity

T = rise time of the ramp source time function

a = α/V

b = β/V .

The dislocation source models adopted in Burridge and Knopoff's (1964) and Haskell's (1964) works are equivalent sources that are not realized in earthquakes. The introduction of a dislocation in a medium requires a very large amount of energy to be put into the medium. This energy is not generally available in natural circumstances. Archambeau (1964) proposed a relaxation model which incorporated a finite non-linear zone, the propagating rupture and release of tectonic strain. Such a source model provides more parameters to fit an actual radiation field. His preliminary results show that E_s/E_p values depend on source parameters, but in general are of the same order as the values we arrived at for dislocation model.

Data and Data Analysis

1. Instruments Used

To ensure that the quality of the data be uniform it is desirable to use only data from those instruments that have very similar frequency characteristics. Therefore, wherever it is possible, we will use the WWNSS seismograms. Even the responses of these standardized seismometers exhibit a certain amount of deviation from the published curves; this can be seen from the difference in the shape of the calibration pulses on the seismograms (figure 4). However, in most cases, the calibration pulses are quite similar and the response of the instrument obtained by Fourier analyzing these traces is very close to the ones published in the handbook: World-Wide Standard Seismograph Network.

The amplitude response of a critically damped and zero-coupling galvanometer-seismometer system can be expressed as

$$A(\omega) = \frac{\omega^3}{\omega_0^2 \omega_g^2 + \omega_0^2 \omega^2 + \omega_g^2 \omega^2 + \omega^4}$$

as $\omega \rightarrow \infty$, $A(\omega) \rightarrow 1/\omega$

and as $\omega \rightarrow 0$, $A(\omega) \rightarrow \omega^3/\omega_0^2 \omega_g^2$.

That is to say, at short periods the instrument reacts like an integrating circuit and at long periods, a differentiating circuit.

And at intermediate periods we would expect the instrument to respond in a rather complicated way. Thus a direct use of the amplitude of a trace is not desirable in that equalization or other frequency-dependent operations cannot be carried out without ambiguity. Amplitude of ground displacement, acceleration, and velocity could be obtained by deconvolving with the instrument response in the time domain or multiply by the proper instrument response in the frequency domain.

The frequency response of a velocity transducer is given as

$$A(\omega) = Q\omega^3 \left(\chi^2(\omega) + \gamma^2(\omega) \right)^{-1/2} \quad (\text{Amplitude})$$

$$\phi(\omega) = \tan^{-1} \left(\chi(\omega) / \gamma(\omega) \right) \quad (\text{Phase})$$

where

$$\omega = \text{frequency (radians/sec)}$$

$$\chi = \omega^4 - \omega^2 \left[n_1^2 + n_2^2 + 4 k_1 k_2 (1 - \sigma^2) \right] + n_1^2 n_2^2$$

$$\gamma = -2\omega^3 (k_1 + k_2) + 2\omega (n_2^2 k_1 + n_1^2 k_2)$$

n_1 = natural frequency of the pendulum

n_2 = natural frequency of the galvanometer

k_1/n_1 = h_1 damping factor for the pendulum with the galvanometer clamped ($h_1 = 1$ for critical damping)

$k_2/n_2 = h_2$ damping factor for the galvanometer with the
pendulum clamped ($h_2 = 1$) for critical damping

σ = coupling factor

Q = constant determined by parameters of the electrical
and mechanical system (see Hagiwara, 1958)

This formula was programmed and was used to reduce the trace spectrum to ground displacement spectrum. For our purpose, the calculated response is close enough to the actual response of the instrument obtained by Fourier analyzing the calibration pulse (figure 5).

2. Analysis of Body Waves

Body waves P and S are usually present on a seismogram as a pulse at suitable distances from the source. Great care must be taken to choose waves that are not contaminated by later or earlier phases. For example, PcP often follows P and gradually merges into P.

In most cases, the signal-noise ratio is very high and pre-processing of data is not necessary. However, one difficulty arises owing to the finite time window we take for P and S waves. The response of the instrument is such that after an impulsive ground displacement it takes a long time for the trace to return to its zero-line; the next phase invariably comes in before the previous phase dies down completely (see, for example, Berckheimer

and Schneider, 1964). Thus, when we wish to isolate a P wave or an S wave by applying a finite velocity window, we will cut off a part of the signal. From the expression for instrument frequency-response, the zero frequency will not be sensed by the instrument. As a result of the velocity filtering, a part of the signal is discarded; the areas enclosed by the trace above and below the zero-line are not equal, i.e. a dc component is introduced into the spectrum. When we divide the spectrum by $A(\omega)$, the error is drastically magnified. In the process of numerical Fourier analysis, this component will contaminate the values at other frequencies, unless we either detrend the trace or use

$$\Delta f = \frac{1}{2T} = \frac{1}{2 \times \text{record length}}$$

as frequency increment, in the interval

$$0 \leq f \leq \frac{1}{2\Delta t} = \frac{1}{2 \times \text{digital interval}}$$

Another technique which is useful in rendering the spectrum smooth is tapering the trace at both ends, so that the trace has a value of zero and a slope of zero at these points. Since the Fourier transform operation is assuming the trace is zero outside the data range the tapering will eliminate possible jumps at the ends.

3. Surface Waves

The analysis of surface waves is done in much the same way as in previous studies of surface wave phase velocities (see, for example, Toksoz and Ben-Menahem, 1963). Instead of using phase spectrum, as was in the work on phase velocity, we are concerned here mainly with the amplitude spectrum. We will outline the procedure we used.

a. Identification of Waves

A Fortran program was written to calculate the arrival time of the surface waves G_1 through G_5 and R_1 through R_5 , given the epicenter and origin time. As the group velocity would vary for waves that propagate by different great circle paths, we cannot set a rigid velocity window for all the seismograms; instead, judgement has to be used as to when to start and when to stop. This is especially crucial when we employ G_1 or R_1 . The orbital motion of the wave will help in identification, when distinguishing between G and R waves.

b. Digitization

After the group velocity window for each wave is determined, the traces are then digitized at intervals controlled by the highest frequency we wish to look at. In the present work, we used 3 second intervals. As we shall see later, we will not look at waves below

15 seconds; 20 points per minute is therefore quite sufficient. Tapering of data at both ends of the trace can be performed before digitizing.

c. Detrending

The digitized data are then put through a detrending process on the computer to remove the mean and the tilt of the trace (remove trend of degree 1). This will eliminate the dc component as well as the very low frequency content which comes into the data through some instability of the seismometer system.

d. Filtering

Not infrequently the wave traces are mixed with short-period or long-period "noises": microseisms, multiply reflected body waves, instrumental noise, etc. The presence of these noises render the spectrum rugged and sometimes cause a significant modification of the amplitude at periods that we are interested in. Digital filtering can be used to remove these interferences.

The response $H(\omega)$ of the low-pass filter we employed is such that

$$H(\omega) = 1 \quad |\omega| \leq \omega_c$$
$$= \frac{\omega + \omega_r}{\omega_r - \omega_c} \quad -\omega_r \leq \omega \leq -\omega_c$$

$$\begin{aligned} &= \frac{\omega_r + \omega}{\omega_r - \omega_c} && \omega_c \leq \omega < \omega_r \\ &= 0 && |\omega| > \omega_r \end{aligned}$$

where ω_c = cut-off frequency

ω_r = roll-off frequency

The center of the filter may be shifted to ω_o ;
thereby we may generate a band-pass filter. A detailed
treatment can be found in a work by Ormsby (1961).

Total Energy and Partitioning of Energy for a
Shallow Earthquake

Introduction

The classification of earthquakes into shallow, intermediate and deep has an element of arbitrariness in it since there is hardly a discontinuity involved in the depth distribution of hypocenters. It is nevertheless convenient to employ such terms for general descriptive purposes. In the present context a "shallow" earthquake is one that generates a relatively large amount of fundamental surface waves, while in an "intermediate" or "deep" earthquake the fundamental surface wave will either be absent or higher mode surface waves become dominant among the later arrivals.

The procedures involved in either case would be the determination of radiation pattern or equivalently in our method, the source mechanism, of an earthquake and then integration of the individual phases on the seismogram. The method is summarized in the flow diagram in figure 6. For shallow shocks we are going to take into account the surface waves. As we have found out that even for a shallow shock the surface wave energy in the frequency band considered is about two to three orders of magnitude smaller than that of body waves P and S; we have neglected the surface wave energy for deep earthquakes completely, although the higher mode surface wave energy can be of considerable theoretical interest.

In this section we will give an example of integration of energy for the shallow Iranian shock of 1 September 1962. We will first determine the radiation pattern of the source and obtain thereby the source mechanism; based on these radiation patterns we will on the one hand integrate the surface wave energy and on the other hand calculate the corresponding body wave radiation patterns. These body wave radiation patterns are used later in body wave integration, after the body waves, which are a mixture of P and pP, and, S and sS, are unscrambled. Extraction of P and S from mixed pulses is done by assuming crustal structure above the source and the radiation pattern of the source. Considerable error could be introduced in this procedure; however, by using a large number of P + pP and S + sS waves, the error will be reduced.

Radiation Pattern of Surface Waves and Source

Mechanism of 1 September 1962, Iran Earthquake

1. Introduction

For an earthquake source that is not spherically symmetric, the azimuthal dependence of wave amplitude and initial phase, or radiation pattern, is involved. Since the radiation pattern is controlled by the characteristics of the source, a study of the radiation pattern will provide a better understanding of the source mechanism and improvement in energy measurements. Gutenberg (1936) discussed the different azimuthal distributions of surface wave energy for two shocks that occurred in the neighborhood of each other and inferred the different mechanisms, and later (1955) he plotted the azimuthal dependence of amplitude of surface waves and magnitude derived therefrom. Brune (1961) determined the Rayleigh wave radiation pattern for the 1958 Alaska earthquake using time domain measurements. He found the lobe structure of the pattern to conform to the fault motion determined by first motion method. Ben-Menahem and Harkrider (1964) formulated the problem of radiation pattern for Rayleigh and Love waves from Dipolar point sources in multilayered media. They showed the dependence of the radiation pattern on type and depth of source, orientation of the motion vector and frequency. We will now find the actual radiation pattern of Rayleigh and Love

waves generated by the Iran shock of September 1, 1962 at different frequencies and derive therefrom, by comparing with Ben-Menahem and Harkrider's result, the fault parameters, namely, strike, dip, slip angle and depth.

2. Data Analysis

Three component long-period seismograms from USCGS WVNSS, Columbia stations in Canada, Japan and Honolulu and some other individual stations were collected (Table IV). Azimuthal coverage is sufficiently dense in the second and fourth quadrants and is relatively scanty in the other two quadrants (figure 7). With few exceptions R_1 or G_1 through R_3 or G_3 could be traced. On a number of seismograms the magnifications were high enough for R_4 or G_4 and R_5 or G_5 to be distinguished. Thus each station might provide one or more points on the radiation pattern. The determination of the time window was done in much the same way as in previous surface wave phase velocity works (see, for example, Toksoz and Ben-Menahem, 1963). Owing to the fact that the observed seismic signals traveled over different paths, it was necessary to use a slightly different group velocity window for each case.

The traces were digitized at three seconds interval and subjected to Fourier analysis. Preprocessing consisted of removing trend of degree 1 and passing through a 61 coefficient low-pass filter, with cut-off at 50 seconds and roll-off at 40 seconds. Shorter periods were not included because of the lack

of power for waves of period less than 40 seconds and of the sensitivity of these waves to the crustal structure and diffraction effects at the crustal margin; a more refined technique would be required to extract information from this shorter period range. Moreover, the fault length, as deduced from geological observations, is 100 km; the finiteness of source causes the presence of sharp minima in spectra for periods shorter than 100 seconds.

The spectra so obtained were corrected for instrumental response and converted to ground displacement spectrums. They were then equalized to a fixed distance from the epicenter by removing the effects of dissipation and geometrical spreading on a sphere. The operations involved can be summed up as follows:

$$\begin{aligned} f(t) &= \text{seismogram trace} & T_0 < t < T_1 \\ &= 0 & t < T_0, t > T_1 \\ F(\omega) &= \int_{T_0}^{T_1} f(t) e^{-i\omega t} dt \\ A(\omega) &= F(\omega) \cdot I(\omega)^{-1} \cdot e^{\gamma(\omega)\Delta} \cdot \sin\Delta \end{aligned}$$

where

T_0 = arrival time of the wave

$T_1 - T_0$ = time window

$F(\omega)$ = trace spectrum

Δ = distance of station from epicenter

$\gamma(\omega)$ = absorption coefficient

R_o = the radius of the Earth

$I(\omega)$ = instrumental response

$A(\omega)$ = equalized displacement spectrum

The instrument response we used was the theoretical formula derived by Hagiwara (1958) for electromagnetic seismographs.

The response could be calculated quite easily provided the coupling and damping factors are given. In the case of WWNSS seismograms it was found that the formula yielded a response quite close to the curve obtained analyzing the calibration pulse (figure 5).

Absorption coefficients used were those obtained by Ben-Menahem (1965) (figure 8). This factor is extremely important when equalizing waves that have traveled over a long distance due to the factor $e^{\gamma(\omega)\Delta}$.

The resulting displacement spectra were then plotted as a function of azimuthal angle around the source. For Rayleigh waves we used the vertical component; the equalized spectra were plotted directly. For Love waves it was necessary to add the two horizontal components vectorially or correct for the angle of incidence before plotting. The angles between north and the geodesic connecting the epicenter and the station at the source (azimuth) and at the station (back azimuth) were computed and listed in Table IV.

A separate program calculated and plotted the theoretical radiation pattern as formulated by Ben-Menahem and Harkrider by assuming a singlet, a couple or double couple force system for various spatial orientations of the motion vector and depth. These theoretical patterns were compared with the result obtained from data analysis to find a pattern that fitted the data best. The set of parameters that generated the best-fitting patterns were taken to be the possible fault parameters of the earthquake. This method is essentially a trial and error one but the variations of the theoretical pattern is a continuous function of the parameters; once the trend is found the range of variations of the parameters could be narrowed down quickly.

Time domain analysis was also attempted; however, the scatter of the data was found to be too severe to yield any significant result.

3. Discussion of Results

The Iran shock of September 1, 1962 was investigated by Ambrasey (1963), Mohjer and Pierce (1963) and Petrescu and Purcaru (1964). Ambrasey and Mohjer and Pierce concentrated their attention on surface features and damages caused by the earthquake while Petrescu and Purcaru did a first motion study.

Results of the first motion study and the present work are listed in Table V. The observed and theoretical radiations are

plotted in figure 9. In figure 10 we show the calculated radiation patterns for a 100 second wave at several depth with different orientations of the motion vector.

The present study reveals that the source is a double couple equivalent to a shear dislocation on a sinistral reverse fault with strike oriented N 80° W, dip 78° , toward southwest, slip angle 63° and at a depth of 11 km. This result as we can see from Table V is very close to the conclusion reached by Petrescu and Purcaru. The depth, however, is different from the depth given by USCGS (20 km) or BCIS (27 ± 9). This may be explained by the fact that what we see in the surface waves is an average feature. Geological observations show (Ambrasey, 1963) that the fault surface reaches up to the surface; it is very difficult to define the "depth" of this earthquake.

Apparent on the data plot is the fact that data scatter to the west of the source is greater than in the opposite direction. This phenomenon is not so obvious for 200 second wave while for shorter period waves both the Rayleigh and Love wave data show some asymmetry. Part of this fact can be explained by moving source theory (Ben-Menahem, 1961). Plotted in figure 12 are frequencies at which the maximums in the spectrum ratio occurs for several stations and the solution of the directivity function

$$D = \left| \begin{array}{cc} \left(\frac{C}{V} + \cos\theta_o\right) & \sin\frac{\pi b}{CT} \left(\frac{C}{V} - \cos\theta_o\right) \\ \left(\frac{C}{V} - \cos\theta_o\right) & \sin\frac{\pi b}{CT} \left(\frac{C}{V} + \cos\theta_o\right) \end{array} \right|$$

where

$C = C(\omega)$ phase velocity

$V =$ rupture velocity

$\theta_o =$ counter-clockwise azimuthal angle measure from strike
direction

$b =$ fault length

$T =$ period.

By fitting the phase velocity with an analytical function and then solve $D = 0$ for frequency we can find the displacement of the maximums in spectrum-ratio as a function of θ_o . In the present case, some of the data points are consistent with the theoretical calculations for a fault length of 100 km and rupture velocity 1.5 km/sec moving toward west. But there are maximums that cannot be explained this way. This fault is probably more complicated than a simple horizontal rupture model can explain.

Reduction of Body Waves

Consider two signals $f_1(t) = f(t)$ and $f_2(t) = \beta f(t)$ and let $g(t)$ be the sum of these two signals after $f_2(t)$ has gone through a "black box" with impulse response $h(t)$:

$$g(t) = f(t) + \beta \int_{-\infty}^{\infty} f(\tau) h(t-\tau) d\tau$$

then, in the frequency domain we have

$$G(\omega) = F(\omega) \{ 1 + \beta H(\omega) \}$$

where $G(\omega)$, $F(\omega)$ and $H(\omega)$ are the complex Fourier transforms of $g(t)$, $f(t)$ and $h(t)$ respectively. Or, more explicitly, we can write

$$G(\omega) = |F(\omega)| e^{i\phi_0(\omega)} \left\{ 1 + \beta |H(\omega)| e^{i\phi_1(\omega)} \right\}$$

where the amplitude and phase factors are separated. Note that $\phi_1(\omega)$ includes the time delay between $f_2(t)$ and $f_1(t)$ after $f_2(t)$ has passed through the "black box". It is evident that the expression in the parenthesis will add a phase shift to $\phi_0(\omega)$ and will impose an amplitude modulation on the original spectrum $|F(\omega)|$. In order to visualize the kind of modulation we encounter, a simpler case will be considered first. Let $\beta |H(\omega)| = a$ and $\phi_1(\omega) = \omega t_0$, the expression can be written as

$$A(\omega) = 1 + a e^{i\omega t_0}$$

The behavior of the amplitude and the phase is plotted in figure 11 for various a 's. We see that if $F(\omega)$ is a slowly varying function of ω , from the shape of $G(\omega)$ we may obtain t_0 , and conversely, if we know t_0 , we may recover $F(\omega)$ from $G(\omega)$.

Now to be more specific, we refer to $f_1(t)$ as P and $f_2(t)$ as pP . Then $h(t)$ is the impulse reflection response of the crust above the source, and β is the amplitude ratio at the source between P and the wave that later becomes pP . Owing to the complicated nature of $H(\omega)$ in this case the dips will not be regularly spaced as in the case when we let $\beta|H(\omega)| = a$, neither will the phase variations be as simple. We have calculated

$$1 + \beta|H(\omega)| e^{i\phi(\omega)}$$

for the Central U.S. Crust (McEvelly, 1964) and for several β 's (figure 13).

We have neglected the attenuation, geometric dispersion and the crustal effects at the receiver. But since we assume we are dealing with a linear system we can remove these factors beforehand using the equalization procedures described in the section on Basic Formulae.

A practical procedure to obtain the source amplitude spectrum of the P wave when P and pP are superposed is outlined as follows:

- (1) Obtain the spectrum $\tilde{G}(\omega)$ for the $P + pP$ wave.
- (2) Remove from $\tilde{G}(\omega)$ the effects of attenuation, geometric spreading, instruments, and the crustal influence at the

receiver, to obtain $\tilde{G}(\omega)$, namely

$$G(\omega) = \tilde{G}(\omega) / (I(\omega) * S(\omega) * T(\omega))$$

where

$I(\omega)$ = Instrument frequency response

$T(\omega)$ = Crustal transmission response at the receiver

and

$$S(\omega) = r_0^{-1} e^{-f\gamma(\omega, \Delta)} d\Delta \left| \frac{\sin i_s}{\sin \Delta \cos i_0} \right| \left| \frac{di_s}{d\Delta} \right|$$

The integral $e^{-f\gamma(\omega, \Delta)} d\Delta$ in this work was given by Teng (1965), and is described in Appendix I.

Notice that we have treated P and pP as though they have the same i_0 , i_h , $\left| \frac{di_s}{d\Delta} \right|$, and same propagation path.

This is not strictly true, but for shallow shocks it is a good approximation.

- (3) Determine the crustal structure above the source, and compute

$$A(\omega) = 1 + \beta |H(\omega)| e^{i\phi, (\omega)}$$

For various β 's, and also adjust the thickness of the crust such that the relative minima of $G(\omega)$ coincides with those of $A(\omega)$.

(4) Finally, divide $|G(\omega)|$ by $|A(\omega)|$ to obtain $|F(\omega)|$

$$|F(\omega)| = \frac{|G(\omega)|}{|A(\omega)|}$$

In figure 14 we have presented two examples of reduced spectra. The equalized spectra are the Fourier spectra of the P waves recorded at STU and BAG by long-period WWNSS systems compensated for absorption and geometric spreading. The transfer functions were calculated by using Tedzhan structure (Godin et al, 1961) at the source and the Southern Germany and the Oceanic structure (Steinhart and Myer, 1961) for STU and BAG respectively. We have also processed the P wave at ALQ in the same way. Efforts were made to make the shapes of the "source spectra" to be similar. The same technique was applied to the S wave. The resultant spectra were less satisfactory than those for the P waves.

The procedure described here is only an approximate way to eliminate a possible factor of 2 in the average amplitude. The total energy computed after this will be improved by less than an order of magnitude.

Integration for Energy

Based on 8 ^{0.}spectrums for surface waves (Rayleigh and Love waves), 3 for P waves and 2 for S waves the results listed in Table VI were obtained. Also listed in the table are the source parameters and the energy calculated by using Gutenberg-Richter's formula.

The following observations were evident from the Table:

- 1) The sum of P and S energies is an order of magnitude higher than that predicted by Gutenberg and Richter's formula for the total energy of the earthquake.
- 2) The surface wave energy in the band specified is 3 orders of magnitude smaller than body wave energy.
- 3) P wave energy is approximately 1/30 of the S wave energy.

The body wave to surface wave energy ratio is much higher than that obtained by other authors e.g., (Bath, 1958); the magnitude of the surface wave energies itself is comparable, but their body wave energy estimates were much lower (see the discussion in a later section). The ratio we obtained is quite close to that predicted by our simple half-space theory.

The partitioning of energy between P and S is of special interest to us because it is pertinent to our discussion of the cause of earthquakes whether phase change or material failure or whether tectonic strain release is involved. The partitioning seems to conform to our theoretical calculations. This correspondence could be, however, fortuitous; our source model may not be the correct one.

Energy Content of P and S Waves for an
Intermediate and a Deep Earthquake

Introduction

In this section we shall estimate the energy content of the P and S waves from an intermediate and a deep earthquake. It is evident from the seismograms from earthquakes at depth that the source excites both fundamental and higher modes surface waves, but, based on experimental data and theoretical calculations (Harkrider and Anderson, 1966) that we mentioned in the last section, we can expect the energy involved to be not very significant. Besides, the identification of higher modes is not beyond doubt.

It will be shown in the following section that for an intermediate earthquake the radiation pattern of the P wave obtained by frequency-domain analyses of the P pulse on the records conforms quite well to the theoretical pattern calculated from theory (Ben-Menahem et al, 1965) using the fault elements derived from the first motion study as the input parameters. The same conclusion was reached by Teng and Ben-Menahem (1965). It is our contention that when the source mechanisms of earthquakes are determined by first motion studies, we can calculate the energy in P and S for these earthquakes from seismogram records at one station.

In the present section we shall work out in detail the first motion and the radiation pattern of P wave and derive therefrom

the source mechanism of an intermediate earthquake in the Tonga region. We will integrate the seismogram, after proper equalization, to get the energy content of P and S waves. We will also obtain the energy content of an earthquake in Banda Sea, the radiation pattern and source mechanism of which have been published by Teng and Ben-Menahem (1965).

First Motion Study of July 4th, 1963, Tonga Earthquake

The principles regarding the first motion studies of earthquakes have been propounded and summarized by many authors (see, for example, Honda, 1956; Scheidegger, 1957; Hodgson and Stevens, 1964). In general, the physics involved is the same among the different schools, the main differences are the projections they used to plot the data and the drawing of fault-planes. Here we shall follow a procedure summarized by Ritzema (1957):

1. Determine the initial motion data of P and S at stations distributed throughout the world.
2. Determine the azimuths and the distances of the stations from the source, and the azimuth of the source from the station. They can be calculated by using Rudoie's formula (Bomford, 1952).
3. Determine the angle i_h at which the wave left the source. A set of (i_h, Δ) curves for various depths by Ritzema (Ritzema, 1957) can be used for the purpose.

4. Plot the compressions and dilatations of P in a polar diagram in the appropriate azimuth and at a distance of $\tan(i_h/2)$ from the center.
5. Separate the compressions and dilatations by two nodal lines that are perpendicular to each other and follow the course of meridional lines of the Wulff net.
6. Plot the S wave vector.
7. Determine the elements of displacement vectors using the Wulff net.

The advantage of this method is that the fault plane, auxiliary plane and the displacement vector can easily be visualized on a stereographic projection. There is some difficulty in choosing between the two orthogonal planes for the fault plane. If the S pattern follows that of a single couple pattern, this problem can be solved; in our case the S vector pattern seems to result from a double couple source, hence such resolution was impossible. We have to rely on the information as to the prevailing force system in the region concerned, and make the final decision from amplitude data.

The Tonga earthquake of July 4, 1963 had a magnitude of $6\frac{1}{2}$ and a depth of 158 km. The records we used are the matched three component long-period records from the WWNSS stations. The stations we used, the first motions (+ or -) of P the direction of S vector, as well as other data pertinent to the earthquake is presented in Table VII. A few first motion readings were taken from station reports (for non-WWNSS stations), these are marked with asteriks in the table.

The first motions of P are plotted in figure 15 . We can easily draw one meridional line separating the dilatations from the compressions, the other meridional line was fixed by noticing (1) it has to be perpendicular to the other one, (2) the amplitude of P at SPA is vanishingly small, (3) the amplitude at the New Zealand stations are all small. (2) and (3) suggest the proximity of those stations to one of the nodal lines of P. With this information we draw the other nodal line, which was found to be the fault-plane.

We have plotted the S wave vectors in the same figure. The pattern of S wave suggests a double couple source.

Of the two nodal planes we obtained one is parallel to the trend of the Tonga island arc, the other perpendicular to it. Based on the amplitude data of the next section we have chosen the former to be the fault plane. It strikes at N26E, with $\delta = 68^{\circ}$ and $\lambda = 212^{\circ}$.

Radiation Pattern of P Wave

1) Introduction

The method of obtaining the body wave radiation pattern has been discussed by Ben-Menahem et al (1965) and applied to a study of a deep earthquake in the Banda Sea by Teng and Ben-Menahem (1965). Here we shall proceed to describe our data analysis.

2) Data and Data Analysis

The data we used in this investigation were exclusively long-period records from the WWNSS stations. The station abbreviations, epicentral distances, azimuths, and back azimuths are listed in Table VII.

Each P wave trace was digitized from the paper record at irregular intervals, with the intention that linear interpolation will later be used to obtain values at 1 second intervals. The interference of PcP on some traces requires tapering at the end to minimize the effect. The traces were plotted and checked and detrended (degree 1) before we subjected them to Fourier analysis within the frequency window 0. - 0.2. The Fourier spectra are punched on cards for further processing.

3) Equalization of the Spectrum to the "Focal Sphere"

The equalization process can be separated into three steps:

- a) Remove the effects of the crust and the free surface at the receiver. This is done by using

the Haskell matrix method (Haskell, 1962) to calculate the transmission coefficients of a stack of solid layers at the spectral frequencies of our data, and divide the spectrum by the coefficients (for the amplitudes only). The choice of a crustal structure under the receiver presents some problem since we very seldom have the information right under the station. As an approximation we have used published crustal structures in regions adjacent to the place in question. It was pointed out by Ben-Menahem et al (1965) that for periods longer than 10 seconds the influence of the crustal structure is not significantly different from one model to another. We used several continental structures published in a work by Steinhart and Meyer (1961) for continental stations and an average oceanic structure (Raitt, 1963) for oceanic stations.

- b) Remove the effect of geometric spreading along a curved ray.

This is done by multiplying the spectrum by the frequency independent factor

$$r_o \left| \frac{d\Delta}{di_s} \right|^{\frac{1}{2}} \left| \frac{\sin\Delta \cos i_o}{\sin i_s} \right|^{\frac{1}{2}}$$

As before $\frac{d\Delta}{di_s}$, i_o , i_s are obtained from curves published by Ritzema (1958) for a depth of 0.03 Radius of the Earth.

4) Compensate for the anelastic loss of energy.

This is a frequency dependent compensation: the spectrum is multiplied by

$$e^{\int \gamma(\omega, \Delta) d\Delta}$$

$$= e^{\int_c \frac{ds}{Q(r) V(r)}}$$

where r is the distance from the center of the Earth to the point on the ray, Q is the intrinsic loss factor of the material, V the velocity and c is the ray path. (Appendix I)

The above three operations convert the observed spectrum at a station to a point on the focal sphere, namely

$$\tilde{S}(\theta_o, \phi_o, \omega) = r_o F(\omega) T(\omega) I(\omega) \left| \frac{d\Delta}{di_s} \right|^{\frac{1}{2}} \left| \frac{\sin\Delta \cos i_o}{\sin i_s} \right|^{\frac{1}{2}}$$

$$e^{\int \gamma(\omega, \Delta) d\Delta}$$

as prescribed in the section on Basic Formulae.

5) Determination of Source Mechanism

The equalized spectrums are then plotted as a two dimensional curve with amplitudes as ordinates and along the abscissa stations are arranged in the order of increasing azimuthal angle (figure 16). The actual radiation pattern is a three dimensional one; we have suppressed in dimension.

We then calculated the theoretical P wave radiation pattern using the δ , λ and strike direction obtained from the first motion study as trial values, the δ , λ and strike direction are then varied to find a best fit to the observed pattern (figure 16). The answers we arrived at are $\delta = 63^\circ$ $\lambda = 208^\circ$ and strikes at $N24^\circ E$. This is indeed very close to the result of first motion study. We have also shown the corresponding P traces at those stations we used in the radiation pattern plot. (Figure 16).

Integration for Energy

As in the case of a shallow shock, once the radiation pattern has been determined the integration for energy is relatively easy. Theoretically, we should be able to obtain the energy in P or S using one three-component set of seismograms. However, owing to the noise problem, there will be some fluctuations in the spectrum that could cause the frequency integral to vary from one station to another even after the correction for radiation pattern is made. A better approach to this problem is to choose as many spectra as we can, preferably with stations located at the maxima of the radiation pattern as we have done in the case of surface waves in the previous section.

The results of integration for the P wave based on 7 stations and S wave based on 2 stations are listed in Table VIII.

It is seen again that the energy we obtained is considerably higher than that predicted by applying Gutenberg and Richter's formula. The P to S ratio in this case, however, is small compared either to the theoretical results we obtained or to that of Haskell's. We shall discuss this fact in a later section.

Banda Sea Deep Earthquake of 21 March 1964

The first motion study and the radiation pattern of this earthquake had been published by Teng and Ben-Menahem (1965). They had shown also that the fault elements derived from the first motion

study can be used as input parameters to the theoretical radiation pattern given by Ben-Menahem et al (1965) to predict the spatial variation of the P wave amplitudes. The techniques used in Teng and Ben-Menahem's work are essentially the same as those we employed to investigate the Tonga Earthquake.

For the energy integration we have used the P spectra from SEO, BAG, HKC, MUN, TAV, RAB and COL and the S wave spectra from SEO and AFI. The results of integration together with other pertinent data are presented in Table IX.

Calculation of Energy for Earthquakes with Known

Fault Mechanisms

In the previous section we have shown that at least for intermediate and deep earthquakes the amplitude radiation pattern can be predicted by theoretical formulation (Ben-Menahem et al, 1965) with fault elements obtained from first motion studies. We will now use seismograms from one single station (Pasadena 30-90 records) to calculate P and/or S energies from several intermediate and deep earthquakes for which the source mechanisms have been derived from first motion studies by Hodgson and Metzger (1961) and Hodgson and Wickens (1965).

Listed in Table X are the earthquakes we used together with the fault elements, the Richter magnitude and the energies obtained by integrating the Pasadena records.

The wave forms are traced out in figure 17.

Although these earthquakes all have magnitudes around 7, the energy we obtained for them have values that are quite different; some earthquakes with smaller magnitudes have higher energies and vice versa. For example, the earthquake (1) has a larger magnitude than earthquake (6), but the final energy is slightly lower. Indeed the Pasadena record shows a very large P wave for the former and a much smaller one for the latter, but the combined effect of the source being located near the commencement of the high Q zone and that of Pasadena being near to the maximum of a radiation pattern lobe in the

case of earthquake (1) and the opposite for earthquake (6), the energy situation is reversed. The SV wave of earthquake (1) and the SH wave of earthquake (6) yield similar energy in spite of the fact that the SV wave of earthquake (1) has a shorter dominant period than the SH of earthquake (6); the distance and the location of the hypocenter of the latter more than compensated for the difference in period.

From the results presented in Table X it is again evident that the S wave energy is at least an order of magnitude higher than the P wave energy.

This method of determining the energy has two apparent shortcomings:

- a) Uncertainties in source mechanism determination can cause the energy to be overestimated or underestimated. In the Dominion Observatory reports the number of inconsistent polarities is given for each earthquake; the number is quite high sometimes. The inconsistency could be due to instrument polarity uncertainties, but could also be due to the error in choosing the fault-plane solution.

One way to improve the result with the least amount of labor would be to acquire seismograms from WWNSS stations located near to the calculated maxima of the radiation pattern; use these seismograms to check the accuracy of the fault-plane solution and improve the accuracy of the frequency integration.

- b) Each station can only determine the energies of earthquakes in certain regions due to the presence of the shadow zone for the body waves. This can be remedied, of course, by using more stations.

It is hoped that further work in this direction will be done to see whether this method would give a better result.

Free Oscillation Energy

As we mentioned before we can integrate the energy of earthquakes only within a certain frequency band owing to the inhomogeneous and absorbing nature of the Earth at the high frequencies and limited response of the conventional instruments at both ends of the spectrum. However, using special instruments like Benioff strain seismometer, gravity meter or other instruments geared to long-period waves, we can at least extend the estimate to free oscillation frequencies for large earthquakes. We will first investigate the theory and practice for obtaining the free-oscillation energy.

The displacement field for a certain mode can be written as

$$\vec{u}_S = \hat{r} U(r) P_\ell^m e^{im\phi} + r V(r) \vec{\nabla} \left[P_\ell^m (\cos\theta) e^{im\phi} \right]$$

for spherical modes, and for toroidal modes we have

$$\vec{u}_T = -W(r) \vec{r} \times \vec{\nabla} \left[P_\ell^m (\cos\theta) e^{im\phi} \right]$$

Thereby we have

$$\begin{aligned} \vec{u}_S = r U(r) P_\ell^m (\cos\theta) e^{im\phi} + \dot{V}(r) \left[\hat{\theta} P_\ell^m (\cos\theta) \right. \\ \left. + \frac{im\phi}{\sin\theta} P_\ell^m (\cos\theta) \right] e^{im\phi} \end{aligned}$$

The strains in spherical coordinates are

$$e_{rr} = \frac{\partial u_r}{\partial r} = U'(r) P_\ell^m(\cos\theta) e^{im\phi}$$

$$e_{\theta\theta} = \frac{1}{r} \frac{\partial u_\theta}{\partial \theta} + \frac{u_r}{r} = \frac{1}{r} \left[V(r) P_\ell^m(\cos\theta)'' + U(r) P_\ell^m(\cos\theta) \right]$$

$$e^{im\phi}$$

$$e_{\phi\phi} = \frac{1}{r} \left[V(r) P_\ell^m \cot\theta - \frac{m^2}{\sin^2\theta} V(r) P_\ell^m(\cos\theta) + U(r) P_\ell^m(\cos\theta) \right]$$

$$e^{im\phi}$$

$$e_{r\theta} = \left[\frac{1}{r} V(r) P_\ell^m(\cos\theta)' + \left(V'(r) - \frac{V(r)}{r} \right) P_\ell^m(\cos\theta)' \right] e^{im\phi}$$

$$e_{r\phi} = \left[\frac{im}{r \sin\theta} V(r) P_\ell^m(\cos\theta) + \left(V'(r) - \frac{V(r)}{r} \right) P_\ell^m(\cos\theta) \frac{im}{\sin\theta} \right] e^{im\phi}$$

$$e_{\theta\phi} = \frac{2 im V(r)}{r \sin\theta} \left[P_\ell^m(\cos\theta)' - \cot\theta P_\ell^m(\cos\theta) \right] e^{im\phi}$$

From the expressions for e_{rr} , $e_{\theta\theta}$ and $e_{\phi\phi}$, and the associated

Legendre equation we have

$$\Delta = (e_{rr} + e_{\theta\theta} + e_{\phi\phi}) = \left[U'(r) + \frac{2U(r)}{r} - \frac{\ell(\ell+1)V(r)}{r} \right] P_\ell^m(\cos\theta) e^{im\phi}$$

For the torsional modes, we have

$$\vec{u}_T = w(r) e^{im\phi} \left[\frac{\hat{\theta} im}{\sin\theta} P_\ell^m(\cos\theta) - \hat{\phi} P_\ell^m(\cos\theta)' \right]$$

The strains are

$$e_{\theta\theta} = -e_{\phi\phi} = \left\{ \frac{im W(r)}{\sin\theta} \left[(1-m) P_\ell^m(\cos\theta) \cot\theta + P_\ell^{m+1}(\cos\theta) \right] \right\} e^{im\phi}$$

$$e_{\phi\phi} = -W(r) \left[\frac{m^2}{\sin^2\theta} P_\ell^m(\cos\theta) - P_\ell^m(\cos\theta)' \cot\theta - P_\ell^m(\cos\theta)'' \right] e^{im\phi}$$

$$= -W(r) \left[2 P_\ell^m(\cos\theta)'' = \ell(\ell+1) P_\ell^m(\cos\theta) \right] e^{im\phi}$$

$$e_{r\theta} = \left(w'(r) - \frac{W(r)}{r} \right) \frac{im e^{im\phi}}{\sin\theta} P_\ell^m(\cos\theta)$$

$$e_{r\phi} = - \left(W'(r) - \frac{W(r)}{r} \right) P_\ell^m(\cos\theta)' e^{im\phi}$$

In These expressions

P_ℓ^m = associated Legendre Polynomial

$\hat{r}, \hat{u}, \hat{\theta}$ = unit vectors in the direction of r, θ and ϕ

$e_{rr} \dots$ = strain components

ℓ = polar order number

m = azimuthal order number

The corresponding stresses for both spheroidal and torsional modes can be written as

$$\tau_{ij} = \lambda \Delta \delta_{ij} + 2\mu e_{ij}$$

where $\delta_{ij} = 1$ for $i = j$ and $\delta_{ij} = 0$ for $i \neq j$.

The potential energy can then be calculated by the formula

$$E = \frac{1}{2} \iiint_V \tau_{ij} e_{ij} dv$$

where V is the total volume of the earth.

The results are

$$\begin{aligned} \text{P.E.} = & \frac{\pi/\epsilon_m}{(2\ell+1)} \frac{(\ell+m)!}{(\ell-m)!} \int_0^r \left\{ (\lambda+2\mu) \left(r \frac{\partial u_\ell}{\partial r} + 2 U_\ell - \ell(\ell+1) V_\ell \right)^2 \right. \\ & + \mu \ell(\ell+1) \left(r \frac{\partial V_\ell}{\partial r} - V_\ell + \frac{u}{V_\ell} \right)^2 - 4\mu \frac{u}{V_\ell}^2 - 2 \ell(\ell+1) \mu V_\ell^2 \\ & \left. + 4 \ell(\ell+1) V_\ell \left(\mu \frac{u}{V_\ell} + \mu r \frac{\partial U_\ell}{\partial r} \right) - 8 \mu r V_\ell \frac{\partial U_\ell}{\partial r} \right\} dr \end{aligned}$$

For the spheroidal modes and

$$\begin{aligned}
 \text{P.E.} = & \frac{\pi/\epsilon_m (l+m)! l(l+1)}{(2l+1) (l-m)!} \int_0^r \mu(r) \left\{ \left(\frac{\partial w_l(r)}{\partial r} - \frac{w_l(r)}{r} \right)^2 \right. \\
 & \left. + (l^2 + l - 2) \frac{w_l^2(r)}{r^2} \right\} r^2 dr
 \end{aligned}$$

For the torsional modes (Kovach and Anderson, 1966). These quantities have been calculated by Kovach and Anderson for $m = 0$ using Gutenberg-Bullen A earth model.

Presently, data from three kinds of instruments are used for analyzing the free oscillations of the Earth. Namely, the strain seismometer, the pendulum seismometer and gravimeter. From an energy-measuring point of view three horizontal strain seismometers would suffice to determine the energy in both the spheroidal and torsional modes. In case of pendulum seismometer we need all three components. With a single gravity meter it is impossible to obtain the total energy; it must be coupled with other instruments for the purpose, since the radial gravitational force can be written as

$$\rho \frac{\partial \psi_0}{\partial r} \Delta - \rho \frac{\partial}{\partial r} \left(\psi + U(r) \frac{\partial \psi_0}{\partial r} \right)$$

where, Δ and $U(r)$ have the same meaning as above and ψ is the perturbed gravity potential, which in its unperturbed state is Ψ_0 , ρ is the density. There are three unknowns in this expression, namely $U(r)$, $V(r)$ and $\psi(r)$; they can't be solved by using gravimeter data alone.

When using strain measurements we have to solve $U(r)$, $V(r)$ and $W(r)$ from a combination of $e_{\theta\theta}$, $e_{\phi\phi}$ and $e_{\theta\phi}$.

In general

$$e_{NS} = e_{\theta\theta} \cos^2 \epsilon + e_{\theta\phi} \cos \epsilon \sin \epsilon + e_{\phi\phi} \sin^2 \epsilon$$

and

$$e_{EW} = e_{\theta\theta} \sin^2 \epsilon - e_{\theta\phi} \cos \epsilon \sin \epsilon + e_{\phi\phi} \cos^2 \epsilon$$

where ϵ is the angle between the NS strain instrument and the great circle through the source and the station. Before we can solve for U , V , and W we have to have some information of m , the azimuthal order number. This number is determined by the source radiation pattern. If the recording stations are very densely populated around the source a spherical harmonic analysis can actually yield m . Lacking such information we have to obtain the source parameter from other informations, calculate the surface wave radiation pattern and apply it to this case. Since the wave lengths under consideration are very long compared either to the source dimension or to the depth of the source, the half-space point source solutions of Haskell

(1963) can be applied here as an approximation. The spheroidal oscillations can be taken as very long period Rayleigh waves and the toroidal oscillations as very long period Love waves (guided SH wave) we can use the Rayleigh wave pattern and the SH wave pattern respectively for these two modes of oscillations. Those radiation patterns are linear combinations of $\cos m\phi$ and $\sin m\phi$'s, where $m \leq 2$.

Hence, as can be seen from the expressions for $e_{\theta\theta}$, $e_{\phi\phi}$ and $e_{\theta\phi}$, given θ_0 the polar angle of the station with the source located at the pole, and ϕ_0 the azimuthal angle counted from the direction of the strike of the fault, we can solve for $V(a)$, $U(a)$ and $W(a)$, where a is the radius of the Earth, when the experimental values of the strains are supplied.

Haskell (1963) gave the radiation pattern for horizontal component Rayleigh waves in an homogeneous half-space as follows:

$$\begin{aligned} \chi(\phi, \omega, r, h) = & 2 A(k, r, h) e^{-\pi i/4} \left[3 i f_3 n_3 \left\{ (1 - 2 C_R^2/3\alpha^2) D \right. \right. \\ & - (\gamma - 1)/\gamma \left. \right\} + 2 (v_\alpha/k) (D - 1) \left\{ (f_1 n_3 + f_3 n_1) \cos\phi \right. \\ & \left. \left. + (f_2 n_3 + f_3 n_2) \sin\phi \right\} \right. \\ & \left. - i \left\{ D - (\gamma - 1)/\gamma \right\} \left\{ (f_1 n_1 - f_2 n_2) \cos 2\phi + (f_1 n_2 + f_2 n_1) \sin 2\phi \right\} \right] \end{aligned}$$

where

$$A(K, r, h) = \left\{ k^2 \gamma v_\beta / 4 \rho f^1(k) \right\} \left\{ 2 / \pi k r \right\}^{1/2} e^{-ikr - hv_\beta}$$

$$D = e^{-h(\nu_\alpha - \nu_\beta)}$$

$$\nu_\alpha^2 = k^2 - (\omega/\alpha)^2$$

$$\nu_\beta^2 = k^2 - (\omega/\beta)^2$$

$C_R = \omega/k =$ phase velocity of Rayleigh Wave

$n_i =$ the component of the unit vector normal to the fault plane.

$f_i =$ the component of the unit vector in the direction of displacement.

(Table XI)

$$\gamma = 2(\beta k/\omega)^2$$

Values of f_i in terms of the dip angle δ of the fault plane are listed in Table XI. It is to be noted that we can obtain the solutions for fault with arbitrary slip-angles, i.e.

$$\lambda \neq 0^\circ \text{ or } 180^\circ \text{ (strike-slip) and } \lambda \neq 90^\circ \text{ or } 270^\circ \text{ (dip-slip)}$$

by combining properly the solutions for strike- and dip-slip fault.

For our purpose we shall put Haskell's solution in complex-form:

$$\chi(\phi, \omega, r, h) = 2 A(k, r, h) e^{-\pi i/4} \left[B_1 i + \text{Re} \left\{ B_2 e^{i(\phi - \theta')} \right. \right. \\ \left. \left. i \text{Re} \left\{ B_3 e^{i(2\phi - 2\theta'')} \right\} \right\} \right]$$

where

$$B_1 = 3 f_3 n_3 \left\{ (1 - 2 C_R^2/3\alpha^2) D - (\gamma - 1)/\gamma \right\}$$

$$B_2 = 2(v_2/k) (D - 1) \sqrt{(f_1 n_3 + f_3 n_1)^2 + (f_2 n_3 + f_3 n_2)^2}$$

$$\theta' = \tan^{-1} \left(\frac{f_1 n_1 + f_2 n_1}{f_1 n_1 - f_2 n_2} \right)$$

$$B_3 = \left\{ D - (\gamma - 1)/\gamma \right\} \sqrt{(f_1 n_1 - f_2 n_2)^2 + (f_1 n_2 + f_2 n_1)^2}$$

$$\theta'' = \tan^{-1} \left(\frac{f_1 n_2 + f_2 n_1}{f_1 n_1 - f_2 n_2} \right)$$

Referring now to the formulas for the displacement as well as the strain expressions, we have defined the weighting factors for the m dependent part. Namely

azimuthal order No.	weighting factor
m = 0	iB ₁
m = 1	B ₂ e ^{-iθ'}
m = 2	iB ₃ e ^{-iθ''}

For torsional modes, as a first approximation, we can use the radiation pattern of SH in an infinite space (Ben-Menahem et al, 1965). For i_h large (beyond critical angle) the source can be taken as $m = 2$.

Free Oscillation Energy of Alaskan Earthquake

The great Alaskan Earthquake of March 28, 1964, excited very long waves that were recorded at Isabella on strain seismometer (Smith, 1966) and ultra-long period seismograph at Berkeley (Nowroozi, 1965) among others. Using this data we are able to determine the energy of fundamental mode oscillations for orders from 2 to 15. The source mechanism of this earthquake has been worked out by Toksöz from long period Rayleigh and Love waves (Toksöz, M. N., personal communication, January 15, 1966). The results are:

Strike	N 41° E
Dip 65° ± 5°	S 49° E
Slip 300°	
Force system	double couple

These parameters will be used to determine the m 's and the weights.

1. Calculation of $U_{\ell}(a)$ from Isabella strain data.

The data was in the form of power spectrum densities (Smith, 1966); these can be reduced to strain² by multiplying to them the band width. The squareroot of the reduced quantity is the absolute value of the strain. In order to use the displacement-energy table calculated by Kovach

and Anderson (1966 ; see Table XII), we must solve a system of simultaneous absolute value equations of the form ($\mathcal{E} \cong 0$; $e_{NS} \cong e_{\theta\theta}$, $e_{EW} \cong e_{\phi\phi}$)

$$|a' U_\ell + b' V_\ell| = |e_{\theta\theta}|$$

$$|c' U_\ell + d' V_\ell| = |e_{\phi\phi}|$$

where

$$a' = \sum_{m=0}^2 A_m P_\ell^m(\cos\theta_0) e^{im\phi_0}$$

$$b' = C \sum_{m=0}^2 A_m P_\ell^m(\cos\theta_0)'' e^{im\phi_0}$$

$$c' = a'$$

$$d' = C \sum_{m=0}^2 A_m \left(P_\ell^m \cos\theta_0 - \frac{m^2}{\sin^2\theta_0} P_\ell^m(\cos\theta_0) \right) e^{im\phi_0}$$

where

$$A_0 = i B_1$$

$$A_1 = B_2 e^{-i\theta'}$$

$$A_2 = i B_3 e^{-i\theta''}$$

$$C = -i k (\gamma - 1) / \gamma \nu_\alpha$$

B_i 's are functions of source parameters and frequency, the four coefficients a', b', c', and d' are therefore also functions of the same quantities plus ℓ and m. We have solved the system of two simultaneous absolute value equations numerically on the computer for orders 2 to 6. Although we also have the higher order strain data, but because the values of $\frac{d}{d\theta} P_\ell^m(\cos\theta)$ vary very fast for large ℓ , the effect of assumed radiation pattern as well as epicenter location error can cause great uncertainties in the values of $U_\ell(a)$ we obtain. It is advisable to use vertical displacement data for large ℓ since only P_ℓ^m are involved in reducing the data to $U_\ell(a)$.

For the torsional modes, it is relatively easy to solve for $W(a)$. Using the relation $e_{\theta\theta} = -e_{\phi\phi}$ for torsional modes, we have

$$|W_\ell(a)| = \frac{\sum_{m=0}^2 \frac{mA_m}{\sin\theta} \left[(1-m) P_\ell^m(\cos\theta_o) \cot\theta_o + P_\ell^{m+1}(\cos\theta_o) \right] |e^{im\theta_o}|}{|e_{\theta\theta}|}$$

After $U_\ell(a)$ or $W_\ell(a)$ is obtained we correct it for attenuation by using published Q values (Benioff et al, 1961; Alsop et al, 1961) the measured value $U_\ell(a)$ can

be expressed as

$$U_{\ell}(a) = - \frac{QT}{\pi\tau} \left(e^{-\frac{\tau\pi}{QT}} - 1 \right) A_{\ell 0}$$

where T = period, τ = record length and $A_{\ell 0}$ the original amplitude. (Kovach and Anderson, 1966); it is easy to obtain $A_{\ell 0}$ from this expression.

2. Calculation of $U(a)$ from Berkeley Pendulum data.

The displacement field can be written as

$$\vec{u}_r = \vec{a}_r \sum_{\ell=0}^m \sum_{m=-\ell}^m P_{\ell}^m(\cos\theta) e^{im\phi} {}_n U_{\ell}(r)$$

$$\vec{u}_{\theta} = \vec{a}_{\theta} \sum_{\ell=0}^m \sum_{m=-\ell}^m \frac{dP_{\ell}^m}{d\theta} e^{im\phi} {}_n V_{\ell}(r)$$

$$\vec{u}_{\phi} = \vec{a}_{\phi} \sum_{\ell=0}^m \sum_{m=-\ell}^m \frac{i m P_{\ell}^m(\cos\theta)}{\sin\theta} {}_n V_{\ell}(r)$$

for spheroidal modes.

When we use one station to find $U_{\ell}(r)$ we have to normalize it by dividing the amplitude with

$$\sum_{m=0}^2 A_m P_{\ell}^m(\cos\theta_0) e^{im\phi_0}$$

θ_0 and ϕ_0 are the coordinates of the station with the source located at the pole and ϕ_0 counted from the direction of the fault. A_m has the same values as before. After we have obtained $U_\ell(a)$ we can use the same procedure as in the case of strain data to obtain $A_{\ell 0}$. $A_{\ell 0}$ can now be used in connection with displacement energy tables to calculate the energy in each order. The total energy for each order will be a weighted sum of energies for $m = 0, 1, 2$ (Table XII). The weights are the squares of the ones we used for amplitudes. Namely

$$\bar{E}_\ell = A_0^2 E_0 + A_1^2 E_1 + A_2^2 E_2$$

The energy in order ℓ will then be

$$E_\ell = A_{\ell 0} * \bar{E}_\ell$$

The results for the spheroidal oscillations are presented in Table XIII.

The sum of the fundamental mode energy from order 2 to 15 is of the order 10^{23} ergs. Alaskan earthquake has a magnitude of 8.3 (± 0.3); using an energy-magnitude formula of the form

$$\log E = 11.8 + 1.5 M$$

will give a total energy of 3.3×10^{24} ergs. But, as we asserted before that the earthquake generated a very

complicated P wave, the actual energy could be higher than that calculated from the energy-magnitude relation, assuming the relation to be correct. In other words, it is possible that the energy in the low order spheroidal oscillations is at least one to two orders of magnitude smaller than in the body waves.

Energy Estimates of Jeffreys, Gutenberg and Richter and Others

The results presented in the previous sections all indicated that the energies we obtained for earthquakes around magnitude 7 are at least one order of magnitude higher than that calculated from Gutenberg-Richter energy-magnitude formula.

Given seismograms recorded all around the source, the density of the material and the velocities of the source, we can obtain the energy for each phase, P, S, Rayleigh or Love wave, by (1) equalizing the spectra of seismic waves back to the source (2) obtain the radiation pattern from the data or from calculations using source mechanism, and (3) integrate the square of velocity spectra. This is essentially what we have done. We shall now outline the methods used by other authors, so that we can have some idea of where the discrepancy might come in.

1. Jeffreys (1923) modified an earlier (Galitzin, 1915) method to estimate the energy of the Pamir landslide of 1911, February 18. The formula he used was

$$E = 4\pi^3 \Delta^2 \rho e^{\gamma\Delta} \int v \frac{a_Z^2 + a_{EW}^2 + a_{NS}^2}{T} dt$$

for body waves, where the definition of Δ , ρ , γ , v are the same as elsewhere in the present work and a 's are the amplitudes on the three components, T is the period of the "sine wave". This formula was essentially what Galitzin

used; however, Galitzin used this same formula indiscriminately to all the waves on the seismogram, body waves as well as surface waves, while Jeffreys assumed all the "long waves" are Rayleigh waves and employing the following formula for energy

$$E = 8\pi^3 \rho R \sin\Delta \int \frac{a^2 HV}{T^2} dt$$

where, in addition to the factors we have already encountered we have $H = 7.061f$, $V =$ Rayleigh wave velocity, and a here denotes the horizontal component of the ground motion. H is actually a conversion factor for the half-space Rayleigh wave, such that given the amplitude on horizontal component, the energy can be evaluated by the formula above.

2. Gutenberg and Richter's approach to energy calculations consists mainly in the establishment of a functional relation between a parameter measurable on the seismogram and the independently assessed energy of the earthquake. We shall therefore discuss two problems pertinent to this approach:

- (a) Is it possible to obtain, from the three component records of a single station one parameter, such that it completely describes the characteristics of an earthquake.

- (b) What is the significance of the Richter magnitude scale.
- (a) Because of the non-spherical radiation pattern, the amplitude of a single phase P, S, R or G will depend on the position of station with regard to the orientation of the motion vector. It might be suggested that the maximum of P often coincides with the minimum of S and vice versa; the same relation also appears to hold for G and R waves. However, it is clear that the body wave radiation patterns are functions of the form $f(\theta, \phi; \delta, \lambda)$ and fundamental mode surface waves radiation patterns are of the form $g(\phi; \delta, \lambda, h; \omega)$ h being the depth of the source, the other variables have the same meaning as elsewhere in the present work. Therefore, even neglecting the problem of signal-noise ratio, and phase identification, it is not possible to locate a station on the radiation pattern. In other words, it is impossible to determine the source mechanism of an earthquake from a single station. There is some hope that the spectrum of P, S, R or G waves may

indicate the "size" of an earthquake.

Empirically, it is true that large earthquakes do give rise to longer waves; more studies of source time function and areal extent of the earthquake are needed before we can extract one or two parameters from the spectra to determine the "size" of the earthquake.

- (b) The Richter magnitude was devised mainly for the purpose of earthquake statistics studies (Richter, 1963), that is to say, one single determination of the magnitude of an earthquake may not be significant, but, over a period of time, with reports from a few stations around the world, the spatial and temporal distributions of magnitude is a good measure of the seismicity of a region. However, Richter (op. cit.) repeatedly warned that the magnitude may not be definitely a measure of energy, and that, physically, the assumption under which the magnitude scale is constructed, namely, one earthquake differs from another only in a constant multiplying factor applied to all the

displacements, velocities, and accelerations in the elastic waves at any distance from the epicenter, is an unlikely one. Not infrequently, the magnitude estimated by different stations differ by 1 or more, evidently as a consequence of the asymmetric radiation pattern (Gutenberg, 1955). Further complications arise when large earthquakes like the Chilean earthquake of 1960, Alaskan earthquake of 1964 and the Rat Island earthquake of 1965, the body waves are long and complicated, suggesting that for a fault extending for a length of several hundreds of kilometers the motion could consist of several impulses in succession. Underestimation of the magnitude would ensue if only one maximum amplitude of the P wave train was measured. But barring such extreme cases, magnitudes for relatively small or deep earthquakes, for which the wave shapes are relatively simple and similar, may sufficiently define the "size" of the event.

In order to determine the coefficients of a relation between energy and magnitude of the form $\log E = a + b M$

where E is the energy and M the magnitude, we have to evaluate E independently. Gutenberg and Richter (1942) used a simplified version of the formula for kinetic energy:

$$E = 8\pi^3 \rho \left\{ h^2 + 4 r_o (r_o - h) \sin^2 \frac{1}{2} \Delta \right\} \int v A^2 T^{-2} dt$$

(Bullen, 1963). This was derived under the assumption of uniform radiation in all directions, the wave path being a straight line and the waves diminishes as $1/R^2$, R being the straight-line distance, the expression in the parenthesis is the square of the distance. A is the amplitude of the wave, T its dominant period, and V the velocity. In practice, the integration is converted to summation. Gutenberg and Richter (op. cit.) tried to use near epicenter data, i.e., $\Delta \approx 0$. For which

$$E = 8\pi^3 h^2 \int v A^2 T^{-2} dt$$

Further assuming 1) the radiated energy consists of a series of n equal sinusoidal waves of length λ , amplitude A_o and period T_o , 2) acceleration = $4\pi^2 A^2 / T^2 = a$, 3) $n\lambda = vt_o$,

$$E = \frac{1}{4\pi} h^2 v t_o \rho a^2 T_o^2$$

with $v = 3.0$ km/sec, E in ergs, we then have

$$\log E = 14.9 + 2 \log h + \log t_o + 2 \log T_o + 2 \log a_o$$

From this point on the authors used empirical relations between t_o , the duration of the strong shaking, and M , between T_o , the dominant period of the wave, and M , between a_o , the acceleration, and M . h is supposed to be 18 km, the "normal" depth for California shocks. The functional relation arrived at was

$$\log E = 11.3 + 1.8 M.$$

In a subsequent paper (Gutenberg and Richter, 1955) the relation between t_o , T_o , a_o and M are revised, and $\log E$ was related to A_o/T_o and M , the relation was changed to

$$\log E = 9.4 + 2.14 M - 0.054 M^2$$

The method of obtaining the coefficients was more or less the same as used in previous papers.

It is to be noted that the data on which these relations were derived are from local earthquakes, at distances of a few kilometers to 400 km., and the amplitude read was mostly S wave amplitudes for the 1942 formula and a value of $E_S/E_P = 2$ was assumed in the 1956 formula.

The values of total energy obtained by the energy-

magnitude relations seem to be on the low side. This is especially true if one is using USCGS data, which are averages of the magnitude determinations at several stations, and are often lower than the Pasadena, Palisades or Berkeley results.

There are several causes for the apparent discrepancy between the values obtained in the present work and those obtained by using the relations above; some of the factors lead to over-estimation of the value while others lead to underestimation:

- a) Azimuthal dependence of amplitudes, this may cause error in either direction of an order of magnitude or so.
- b) Most of the observations were made on narrow band, short-period instrument recordings; t_0 and a_0 might be underestimated, hence $\log E$.
- c) Frequency dependent attenuation has not been considered; causes underestimation.
- d) The most severe error could be due to the fact that in distances within which Sn or Pn, as the case may be, is the maximum phase. And these conical waves fall off theoretically as inverse distance squared in amplitude (Brekovskikh, 1960). The distance compensation in the energy formula is therefore inadequate.

3. Bath (1955, 1958) used for body waves the full version of the formula

$$E_{P,S} = 8\pi^3 \rho \left\{ h^2 + 4 r_o (r_o - h) \sin^2 \frac{\Delta}{2} \right\} \int v \left(\frac{A}{T} \right) dt$$

where $\rho = 2.78/\text{cm}^3$, $h = 20 \text{ km}$, $r_o = 6370 \text{ km}$, $c = 6.0 \text{ km/sec}$. for P wave and 3.4 km/sec for S wave. And a formula similar to Jeffreys' (1923).

$$E = 4\pi^3 \rho r_o \sin \Delta e^{\gamma \Delta} \int H v (A/T)^2 dt$$

for surface waves, where $\rho = 3.3 \text{ g/cm}^3$, $r_o = 6.37 \times 10^8 \text{ cm}$, $\gamma = 3 \times 10^{-4}/\text{km}$ and $v = 4 \times 10^5 \text{ cm/sec}$. $H = 1.1 vT$ as in Jeffreys'.

As pointed out by Bath (1955), in the body wave energy calculations he had neglected radiation patterns of the source, the attenuation and the crustal effects at the receiver. In addition to these, he also neglected the effects of the curved path; the combination of this factor with the attenuation has been called "diminishing factor" and been calculated for various epicentral distances and frequencies by Teng (1965). It was estimated that at an epicentral distance of 70° , 10 second P wave energy will be attenuated approximately 10 times, and 1 second P wave energy will be attenuated 200 times. S wave will suffer a much more

severe attenuation. These may be the reasons why the total energy and the ratio $E_S/E_P = 1.5$ are low. Bath's (1955) surface wave energy might be slightly higher because of the high attenuation coefficient he used ($3 \times 10^{-4}/\text{km}$), his neglect of radiation pattern, and inclusion of 20 second oceanic Rayleigh wave in some cases. (Appendix IV)

4. Russian seismologists working in the field of earthquake energy are mainly concerned with the evaluation of seismicity in a region. There are several slightly different versions of formulas for estimating the energy, but the one commonly referred to is the TESE (the Tadzhik Combined Seismological Expedition) formula. We will discuss here a work by Aronovich (1963), who used a similar formula and gave a rather detailed treatment of the energy of Crimean earthquakes.

The basic formula used was

$$\overline{E_P}, \overline{S} = 4\pi\rho v_{P,S} \int_0^r \frac{r^n}{R^{n-2}} \dot{U}_{P,S}(t) dt$$

Here r is the hypocentral distance and $U(t)$ is the velocity of P or S. The evaluation is done within an epicentral range of 100-150 km, the direct P and S waves are the principle energy carrier. They are denoted by P and S. n is empirically determined by observing energy density decay with distance. R is the radius of integration, estimated from the duration of S waves.

The formula is otherwise similar to that of the other authors except the exponent n and the "radius of integration" concept. The exponent n was actually measured; if the identification of waves was consistent, the error for geometric spreading correction can be minimized for near 0 shock distances. The factor R^{n-2} does not have any physical significance; it gives the formula the correct dimension.

Energy Budget of Earthquakes

The energy we obtained by integrating seismograms around the source is the far field radiation part of a source which also generates the near field waves (waves diminish more rapidly as a function of distance) as well as other types of energy "generated" by the source. By generation of energy we mean the conversion of energy from one form to another occurring during the earthquake process. In general, the following relation must hold:

$$\begin{aligned} & (\text{Elastically stored energy})_{\text{before}} + (\text{Physico-chemical energy})_{\text{before}} \\ = & (\text{Elastically stored energy})_{\text{after}} + \text{heat energy} \\ & + \text{work done against gravity} + (\text{Physico-chemical energy})_{\text{after}} \\ & + \text{seismic wave energy} \end{aligned}$$

In this relation we are asserting that both physico-chemical processes, often described as phase change, and elastic strain can contribute toward the occurrence of earthquakes. In other words, a physico-chemical process such as phase change can have mechanical effects that precipitate the release of strain in large amounts.

In term of Archambeau's tectonic source theory (Archambeau, 1964), the rupture zone can be created either as a result of the elastic strain being in excess of the "material strength", or as a result of an unstable physico-chemical state caused by localized pressure-temperature conditions.

The problem of energy conversion has been tackled by several authors.

A classical theorem of elasticity asserts that the potential energy of deformation of a body which is in equilibrium under given load is equal to half the work done by the external forces acting through the displacement from the unstressed state to the state of equilibrium. It was pointed out by Fu (1945) that this theorem implies an instantaneous adjustment of the medium to the external force. Under such condition half of the work done by the external force will go into potential energy which is stored in the medium and half of the energy converts to elastic wave energy and heat energy. However, if we load the medium at such a rate that the process is reversible, then all the energy would be stored in the medium as required by the first law of thermodynamics. Thus Fu concluded that when an external force is applied to a medium at some finite speed, the seismic wave energy derived from the applied force would be between zero and a half. This conclusion is applicable to the situation we have in an artificial explosion, say, in an unstrained medium, and equally well to the building-up of strain before an earthquake. For a natural earthquake, where release of energy stored in the medium is taking place instead of external force being applied, the above statement has to be modified.

Kawasumi and Yoshiyama (1935) set out to prove that in case the medium is prestrained the elastic wave energy is the released strain energy of the medium. They solved an infinite-space problem with a

"box-car" initial time function (of pressure) on a circular surface in the medium. When the length of the box is long enough the solution should approach that in a prestressed medium.

Sezawa (1935) made a further investigation into the dependence of the elastic wave energy on the rate at which force is applied. His solution does show that the amount of energy that goes into elastic wave energy increases concomitantly with the rate at which the force is being applied. His argument that release of accumulated strain is equivalent to the application of a negative force is, however, invalid. In the case of released strain the medium is prestressed; this case is not the same as application of a negative force to an unstressed medium.

A complete theoretical treatment of the problem of earthquake is not yet possible, since the exact nature of earthquakes has not been adequately understood. It is quite possible that there are different types of earthquakes and earthquakes; for example, at different depths the mechanism of earthquakes could be entirely different.

A more realistical approach to the problem had been taken by Archambeau (1964), he included in his model a prestressed linear-elastic medium a non-linear source region; the occurrence of earthquake is a stress relaxation process instead of the introduction of a sudden dislocation as in the works of Burridge et al (1964) and Haskell (1964). Such a model could be used to discuss not only the radiated seismic waves, but also potential energy change before

and after the earthquake; if we have a reasonable model for the non-linear zone we may also discuss the non-linear dissipation of energy in the near source region.

Gravity is usually neglected in the theoretical formulation of the problem. The energy involved, however, may not exceed that of seismic waves (Pshenikov, 1965), considering that an upward vertical movement one side of the fault is often accompanied by a downward movement on the other side.

To know the energy budget near the source more experiments have to be conducted in the non-linear region of an earthquake; heat flow measurements, the strong motion seismometry and a detailed triangulation will enable us to learn more about the actual earthquake source.

Conclusion

We have made an attempt to estimate the energy in earthquakes by considering the source as a radiator which generates signals that propagate through a layered earth; we obtain the energy of the radiator from the signals recorded at large distances by compensating for the effects of attenuation, the inhomogeneities of the medium, the response of the recording instruments, and the free surface.

Several conclusions can be drawn from our observations:

- 1) The sum of the energies in P and S for one earthquake in the frequency band specified exceeds the total energy calculated from Gutenberg and Richter's formula.
- 2) The energy in S wave is greater than that in P wave by at least one order of magnitude. The S wave is the main seismic energy carrier for earthquakes.
- 3) Energies in the Rayleigh and Love surface waves are about three orders of magnitude smaller than those in the P and S waves.
- 4) Assuming that the energy calculated from magnitude-energy formula for earthquakes (usually magnitude 8 or higher) that excites lower order free oscillations will be upgraded at least by one order of magnitude (for Alaskan earthquake, it would then be $> 10^{25}$ ergs), the total energy in the spheroidal modes (from order 2 to 15) is two orders less than the "total energy".

- 5) Because of our inability to record the complete signal, our estimates are the lower limits of seismic radiation for each earthquake.
- 6) It is possible to use three component records from a few stations to obtain the energies in P and S wave for intermediate and deep earthquakes whose fault mechanisms are given.

The main uncertainties of our estimates could be due to the uncertainties in our knowledge regarding the attenuation of seismic waves.

In order to obtain a closer estimate of the total energy involved in an earthquake, near field observations of possible non-linear waves, heat flow and strain fields are needed. It is not impossible that the energy involved in an earthquake is considerably higher than heretofore assumed.

References

Alsop, L. E., G. H. Sutton and M. Ewing

- 1956 "Measurement of Q for Very Long Period Free Oscillations,"
J. Geophys. Res., 66: 2911-2916.

Ambrasey, N. N.

- 1963 "The Buyin-Zara (Iran) Earthquake of September 1, 1962,"
A Field Report, Bull. Seismol. Soc. Am., 53: 705.

Anderson, D., and M. N. Toksöz

- 1963 "Surface Waves on a Spherical Earth, 1. Upper Mantle
Structure from Love Waves," J. Geophys. Res., 68: 3483-3499.

Anderson, D. L. and C. B. Archambeau

- 1964 "The Anelasticity of the Earth," J. Geophys. Res., 69:
2071-2084.

Anderson, D. L., and B. Julian

- 1965 "Travel Times, Velocities and Amplitudes of Body Phases",
Presented at Seismol. Soc. Am. 1965 Annual Meeting,
St. Louis, Missouri.

Aronovich, Z.I.

- 1963 "Determining the Energy of Crimean Earthquakes", Izv.
Akad. Nauk SSSR, Ser. Geofiz.: 332-340.

Bath, M.

- 1955 "The Relation Between Magnitude and Energy of Earthquakes",
Trans. Am. Geophys. Union, 36: 861-965.

Bath, M.

- 1958 "The Energy of Seismic Body Waves and Surface Waves",
Contributions in Geophysics (In Honor of Gutenberg),
Pergamon Press: 1-16.

Ben-Menahem, A.

- 1961 "Radiation of Seismic Surface-Waves from Finite Moving
Sources", Bull. Seismol. Soc. Am., 51: 401-435.

Ben-Menahem, Ari, and David G. Harkrider

- 1964 "Radiation Pattern of Seismic Surface Waves from Buried
Dipolar Point Sources in a Flat Stratified Earth,"
J. Geophys. Res., 69: 2605-2620.

Ben-Menahem, A., S. W. Smith, and T. L. Teng

- 1965 "A Procedure for Source Studies from Spectrums of Long-
Period Body Waves," Bull. Seismol. Soc. Am., 55: 203-206.

Ben-Menahem, Ari

- 1965 "Observed Attenuation and Q Values of Seismic Surface Waves
in The Upper Mantle," J. Geophys. Res., 70: 4641-4651.

Benioff, H., F. Press, and S. W. Smith

- 1961 "Excitation of the Free Oscillations of the Earth by
Earthquakes," J. Geophys. Res., 55: 605-615.

Bomford, B. G.

- 1952 Geodesy, Oxford University Press, Amen House, London.

Berckhemer, H., and G. Schneider

- 1964 "Near Earthquake Record with Long-Period Seismographs,"
Bull. Seismol. Soc. Am., 54: 973-986.

Brekhovskikh, L. M.

- 1960 "Waves in Layered Media", Academic Press, New York.

Brune, J. N.

- 1961 "Radiation Pattern of Rayleigh Waves from the Southeast
Alaska Earthquake of July 10, 1958", Publ. of Dom. Obs., Vol.
XXIV , No. 10.

Burridge, R., and L. Knopoff

- 1964 "Body Equivalents for Seismic Dislocations", Bull. Seismol.
Soc. Am., 54: 1901-1914.

Burridge, R., E. R. Lapwood, and L. Knopoff

- 1964 "First Motions from Seismic Sources Near A Free Surface",
Bull. Seismol. Soc. Am., 54: 1889-1913.

Chander, R., and J. N. Brune

- 1965 "Radiation Pattern of Mantle Rayleigh Waves and The Source
Mechanism of the Hindu-Kush Earthquake of July 6, 1962",
Bull. Seismol. Soc. Am., 55: 805-820.

de Hoop, A. T.

- 1958 "Representation Theorems for the Displacement in Elastic
Solid and Their Application to Elastodynamic Diffraction
Theory", Doctoral Dissertation, Delft.

De Noyer, John

- 1958 "Determination of the Energy in Body and Surface Waves",
Part I, Bull. Seismol. Soc. Am., 48: 355-368.

De Noyer, John

- 1959 "Determination of the Energy in Body and Surface Waves",
Part II, Bull. Seismol. Soc. Am., 49: 1-10.

Fu, C. Y.

- 1945 "On the Origin and Energy of Oscillatory Earthquake Waves",
Bull. Seismol. Soc. Am., 35: 37-42.

Galitzin, B.

- 1915 "Earthquake of February 18, 1911", Comptes Rendus, 160:
810-813.

Godin, Y. N., B. S. Vol'vovski, L. S. Vol'vovski, and K. E. Fomenko

- 1961 "Determination of the Structure of the Earth's Crust by
Means of Regional Seismic Investigations on the Russian
Platform and in Central Asia", Izv. Akad. Nauk SSSR, Ser.
Geofiz.: 955-960.

Gutenberg, B., and C. F. Richter

- 1936 "On Seismic Waves", (Third Paper), Gerlands Beitr. Geophys.,
47: 73-131.

Gutenberg, B.

- 1955 "Magnitude Determination for Large Kern County Shocks,
1952; Effects of Station Azimuth and Calculation Method,"
State of California, Dept. of Nat. Resources, Bull. 171.

Gutenberg, B.

- 1956 "The Energy of Earthquakes", Quarterly J. Geol. Soc.,
CXII, Part 1: 1-14.

Hagiwara, T.

- 1958 "A Note on the Theory of the Electromagnetic Seismograph",
Bull. Earthquake Res. Inst., Tokyo Univ., 36.

Hannon, W. J.

- 1964 "An Application of the Haskell-Thomson Matrix Method to
the Synthesis of the Surface Motion and to Dilatational
Waves," Bull. Seismol. Soc. Am., 54: 2067-2080.

Harkrider, D. G., and D. L. Anderson

- "Surface Wave Energy from Point Sources on Plane Layered
Earth," (To Be Published)

Haskell, N.

- 1960 "Crustal Reflection of Plane SH Waves," J. Geophys. Res.,
65: 4147-4150.

Haskell, N.

- 1962 "Crustal Reflection of P and SV Waves," J. Geophys. Res.,
67: 4751-4767.

Haskell, N.

- 1963 "Radiation Pattern of Rayleigh Waves from a Fault of
Arbitrary Dip and Direction of Motion in a Homogeneous
Medium," Bull. Seismol. Soc. Am., 53: 619-642.

Haskell, N.

- 1964 "Total Energy and Energy Spectral Density of Elastic Wave Radiation from Propagating Faults," Bull. Seismol. Soc. Am., 54: 1811-1842.

Hodgson, J. H., and M. E. Metzger

- 1961 "Direction of Faulting in some of the Larger Earthquakes of 1958," Pub. of Dom. Obs. Ottawa, Vol. XXVI: 305-318.

Hodgson, J. H., and A. E. Stevens

- 1964 "Seismicity and Earthquake Mechanism," Chapter 24, Res. in Geophys., MIT Press.

Hodgson, J. H., and A. J. Wickens

- 1965 "Computer-Determined P-Nodal Solutions for the Larger Earthquakes of 1959-1962," Pub. of Dom. Obs., Ottawa, Vol. XXXI: 123-142.

Honda, H.

- 1956 "The Mechanism of the Earthquakes," The Sci. Reports of the Tohoku Univ., Ser. 5, Geophys., Vol. 9, Supplement.

Jeffreys, H.

- 1923 "The Pamir Earthquakes of 18 February 1911, in Relation to The Depths of Earthquake Foci," Monthly Notices Roy. Astron. Soc., Geophys. Suppl., 1: 22-31.

Kawasumi, H., and R. Yosiyama

- 1935 "On an Elastic Wave Animated by the Potential Energy of Initial Strain," Bull. Earthquake Res. Inst., Tokyo Imp. Univ., 13: 49-503.

Kovach, R. L., and D. L. Anderson

1966 "Free Oscillation Energy," (To be published).

Mohajer, G. A., and G. R. Pierce

1963 "Qazvin, Iran, Earthquake," Bull. Am. Assoc. Petrol. Geologists, 47, No. 10.

Morse, P. M. and H. Feshbach

1953 "Methods of Mathematical Physics," Part I, p 151,
McGraw-Hill Co., New York.

Nowroozi, A.

1965 "Eigenvibrations of the Earth after Alaskan Earthquake,"
J. Geophys. Res., 70 : 5145-5156.

Ormsby, J. F.

1961 "Design of Numerical Filters with Applications to Missile
Data Processing," J. Assoc. Computing Mach, 8: 440-466.

Petrescu, G., and G. Purcaru

1964 "The Mechanism and Stress Pattern at the Focus of the
September 1, 1962 Buyin-Zara (Iran) Earthquake," Annales
de Geophysique, 20: 242-247.

Phinney, R. A.

1964 "Structure of the Earth's Crust from Spectral Behavior
of Long Period Body Waves," J. Geophys. Res., 69: 2997-3017.

Pshenikov, K. B.

1965 "The Energy Balance in the Focal Region of a Strong
Earthquake," Izv. Akad. Nauk SSSR, Earth Physics Series,
667-671.

Raitt, R. W.

- 1963 "The Crustal Rocks," The Sea, Edited by M. N. Hill,
Interscience Publishers, pp. 85-102.

Richter, C. F.

- 1963 "Historical Background of the Magnitude Scale," VESIAC
Proceedings, University of Michigan, 1-12.

Ritzema, A. R.

- 1957 "On the Focal Mechanisms of Southeast Asian Earthquakes,"
Publ. of Dominoin Obs., Otta, Vol. XX, No. 2: 341-384.

Ritzema, A. R.

- 1958 "(i - Δ) Curves for Bodily Waves of any Focal Depths,"
Meteorol. and Geophys. Inst., Kjakarta, Verhadlingen,
54: 1-10.

Scheidegger, A. E.

- 1957 "The Geometrical Representations of Fault-Plane Solution
of Earthquakes," Bull. Seismol. Soc. Am., 47: 89-110.

Sezawa, K.

- 1935 "Elastic Waves Produced by Applying Statical Force to a
Body or by Releasing it from a Body," Bull. Earthquake
Res. Inst., Tokyo Imp. Univ., 13: 740-748.

Smith, S. W.

- 1966 "Free Oscillations Excited by the Alaskan Earthquake,"
J. Geophys. Res., 71: 1183-1193.

Stauder, W., and G. A. Bolinger

- 1964 "The S Wave Project for Focal Mechanism Studies, Earthquakes of 1962," Technical Report.

Steinhart, J. S., and R. P. Meyer

- 1961 "Explosion Studies of Continental Structure," Carnegie Inst. Washington, Publication 622.

Teng, T. L.

- 1965 "Amplitudes of Body Waves," Technical Report, Contract AF-49(638)-1337.

Teng, T. L., and A. Ben-Menahem

- 1965 "Mechanism of Deep Earthquakes from Spectrums of Isolated Body-Wave Signals, 1. The Banda Sea Earthquake of March 21, 1964," J. Geophys. Res., 70: 5157-5170.

Toksöz, M. Nafi, and Ari Ben-Menahem

- 1963 "Velocities of Mantle Love and Rayleigh Waves Over Multiple Paths," Bull. Seismol. Soc. Am., 53: 741-746.

Wu, F., and A. Ben-Menahem

- 1965 "Surface Wave Radiation Pattern and Source Mechanism of the September 1, 1962, Iran Earthquake," J. Geophys. Res., 70: 3943-3949.

List of Tables

- Table I. Radiation pattern of body waves from a shear fault (after Ben-Menahem et al, 1965).
- Table II. Rayleigh wave from a surface fault, (a) slip on a horizontal plane, (b) strike-slip on a horizontal plane, (c) dip-plane on a plane dipping at 45° .
- Table III. Partitioning of energy for sources (b) and (c).
- Table IV. Epicentral distances, azimuths and back azimuth of stations used in the study of Iran earthquake.
- Table V. Comparison of results from surface waves study and first motion study.
- Table VI. Source mechanism and energies for September 1, 1962 Iran earthquake.
- Table VII. First motions and station information for the Tonga earthquake.
- Table VIII. Source mechanism and energies for July 4, 1963 Tonga earthquake.
- Table IX. Source mechanism and energies for March 21, 1964 Banda Sea earthquake.
- Table X. Energies for earthquakes with known fault mechanisms. Epicentral distances and azimuth refer to Pasadena and the epicenters.

- Table XI. f_i 's of Haskell's Rayleigh wave radiation patterns.
(Haskell, 1963).
- Table XII. Displacement-energy for spheroidal oscillations.
(Kovach and Anderson, 1966)
- Table XIII. Free oscillation energies.

Table I

Far Field Body Wave Radiation Pattern from a Shear Fault

$$A(\theta, \phi) = c_0 + c_1 \sin\theta + d_1 \cos\theta + c_2 \sin^2\theta + d_2 \cos\theta$$

$$\Omega_1(\phi, \delta, \lambda) = \cos\phi \cos\lambda + \sin\phi \sin\lambda \cos\delta$$

$$\Omega_2(\phi, \delta, \lambda) = \cos\phi \cos\lambda \cos\delta + \sin\phi \sin\lambda \cos^2\delta$$

$$\Omega_3(\phi, \delta, \lambda) = \sin^2\phi \sin\lambda \cos\delta + \cos^2\phi \cos\lambda$$

$$\Omega_4(\phi, \delta, \lambda) = \cos\phi \cos^2\delta \sin\lambda - \sin\phi \cos\lambda \cos\delta$$

	c_0	c_1	d_1	c_2	d_2
P	$\frac{1}{4} \sin\lambda \sin^2\delta$ $-\frac{1}{2} \sin\theta \sin\delta\Omega_1$	0	0	$\Omega_2/2$	$\frac{1}{4} \sin\lambda \sin^2\delta$ $+\frac{1}{2} \sin\theta \sin\delta\Omega_1$
SH	0	$-\sin\delta\Omega_3$	Ω_4	0	0
SV	0	0	0	$-\frac{1}{2} \sin\lambda \sin^2\delta$ $-\sin\phi \sin\delta\Omega_1$	Ω_2

Table II

Source Type	Horizontal Radiation Pattern	Primary Wave Type	Rayleigh Waves	
			Horizontal	Vertical
(a)	cos φ	P	$\frac{\sqrt{2\pi\beta_R} r}{\rho_R} e^{i\beta_R r - i\pi/4}$	$\frac{\sqrt{2\pi\beta_R} r}{\rho_R} e^{i\beta_R r + i\pi/4}$
		SV	$e^{-\gamma\delta z} \frac{\rho_R^2 \sqrt{\rho_R^2 - \beta^2}}{\rho_R} \left[\left(\frac{\omega^2}{2\beta^2} - \beta^2 \right) + (\rho_R^2 - \beta^2) \rho_R^2 \right] \mathcal{R}'(\rho_R)$	$e^{-\gamma\delta z} \frac{\rho_R (\rho_R^2 - \beta^2)^{1/2}}{\rho_R} \left[\left(\frac{\omega^2}{2\beta^2} - \beta^2 \right) + (\rho_R^2 - \beta^2) \rho_R^2 \right] \mathcal{R}'(\rho_R)$
(b)	sin φ • cos φ	P	$e^{-\gamma\alpha z} B_1/R^1(\rho_R)$	$e^{-\gamma\alpha z} B_2/R^1(\rho_R)$
		SV	$e^{-\gamma\beta z} B_3/R^1(\rho_R)$	$e^{-\gamma\beta z} B_4/R^1(\rho_R)$
(c)	(1-2 α ² /β ² +sin ² φ)	P	$e^{-\gamma\alpha z} B_1/R^1(\rho_R)$	$e^{-\gamma\alpha z} B_2/R^1(\rho_R)$
		SV	$e^{-\gamma\beta z} B_3/R^1(\rho_R)$	$e^{-\gamma\beta z} B_4/R^1(\rho_R)$

$$\delta = i \operatorname{sgn} \omega, \gamma_\alpha = (\rho_R^2 - \rho_\alpha^2)^{1/2}, \gamma_\beta = (\rho_R^2 - \rho_\beta^2)^{1/2}$$

$$R^1(\rho_R) = \rho_R \left[2 \left(\frac{\omega^2}{2\beta^2} - \rho_R^2 \right) - 2\gamma_\alpha \gamma_\beta - \gamma_\alpha / \gamma_\beta - \gamma_\beta / \gamma_\alpha \right]$$

$$B_1 = \rho_R^4 (\rho_R^2 - \rho_\beta^2)^{1/2} / \sqrt{\rho_R r}$$

$$B_2 = \rho_R^3 (\rho_R^2 - \rho_\beta^2)^{1/2} (\rho_R^2 - \rho_\alpha^2)^{1/2} / \sqrt{\rho_R r}$$

$$B_3 = \rho_R^2 (\omega^2 / 2\beta^2 - \rho_R^2) (\rho_R^2 - \rho_\beta^2)^{1/2} / \sqrt{\rho_R r}$$

$$B_4 = \rho_R^3 (\omega^2 / 2\beta^2 - \rho_R^2) / \sqrt{\rho_R r}$$

Table III

Source Type	E_P	E_{SV}	E_{SH}	E_{RP}	E_{RS}
	.1253	1.677	6.28	.00342	.00543
b	$E_{SV}/E_P = 11.8$	$E_{SH}/E_P = 50.1$	$E_{RP}/E_P = .0273$	$E_{RS}/E_P = .043$	
	$(E_{SH} + E_{SV})/E_P = 62$	$(E_P + E_{SH} + E_{SV})/(E_{RS} + E_{RP}) = 9 \times 10^2$			
	.825	9.90	6.28	.0222	.0345
c	$E_{SV}/E_P = 11.8$	$E_{SH}/E_P = 7.61$	$E_{RP}/E_P = .0270$	$E_{RS}/E_P = .043$	
	$(E_{SV} + E_{SH})/E_P = 19.4$	$(E_P + E_{SH} + E_{SV})/(E_{RS} + E_{RP}) = 3 \times 10^2$			

Table IV.

USCGS WORLD-WIDE STANDARD STATIONS

ORIGIN IRAN							
LAT	35.600						
LONG	50.000						
STATION	LATITUDE	LONGITUDE	DIST(DEG)	DIST(KM)	AZIMUTH	BACK AZIMUTH	
AAE	9.0297	38.7655	2.83674E 01	3.15631E 03	203.89344	19.52225	
ADE	-34.5801	138.4232	1.07993E 02	1.20172E 04	119.86309	301.07014	
ALQ	34.5630	-106.2730	1.06765E 02	1.18576E 04	339.70713	20.02787	
AQU	42.2114	13.2411	2.91929E 01	3.24539E 03	294.28217	90.76362	
ARE	-16.2744	-71.2929	1.24607E 02	1.38650E 04	274.32983	57.79024	
ATU	37.5822	23.4300	2.14047E 01	2.37995E 03	283.16909	87.21230	
BAG	16.2439	120.3447	6.48862E 01	7.21752E 03	87.51216	302.04902	
BEC	32.2246	-64.4052	8.87319E 01	9.86142E 03	309.46300	47.92906	
BHP	8.5739	-79.3329	1.15151E 02	1.28038E 04	302.32071	44.13658	
BKS	37.5236	-122.1406	1.06881E 02	1.18684E 04	353.47612	6.68766	
BLA	37.1240	-80.2514	9.41642E 01	1.04614E 04	322.29168	38.58187	
BOG	4.3723	-74.0354	1.14264E 02	1.27078E 04	294.99038	47.79818	
CAR	10.3024	-66.5940	1.04836E 02	1.16585E 04	294.45035	48.92617	
COP	55.4100	12.2600	3.24799E 01	3.60941E 03	319.45644	111.73788	
COR	44.3509	-123.1812	1.00184E 02	1.11238E 04	355.03522	5.64175	
DAL	32.5046	-96.4702	1.05314E 02	1.16985E 04	331.05775	27.82214	
DUG	41.1142	-112.4848	1.01982E 02	1.13246E 04	346.55762	14.52073	
FLO	38.4806	-90.2212	9.76108E 01	1.08424E 04	329.56005	31.73977	
GEO	38.5400	-77.0400	9.14547E 01	1.01605E 04	321.23153	40.59573	
GOL	39.4201	-105.2216	1.01925E 02	1.13193E 04	340.62157	20.43159	
HNR	-9.2554	159.5648	1.11223E 02	1.23753E 04	86.22585	304.53608	
IST	41.0236	28.5906	1.76383E 01	1.96100E 03	294.28653	100.95840	
KEV	69.4520	27.0050	3.61887E 01	4.02019E 03	346.49093	147.37160	
KON	59.3900	9.3500	3.54811E 01	3.94245E 03	324.94682	113.84494	
LAH	31.3300	74.2000	2.06174E 01	2.29282E 03	94.99799	288.42860	
LON	46.4500	-121.4836	9.79661E 01	1.08774E 04	354.06543	6.99972	
LPA	-34.5432	-57.5552	1.22006E 02	1.35764E 04	248.14342	66.38873	
LPB	-16.3158	-68.0554	1.21995E 02	1.35746E 04	272.31115	57.99596	
LPS	14.1732	-89.0943	1.17156E 02	1.30221E 04	314.45275	36.85268	
LUB	33.3500	-101.5100	1.06405E 02	1.18187E 04	335.40443	23.90588	
MAL	36.4339	-4.2440	4.33886E 01	4.82401E 03	287.69431	74.30938	
MAN	14.4000	121.0500	6.64434E 01	7.39103E 03	88.81037	302.76928	
MDS	43.2220	-89.4536	9.32812E 01	1.03605E 04	331.57676	32.04880	
MNN	44.5452	-93.1124	9.34947E 01	1.03836E 04	334.53170	29.34615	
MUN	-31.5800	116.1224	9.11724E 01	1.01458E 04	128.68487	311.81003	
NHA	12.1236	109.1242	5.79986E 01	6.45229E 03	98.18925	304.43174	
NNA	-11.5915	-76.5032	1.26208E 02	1.40414E 04	282.53411	54.27936	
NUR	60.3032	24.3905	2.97149E 01	3.30180E 03	334.26582	134.71332	
DGD	41.0400	-74.3700	8.82217E 01	9.80101E 03	321.34181	42.29856	
PMG	-9.2432	147.0914	1.01058E 02	1.12450E 04	93.47089	304.51102	
QUE	30.1118	66.5700	1.49579E 01	1.66351E 03	106.78134	295.78305	
RAB	-4.1133	152.1016	1.02222E 02	1.13734E 04	86.29693	305.38061	
SCP	40.4836	-77.5210	9.02185E 01	9.99006E 03	322.77377	40.26837	
SHA	34.4141	-88.0823	1.00097E 02	1.11200E 04	325.87453	33.57340	
STU	48.4615	9.1136	3.25851E 01	3.62179E 03	306.00071	97.90276	
TAU	-42.5436	147.1914	1.17762E 02	1.31028E 04	124.04485	293.97480	
TOL	39.5253	-4.0255	4.24720E 01	4.72168E 03	292.02929	77.61813	
TRN	10.3900	-61.2406	1.00756E 02	1.12055E 04	291.03145	50.63995	
UME	63.4854	21.1412	3.30463E 01	3.67163E 03	336.59284	133.83775	
WES	42.2304	-71.1920	8.57221E 01	9.52342E 03	320.42355	44.35392	
IRAN	35.6000	50.0000	0.	0.	248.19859	248.19859	

NON-WORLD-WIDE NET STATIONS

ORIGIN IRAN							
LAT	35.600						
LONG	50.000						
STATION	LATITUDE	LONGITUDE	DIST(DEG)	DIST(KM)	AZIMUTH	BACK AZIMUTH	
ABU	34.8660	135.5660	6.75674E 01	7.51105E 03	62.49228	298.47431	
ALE	82.4830	-62.4000	5.77522E 01	6.41287E 03	351.72293	62.98430	
HAL	44.6330	-63.6000	8.00487E 01	8.89340E 03	318.37405	49.30576	
HKC	22.3030	114.1720	5.68062E 01	6.31798E 03	84.94902	298.76723	
HON	21.3030	-158.0950	1.17457E 02	1.30496E 04	29.66262	334.37309	
LND	43.0400	-81.1830	8.99615E 01	1.00183E 04	326.51004	37.83157	
LWI	-2.2500	28.8000	4.25555E 01	4.73564E 03	212.29650	25.83375	
MAT	36.5380	138.2080	6.86511E 01	7.63095E 03	59.80175	299.00626	
MBC	76.2330	-119.3330	6.82314E 01	7.57549E 03	357.26399	9.34806	
MTJ	36.2110	140.1110	7.01486E 01	7.79735E 03	59.29781	299.95266	
OTT	45.3940	-75.1760	8.53879E 01	9.48510E 03	324.70253	41.93565	
PAL	41.0070	-73.9080	8.80101E 01	9.7757E 03	321.06145	42.59142	
PER	-31.9500	115.8330	9.12351E 01	1.01528E 04	129.12418	311.95242	
PIE	-29.6200	30.0960	6.75262E 01	7.51468E 03	198.71167	17.47258	
PNT	49.3160	-119.6160	9.49553E 01	1.05429E 04	353.20041	8.47871	
RDJ	-22.8950	-43.2230	1.05452E 02	1.17350E 04	252.78912	57.58379	
RES	74.6860	-94.9000	6.75745E 01	7.50285E 03	350.48408	30.46014	
SCB	43.7160	-79.2330	8.85477E 01	9.83597E 03	325.81773	39.15715	
SCH	54.8160	-66.7830	7.49279E 01	8.32225E 03	327.64830	48.88956	
SUV	-18.1490	178.4570	1.31404E 02	1.46209E 04	83.07711	301.69971	
UPP	59.8580	17.6270	3.20401E 01	3.56015E 03	329.37899	124.66360	
VIC	48.5200	-123.4160	9.60487E 01	1.06642E 04	355.60339	5.39178	
WIL	-66.2580	110.5830	1.11582E 02	1.24101E 04	157.71066	310.23529	
IRAN	35.6000	50.0000	0.	0.	248.19859	248.19859	

Table V

Comparison of Results

	Present Study	First-Motion Study by Petrescu and Purcaru
Strike Azimuth	280°	283°
Dip azimuth	190°	193°
Dip	78°	80°
Slip Angle	63°	66°

Table VI

Source Parameters of Sept. 1, 1962 Iran Earthquake

	Surface Wave	First Motion
Strike	N80°W	N77°W
Dip	78° toward S10°W	80° toward S13°W
Slip Angle	63°	66°
Force System	Double couple	Double couple

Magnitude and Energy

Richter magnitude = $7\frac{1}{2}$

Energy calculated by using Gutenberg and

Richter's formula $\log_{10} E = 5.8 + 2.4 m$

$$E = 6.3 \times 10^{23} \text{ ergs}$$

Energy in P, S, Rayleigh and Love using present method

$$E_P = 1.95 \times 10^{23} \text{ ergs (0.1 - 0.3 cps)}$$

$$E_S = 5.6 \times 10^{24} \text{ ergs (0.1 - 0.2 cps)}$$

$$E_R = 1.2 (\pm 0.5) \times 10^{21} \text{ ergs (0.005 - 0.015 cps)}$$

$$E_L = 3.2 (\pm 0.8) \times 10^{20} \text{ ergs (0.005 - 0.0 15 cps)}$$

Table VII

Tonga Earthquake of July 4, 1963

First Motion Studies

Station	Azi	Back Azi	Dist(Δ°)	P _z	pP _z	S	i _h
AFI	25.38	203.3	13.5	-			72
ALQ	51.1	238.2	90.8	-	+	63.2 ^o	20.6
ANP	305.8	126.6	78 ^o	-	+	271 ^o	23.5
ANT	118.5	239.2	94.2	-	+	18.2 ^o	20
ARE	111.9	240.2	96.7	-	+	15.2 ^o	
BAG	297.9	124.3	73.5	-	+	259 ^o	27
BHP	85.5	244.9	101.2	?	+		20
BKS	41.4	228.4	82.1	-	+	102 ^o	23.5
BOG	91.9	244.2	104.3	-	+		20
BRS	260.9	94.4	26.3	+			45.6
CAN	245.2	85.4	33.9	+			41.5
CHG	289.6	116.8	92.4	-			21
COR	35.8	227.1	86	-	+	68 ^o	22
CTA	273 ^o	107.5	33.7	-		248 ^o	41.3
NDI	290.8	107.8	114.5	-			20
GUA	313.	137.5	53.8	-			34
HKC	299.6	122.6	81.7	-	+	287 ^o	23.5
HNR	304.	131.	27.4	-	+		44.5
KIP	23.9	202.9	51.	-	+	44 ^o	35.5
LEM	270.6	115.3	73.3	-			26.7

Table VII (Continued)

Tonga Earthquake of July 4, 1963

First Motion Studies

Station	Azi	Back Azi	Dist(Δ°)	P _z	pP _z	S	i _h
LON	35.1	228.3	88.5	-	+	210 ^o	22
LPB	113.6	239.0	99.4				20
LPS	76.7	244.3	94.9	-	+		20.7
MAN	296.7	124.1	72	-	+		27
MAT	324.6	139.8	75.0	-			26
MED	276.1	116.6	85.8	-			22.2
MVN	248.1	102.7	57.0	-		335 ^o	33
NHA	288.6	119.5	80.6	-	+	285 ^o	24
NNA	105.3	240.0	94.7	-	+	23 ^o	20.6
NOU	282.2	108.7	14.8	+			71
PMG	290.3	121.4	37.3	-	+	290 ^o	38.75
PVC	300.5	125.7	15.5	-			70
RAP	302.2	130.4	36.4	-	?		39
SBA	184.1	17.7	52.1	+	+		34
SEO	318.7	131.8	82	-	+	278 ^o	23
SPA	180.	182.3	63.8	-	+	336 ^o	29
TAU	231.5	71.9	32.9	+ ?			42
TNG	270.8	115.5	74.2	-			26

Table VII (Continued)

Tonga Earthquake of July 4, 1963

First Motion Studies

Station	Azi	Back Azi	Dist(Δ°)	P _z	pP _z	S	i _h
WEL	200.7	25.	16.2	+			66.5
WIL	206.7	84.8	58.9	+			31

S polarization angle counts from the vector toward the source, counterclockwise.

Table VIII

Source Parameters of 4 July 1963 Tonga Earthquake

	First Motion	Radiation Pattern
Strike	N26°E	N24°E
Dip	68° toward S64°E	63° toward S66°E
Slip Angle	212°	208°
Force System	Double couple	Double couple

Magnitude and Energy

Richter magnitude $6\frac{1}{4}$ - $6\frac{3}{4}$

Energy calculated from the formula

$$\log_{10} E = 5.8 + 2.4 m:$$

$$E = 2.51 \times 10^{21}$$

Energy in P and S using present method

$$E_p = 1.35 \pm 0.5 \times 10^{22} \text{ ergs (0.01 - 0.2 cps)}$$

$$E_s = 1.1 \times 10^{23} \text{ ergs (0.01 - 0.13 cps)}$$

Table IX

Energy of 21 March 1964 Banda Sea Shock

Source Mechanism

(After Teng and Ben-Menahem)

	First Motion	Radiation Pattern
Strike	S 86° E	N 85° E
Dip	83° N 4° E	84° S 5° E
Slip Angle	310°	315°
Force System	D.C.	D.C.

Magnitude and Energy

Richter Magnitude = 6 3/4

$$E = 10^{(5.8 + 2.4 m)}$$
$$= 10^{22} \text{ ergs}$$

Energy in P and S Using Present Method

$$E_p = 1.05 \times 10^{23} \text{ ergs (0.01 - 0.2 cps)}$$
$$E_s = 1.3 \times 10^{24} \text{ ergs (0.01 - 0.13 cps)}$$

Table X

Date and Epicenter	Δ° (to Pas.)	Azimuth* of Pas.	δ	λ	E_p^\dagger (ergs)	E_s^\ddagger (ergs)	Magnitude (Pas.)
July 26, 1958	66.6°		27°	270°			
(1) Lat. 13.5 S Long. 69° W		133.20			1.35 x 10 ²²	40 x 10 ²³ (SV)	7
June 14, 1959	72.3°	52.9°	83°	213°	1.6 x 10 ²³		
(2) Lat. 20.5° S Long. 68° W							7¼
Jan 15, 1960	63.8°						
(3) Lat. 15° S Long. 75° W		52.2°	66°	137.2°	1.9 x 10 ²¹	20 x 10 ²³ (SH)	7
Mar. 8, 1960	86°						
(4) Lat. 16.5° S Long. 168.5° E		332.20	58°	189.5°	9.1 x 10 ²¹	4.3 x 10 ²³ (SH)	7
Aug 31, 1961	63.2°						
(5) Lat. 10.4° S Long. 70.7° W		86.4°	65°	180°	6.6 x 10 ²¹		7-7½

Table X (Continued)

Date and Epicenter	Δ° (to Pas.)	Azimuth* of Pas.	δ	λ	E_p^+ (ergs)	E_s^s (ergs)	Magnitude (Pas.)
Dec. 8, 1962	79.8 ⁰					7.3×10^{23} (SH)	
(6) Lat. 27.0 S		64.40	21 ⁰	168 ⁰	1.4×10^{22}		6½
Long. 3.6 W						$8. \times 10^{22}$ (SV)	

*Count from the north at the epicenter (counterclockwise)

†Within the frequency range of 0.01 - 0.02 cps

§Within the frequency range of 0.01 - 0.13 cps

Table XI
 Values of f_1 , f_2 , f_3 Corresponding to Various Types of Fault

Type	f_1		f_2		f_3	
	Dip-Slip	Strike-Slip	Dip-Slip	Strike-Slip	Dip-Slip	Strike-Slip
Normal, right-lateral	0	-1	$\cos\delta$	0	$\sin\delta$	0
Normal, left-lateral	0	1	$\cos\delta$	0	$\sin\delta$	0
Reverse, right-lateral	0	-1	$-\cos\delta$	0	$-\sin\delta$	0
Reverse, left-lateral	0	1	$-\cos\delta$	0	$-\sin\delta$	0

Table XII

Energies for ${}_0S_\ell$

Order, ℓ	T (sec)	K. E. (ergs)		
		$m = 0^*$ ($\times 10^{24}$)	$m = 1$ ($\times 10^{24}$)	$m = 2$ ($\times 10^{24}$)
2	3208	.00189	.0113	.0454
3	2120	.00285	.0342	.342
4	1533	.00406	.0812	x 1.46
5	1180	.00510	.153	x 4.28
6	955	.00562	.230	x 9.44
7	807	.00527	.295	1 x 5.9
8	703	.00448	.322	2 x 2.6
9	634	.00400	.360	3 x 1.7
10	579	.00369	.399	4 x 3.8
12	504	.00312	.487	7 x 5.0
13	473.0	.00287	.522	9 x 4.0
14	448.1	.00274	.575	12 x 0.
15	426.5	.00246	.590	14 x 1.

*From Kovach and Anderson (1966)

Table XIII

Energy for Spheroidal Oscillations

ℓ	u(cm)	U_{ℓ} (cm)	Correct for Q	Energy (ergs)
2*		.0024	.0046	6×10^{18}
3*		.00076	.00165	1.55×10^{19}
4*		.00069	.00182	7.3×10^{19}
5*		.00076	.0025	2.94×10^{20}
6*		.00010	.00037	9.65×10^{19}
7 ⁺	.0303	.00445	.0043	6.3×10^{21}
8 ⁺	.0283	.00354	.0039	9.7×10^{21}
9 ⁺	.0220	.00290	.00387	1.21×10^{22}
10 ⁺	.0092	.00184	.0025	1.14×10^{22}
12 ⁺	.0056	.00090	.00153	1.13×10^{22}
13 ⁺	.0136	.00105	.00225	2.1×10^{22}
14 ⁺	.0097	.00054	.0011	1.28×10^{22}
15 ⁺	.0147	.000775	.00177	2.3×10^{22}

u = displacement measured at the station

* Isabella strain data; U_{ℓ} is obtained by solving the two simultaneous absolute value equations as explained in the text. $\tau_0 = 5430$ minutes.

+ Berkeley Ultra-long period data (Nowroozi, 1965).

Figure Captions

Figure 1. Kinetic energy density per centimeter surface displacement for the vertical component Rayleigh wave.....129

Figure 2. Kinetic energy density per centimeter surface displacement for horizontal component Rayleigh wave.....130

Figure 3. Kinetic energy density per centimeter surface displacement for Love wave.....131

Figure 4. Calibration pulses (for step input) of WWNSS. SEO is underdamped and BAG is critically damped.....132

Figure 5. Comparison of instrument response calculated from theory and from calibration pulse.....133

Figure 6. Flow diagram for energy calculations.....134

Figure 7. Distribution of stations for the Iran shock study: coordinates centered at the source. Distances are in degrees.....135

Figure 8. Attenuation coefficient γ and loss factor Q for Rayleigh (R) and Love (L) waves.....136

Figure 9. Observed amplitude-radiation patterns and theoretical fit..137

Figure 10. Calculated radiation patterns at various depths and with different orientations of motion vectors.....138

Figure 11. Amplitude and phase modulation of the common spectrum of two interfering signals. The relative amplitude of the weaker signal is a139

Figure 12. Theoretical (smooth curve) and observed (dots) maxima in spectrum ratio as a function of the azimuth. The counterclockwise angle measured from azimuth 280.....139-A

Figure 13. Amplitude and phase modulation of the common spectrum of two interfering P waves, one of which has been reflected from the crust above the source. β is the ratio of the two P waves. The curves in the upper parts of the figures are the phase shifts; amplitudes are in the lower part.....140

Figure 14. Reduced P wave spectrums.....141

Figure 15. First motion study for the July 4, 1963 Tonga earthquake. Stereographic projections is used.....142

Figure 16. Radiation pattern and P wave traces of the July 4, 1963 Tonga earthquake. M's are the magnifications of the WWNSS instruments at those stations.....143

Figure 17. P and S waves recorded at Pasadena for earthquakes used in single-station energy calculations.....144

Figure 18. Location of singularities and contours of integration.....145

Figure 19. Variations of angle of incidence of Oceanic Rayleigh waves. Waves are recorded on Pasadena digital seismograph, simulated 30-100 instrument.....146

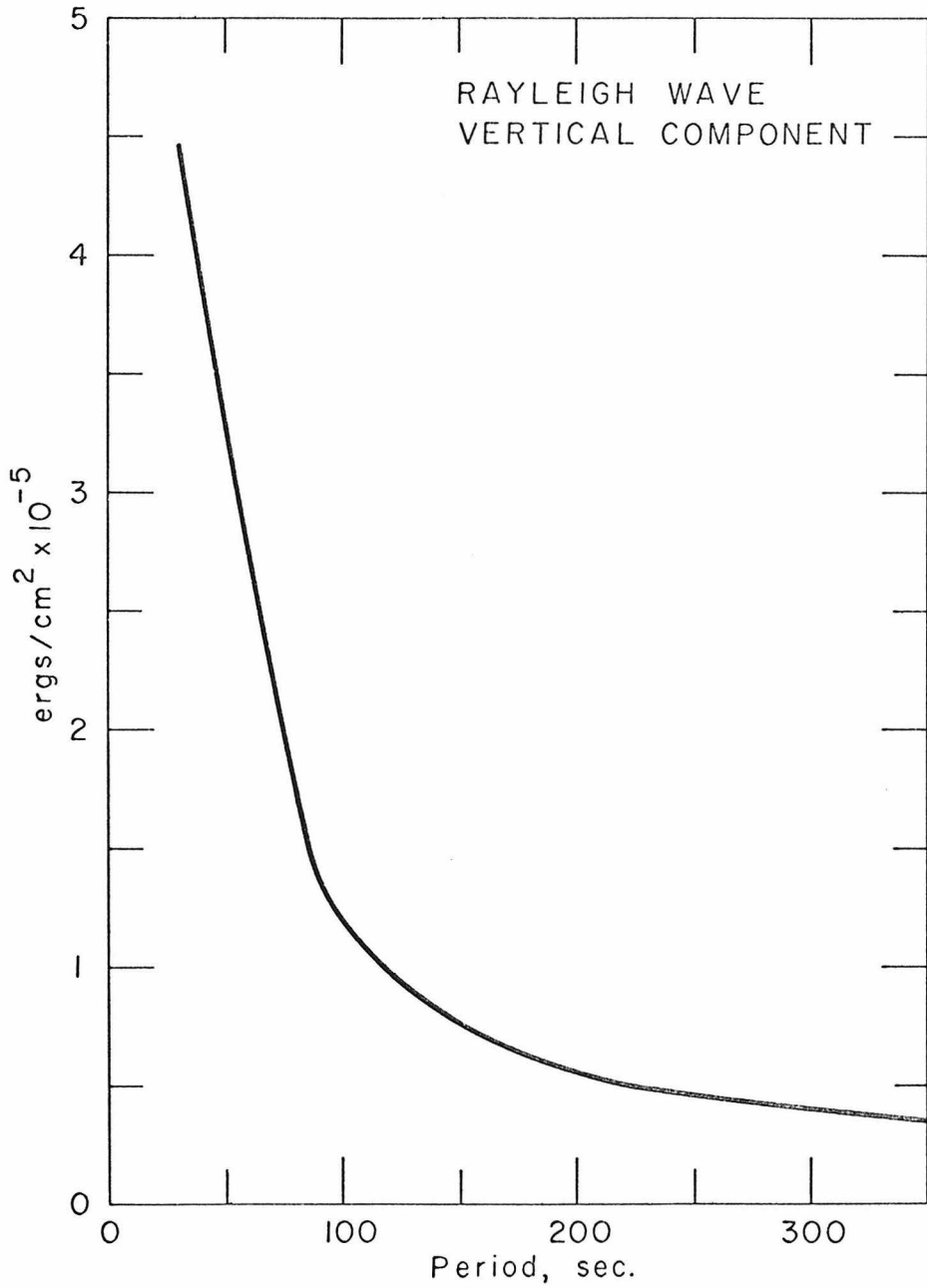


Fig. 1

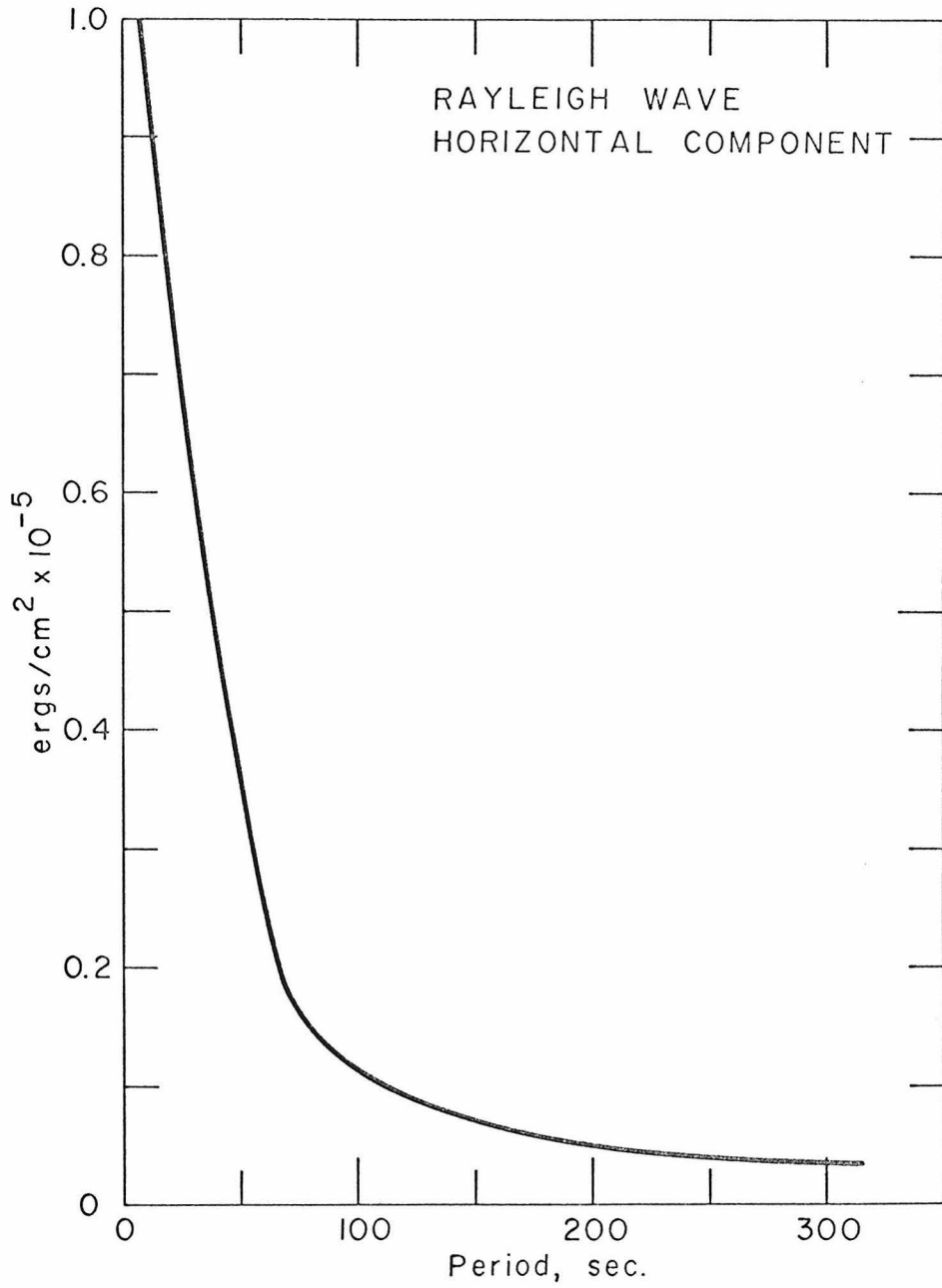


Fig. 2

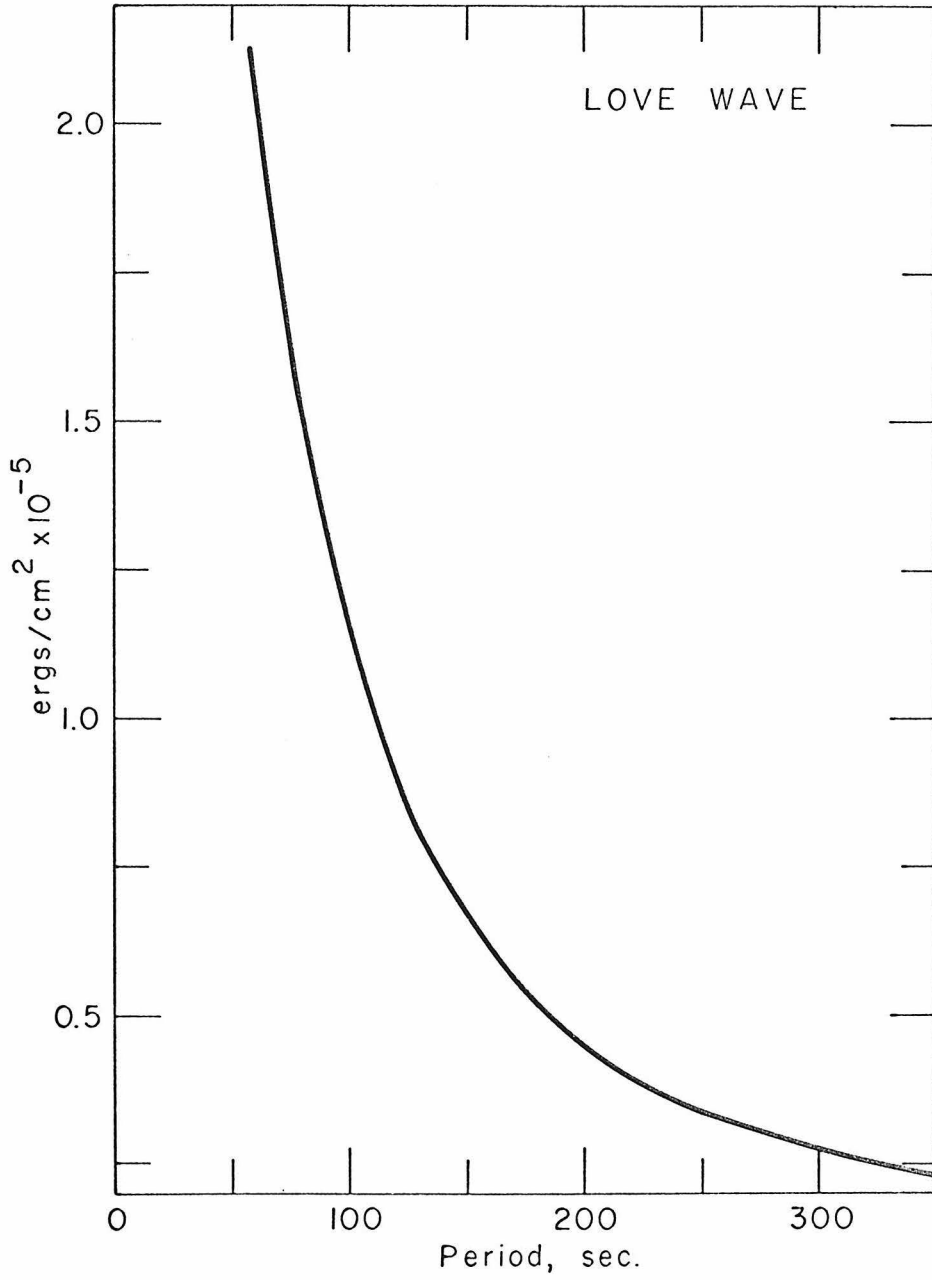
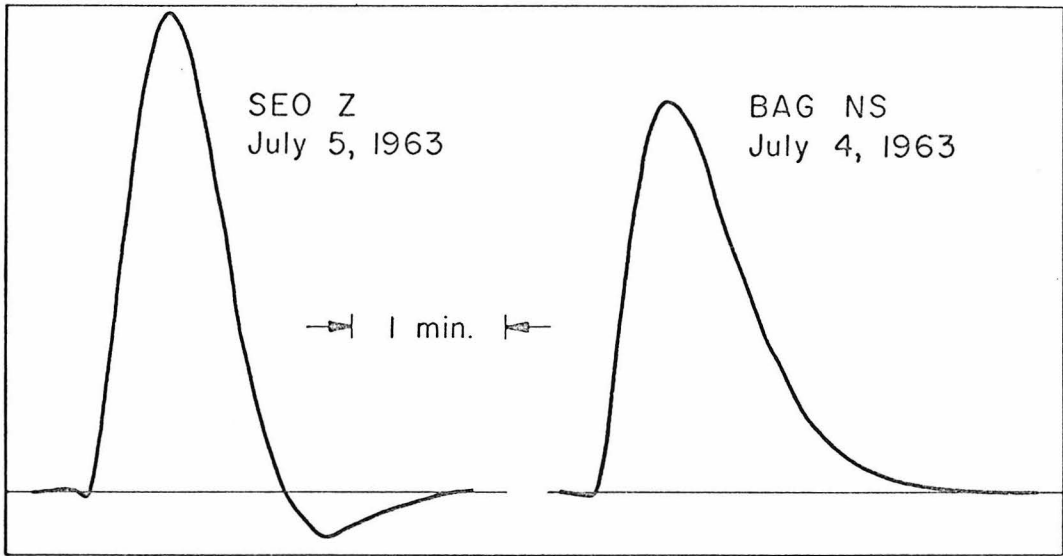


Fig. 3



RESPONSE OF LONG PERIOD WWNSS TO STEP INPUT

Fig. 4

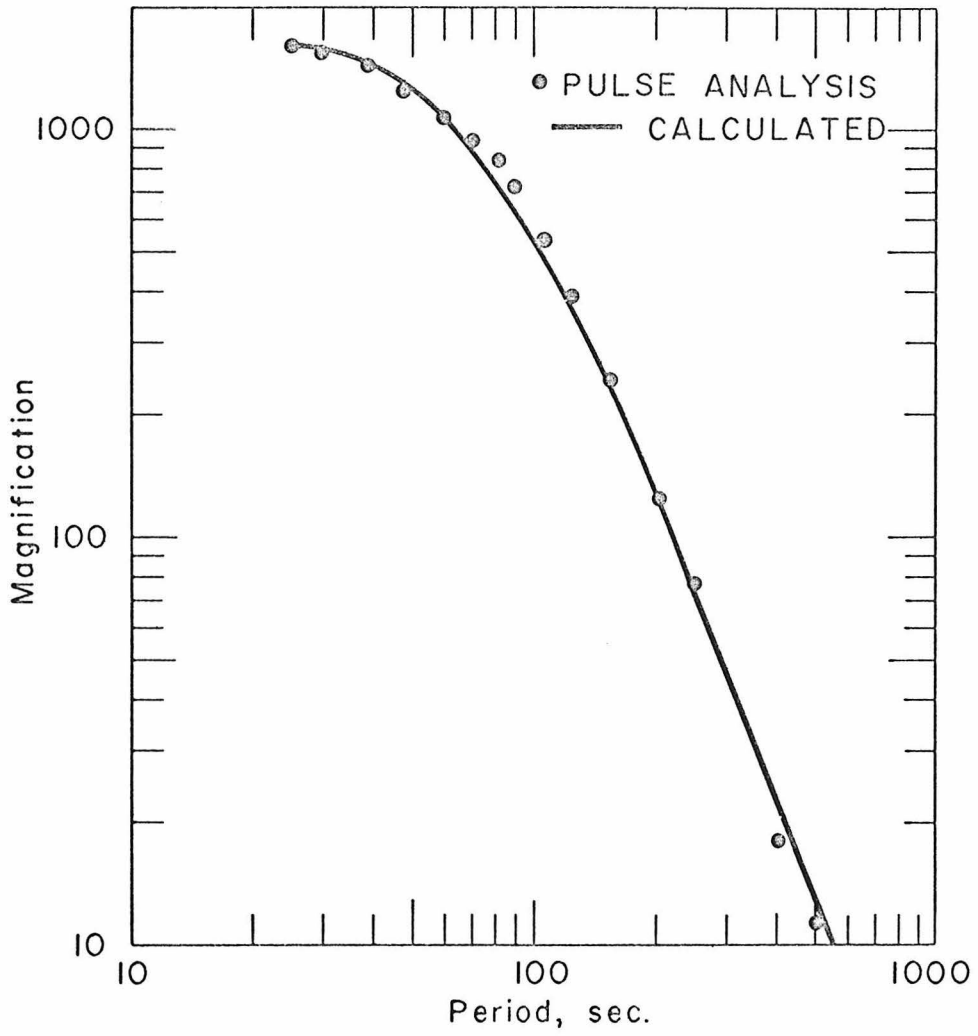


Fig. 5

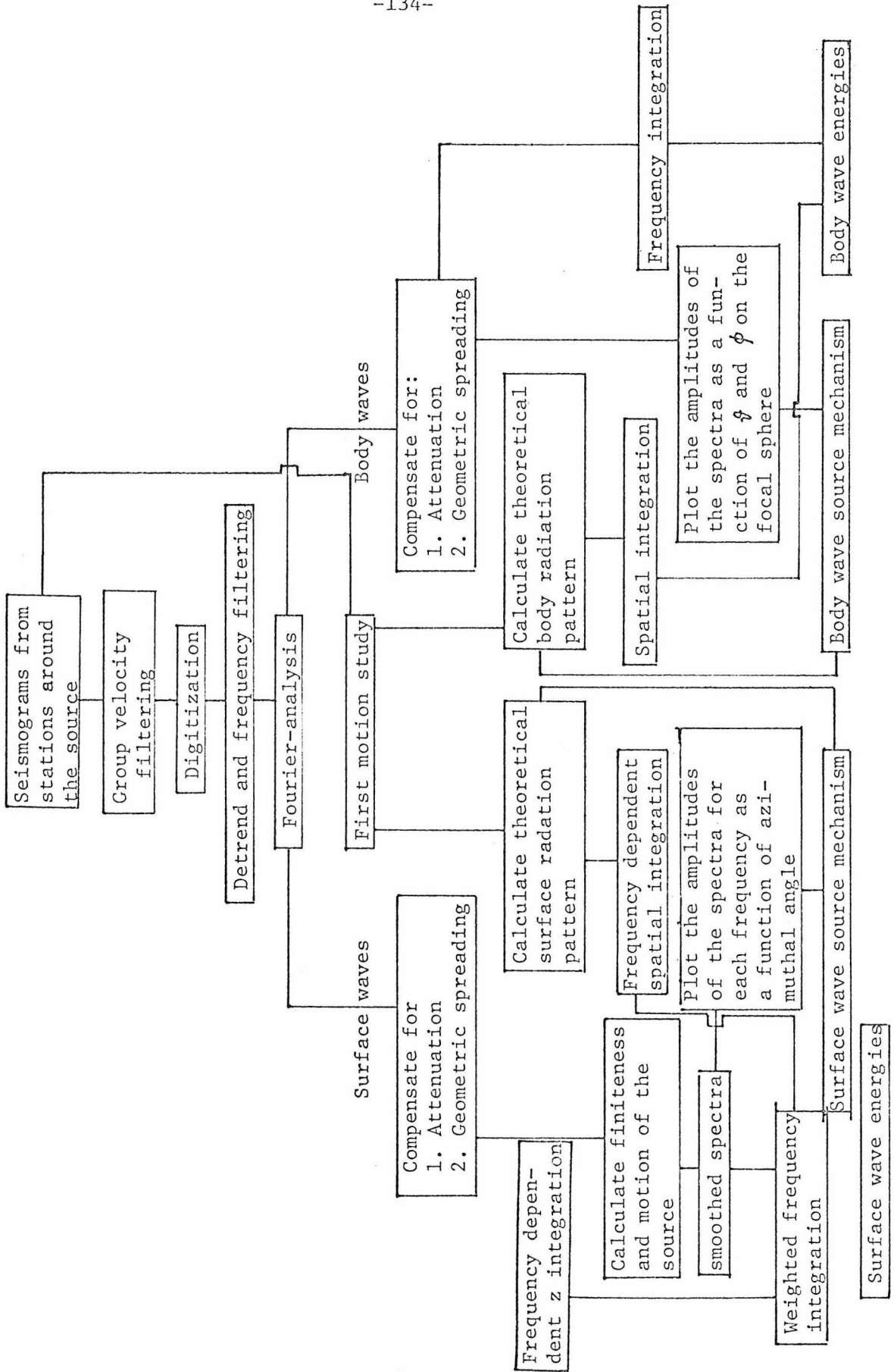


Figure 6

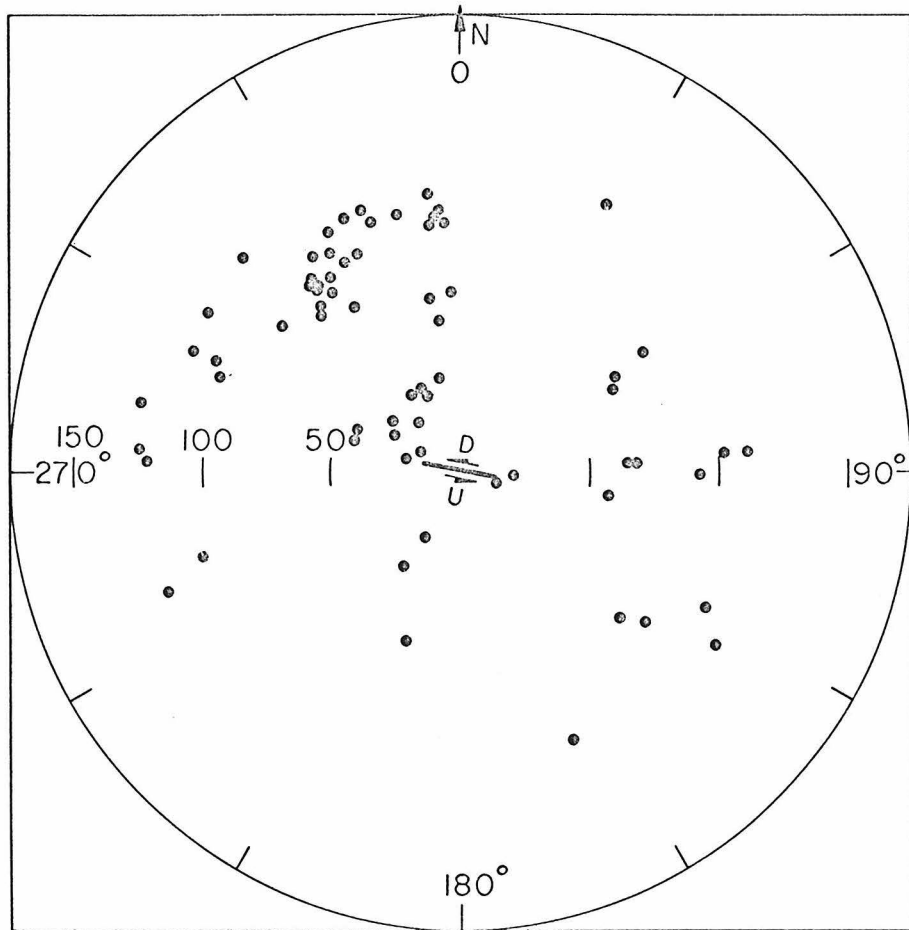


Fig. 7

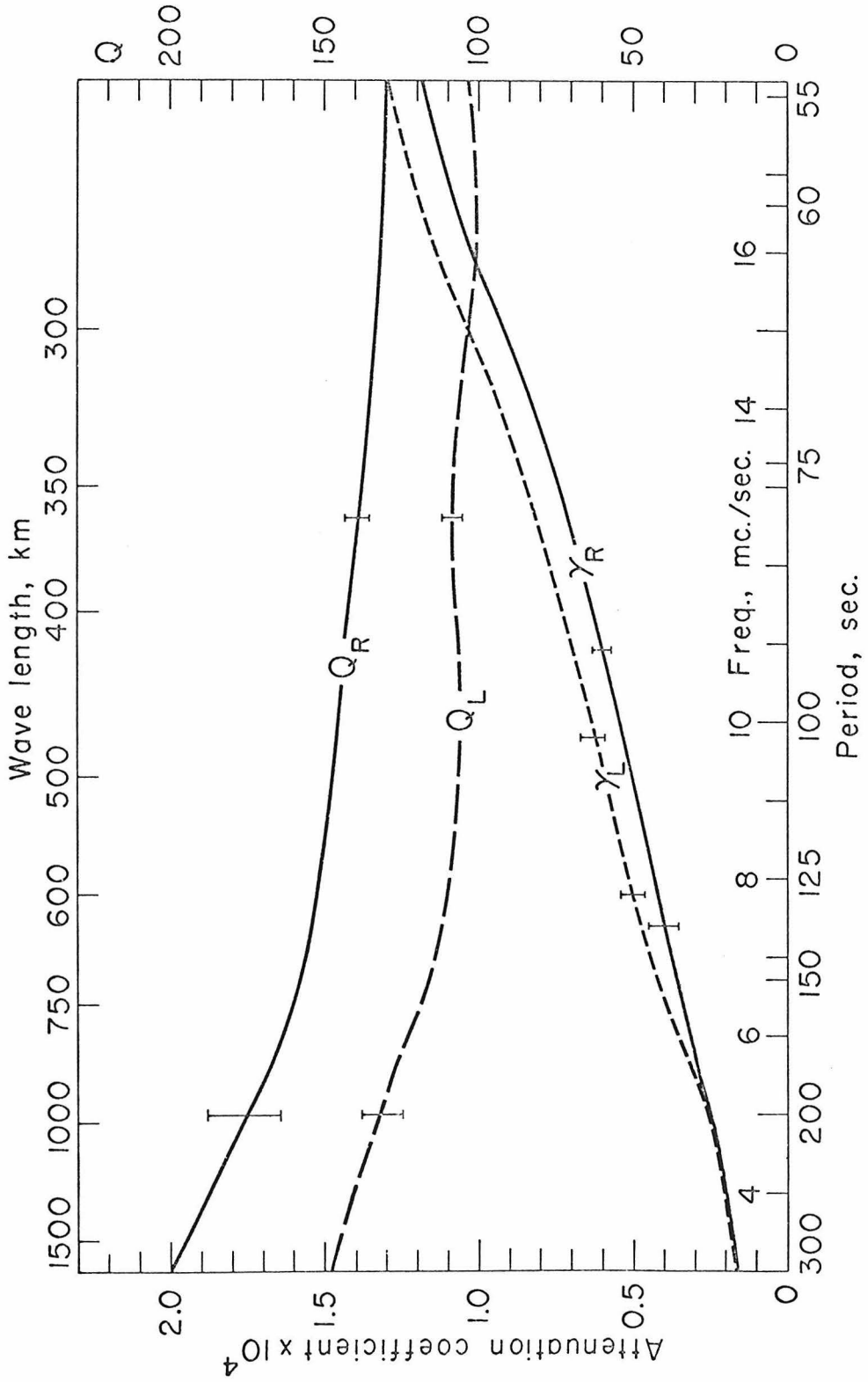


Fig. 8

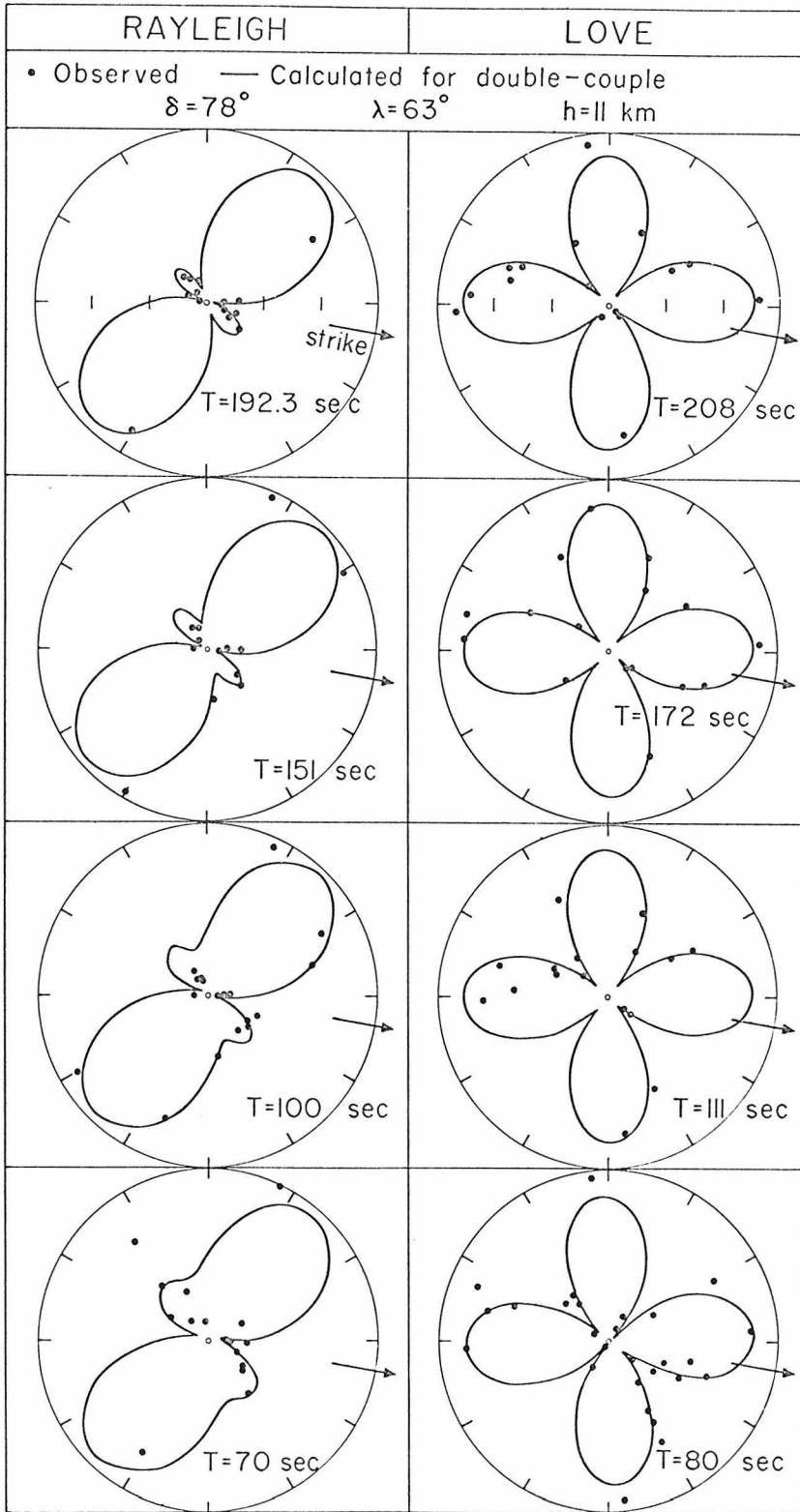


Fig. 9

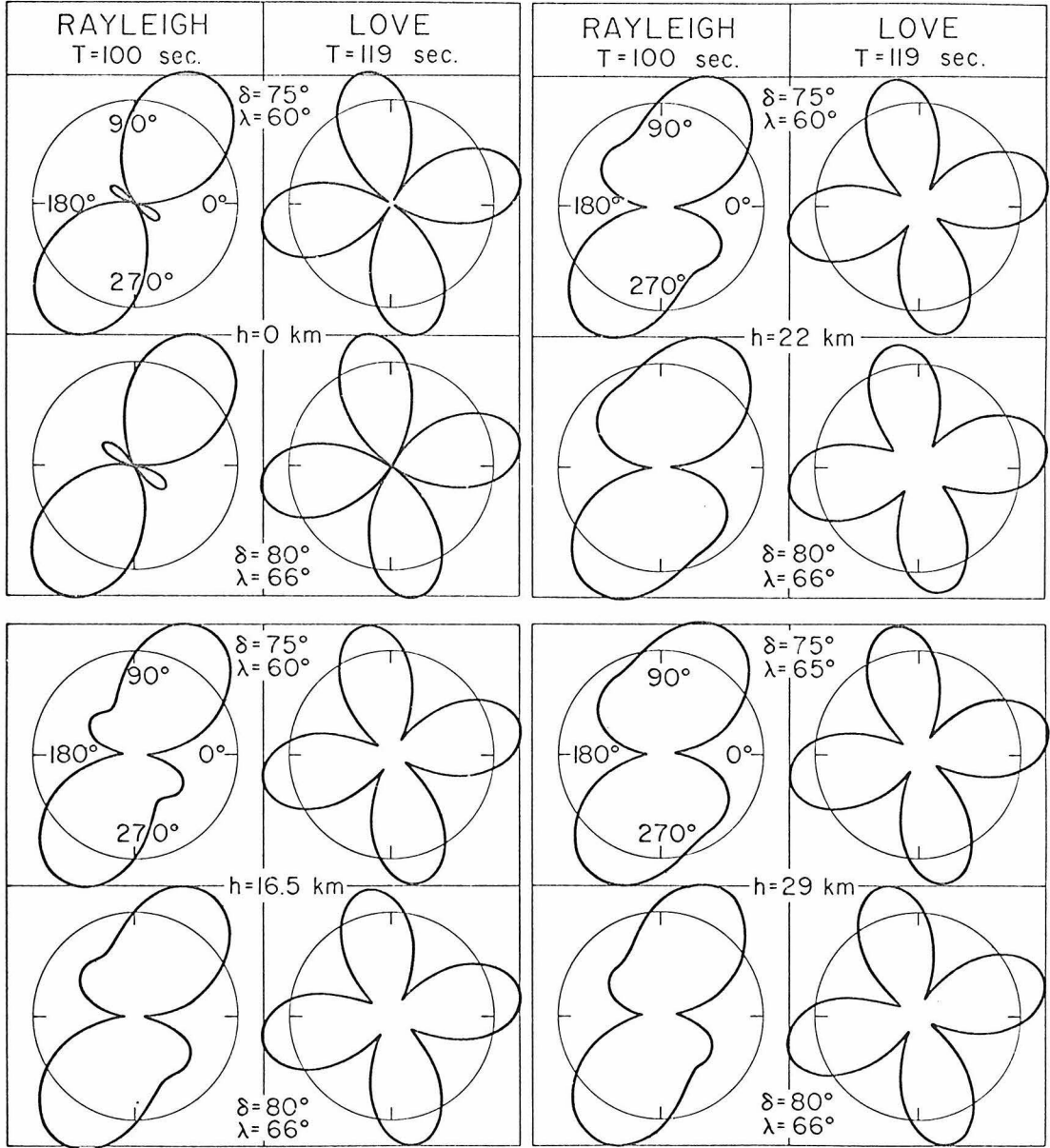


Fig. 10

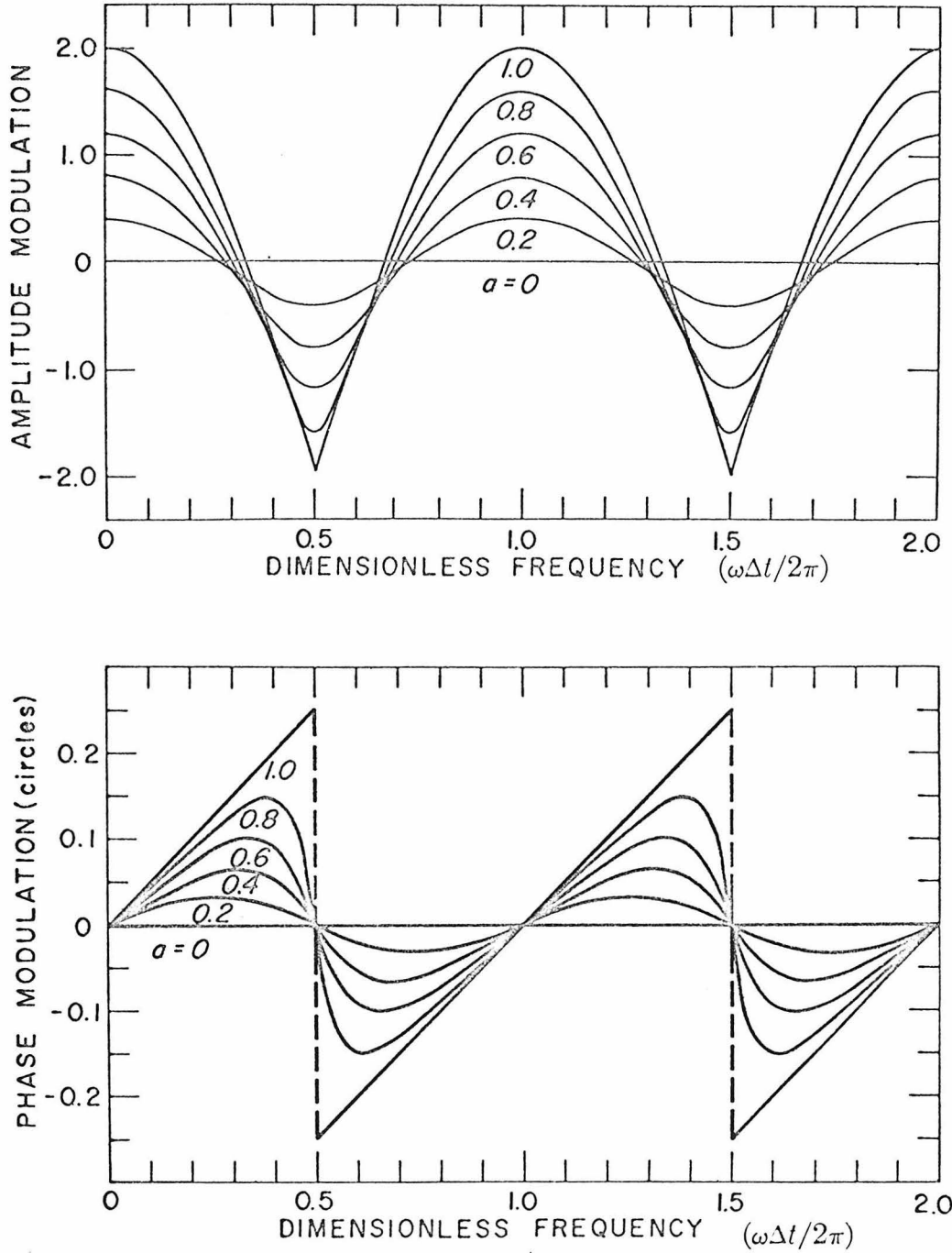


Fig. 11

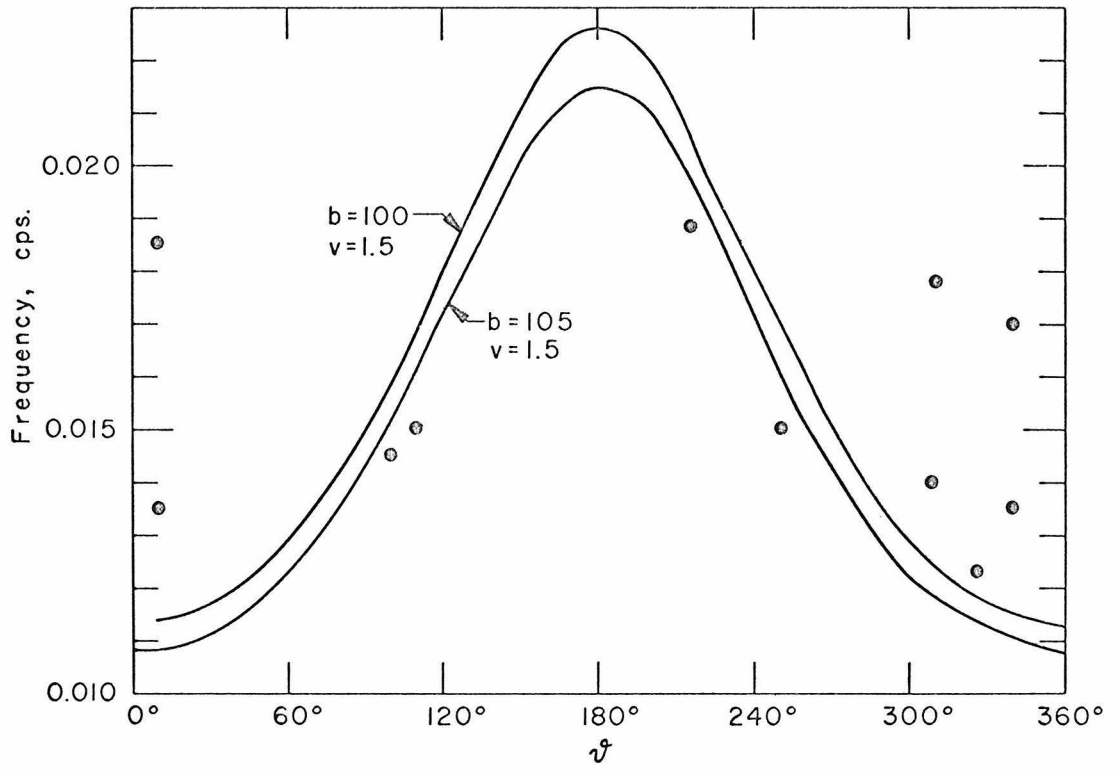


Fig. 12

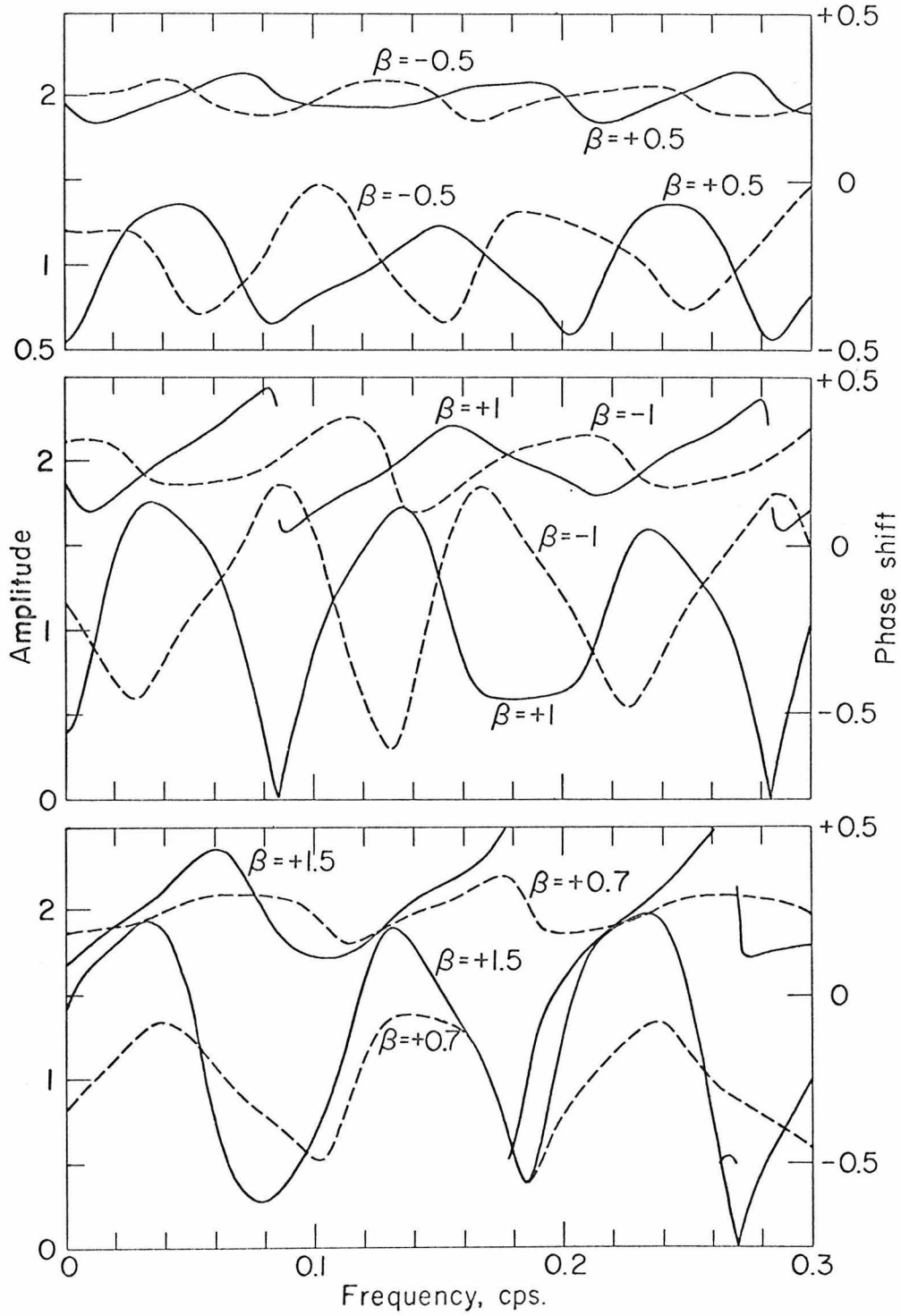


Fig. 13

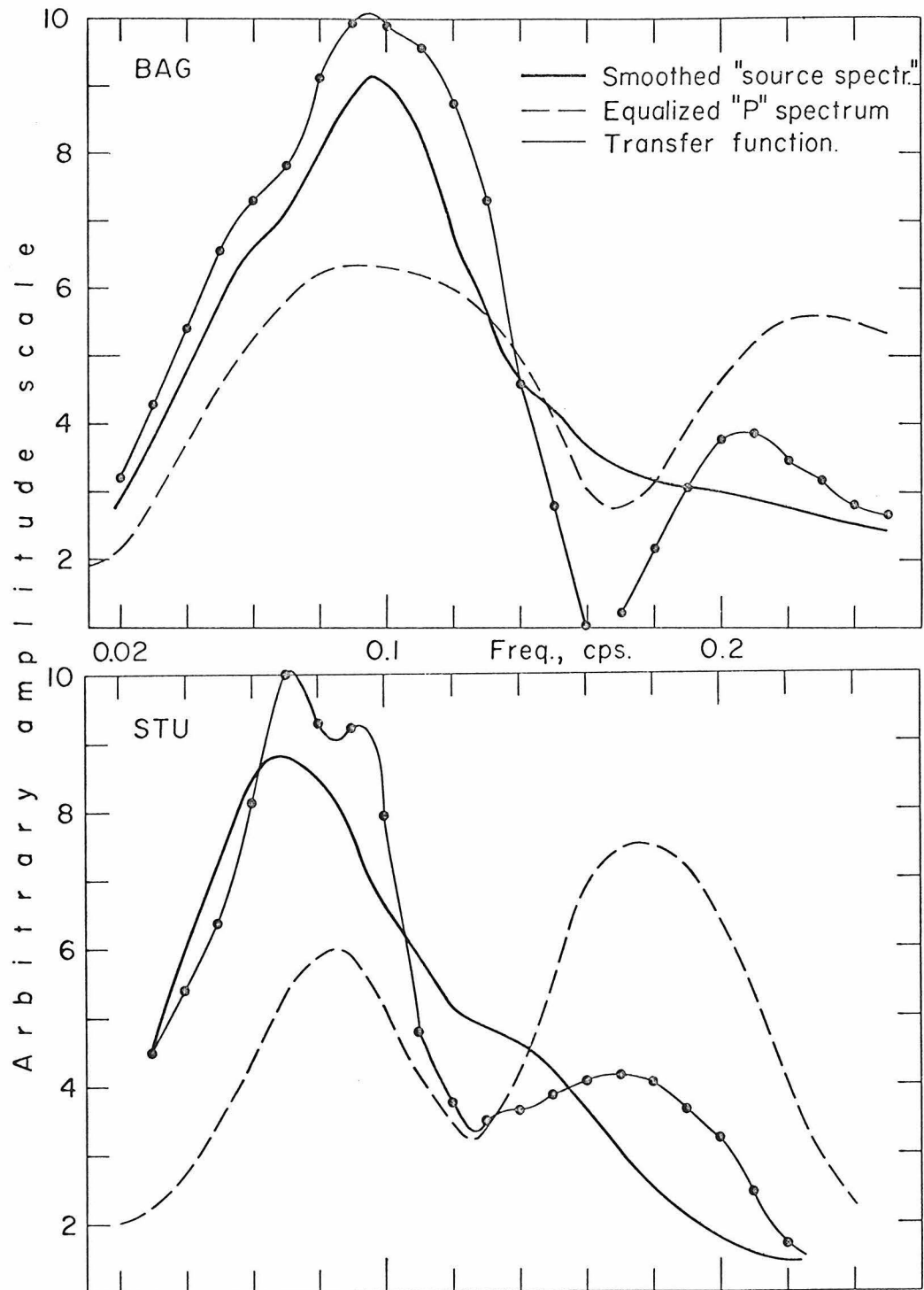


Fig. 14

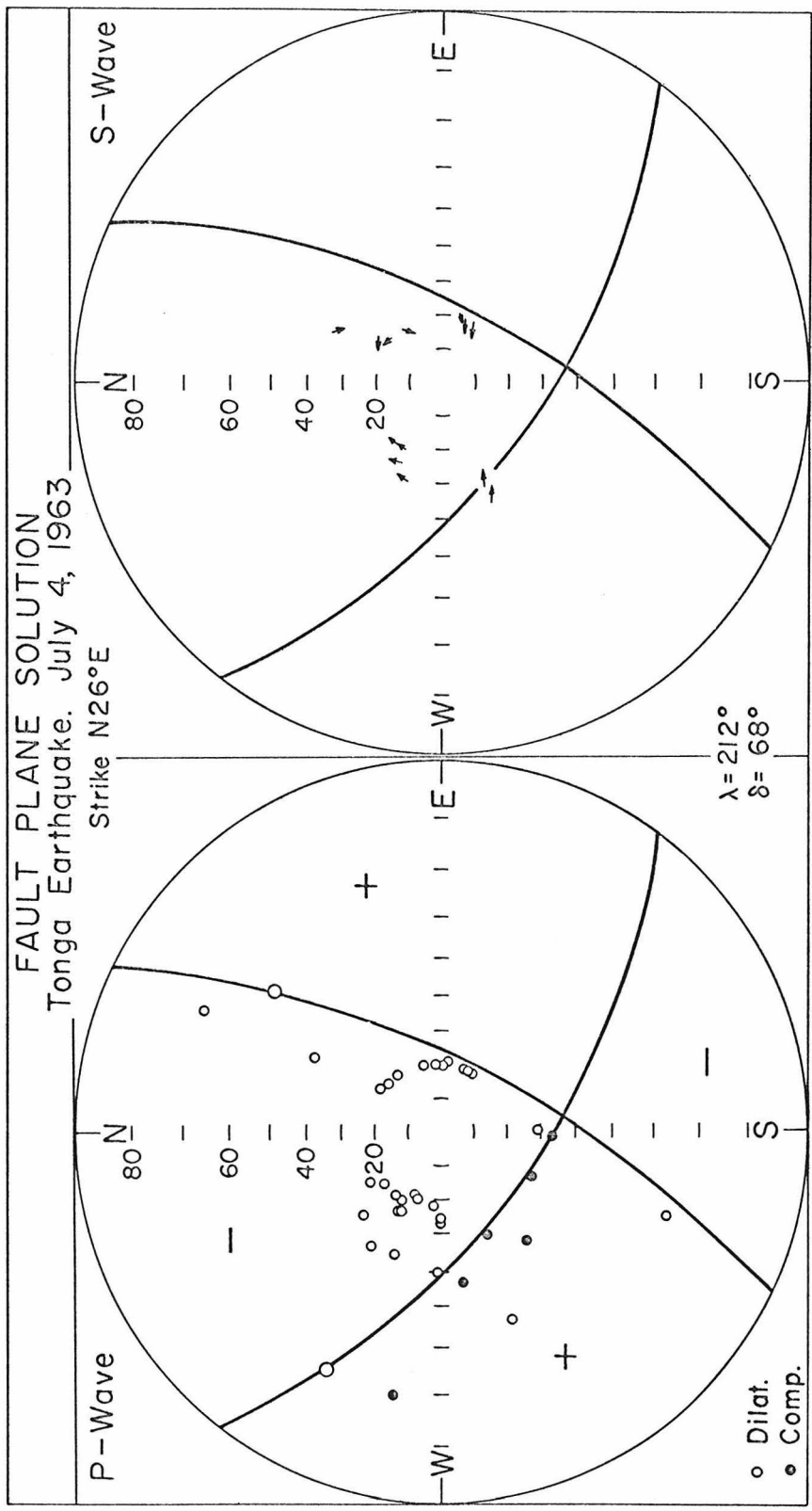


Fig. 15

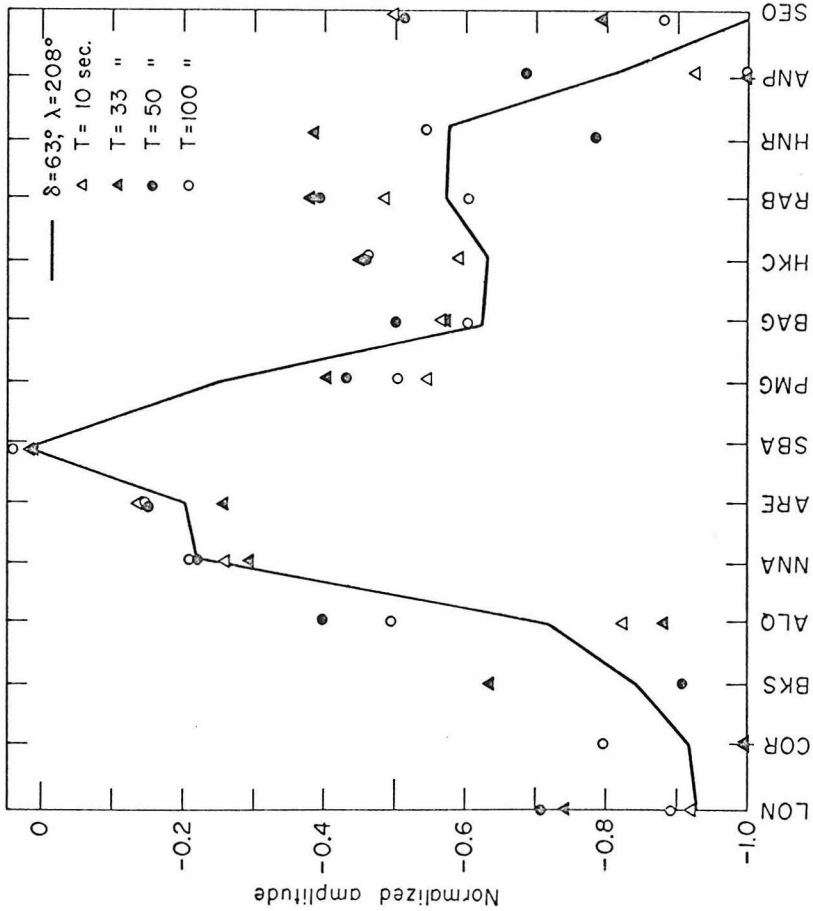
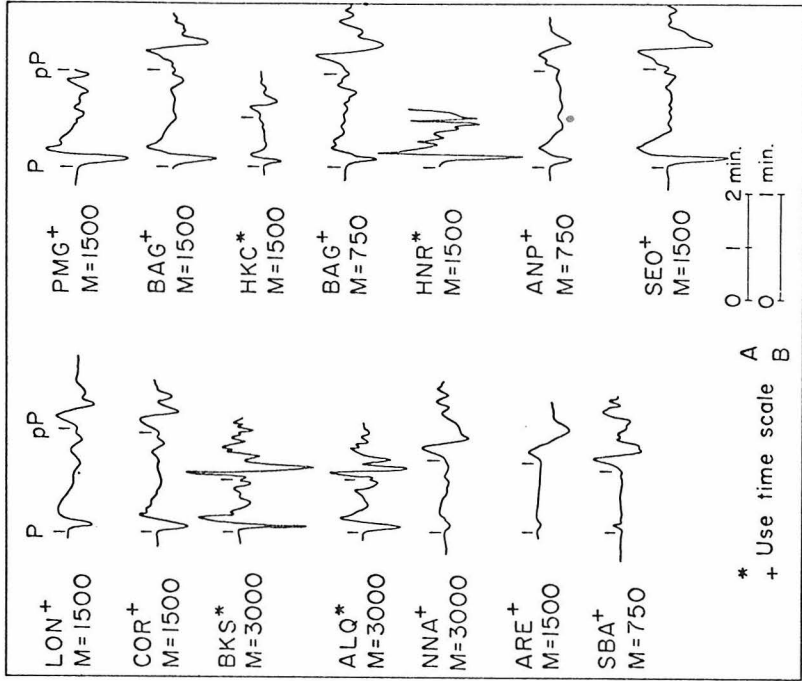


Fig. 16

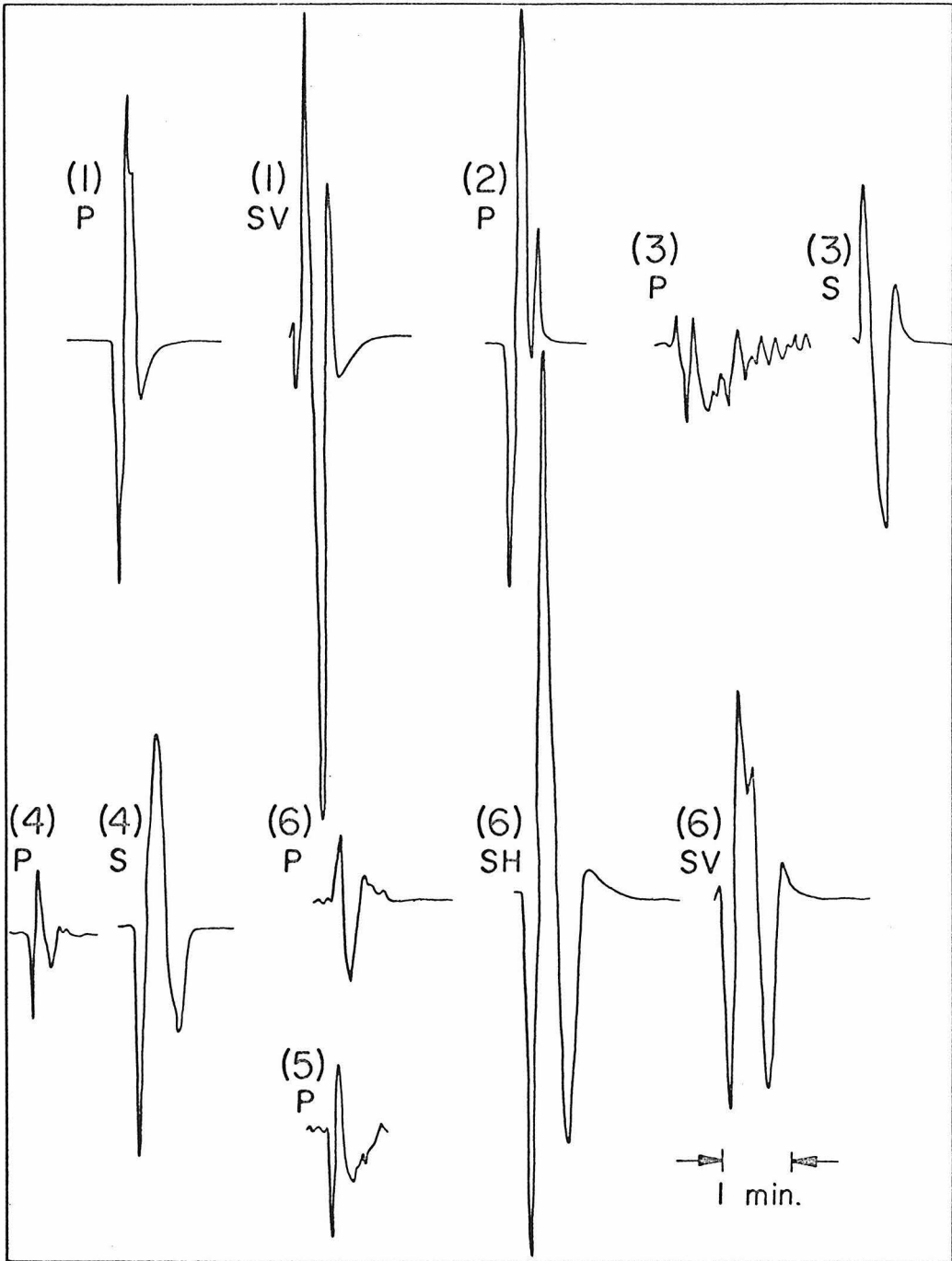


Fig. 17

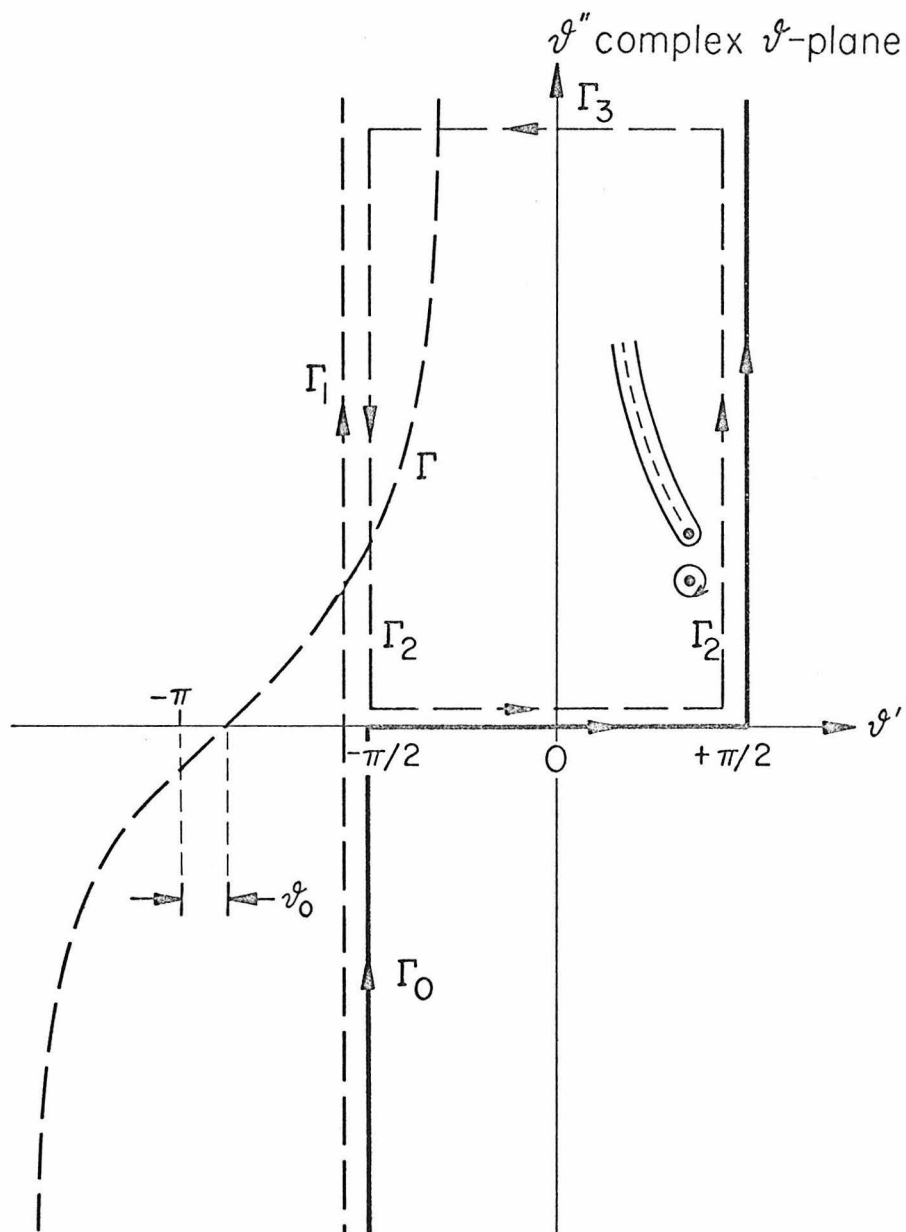


Fig. 18

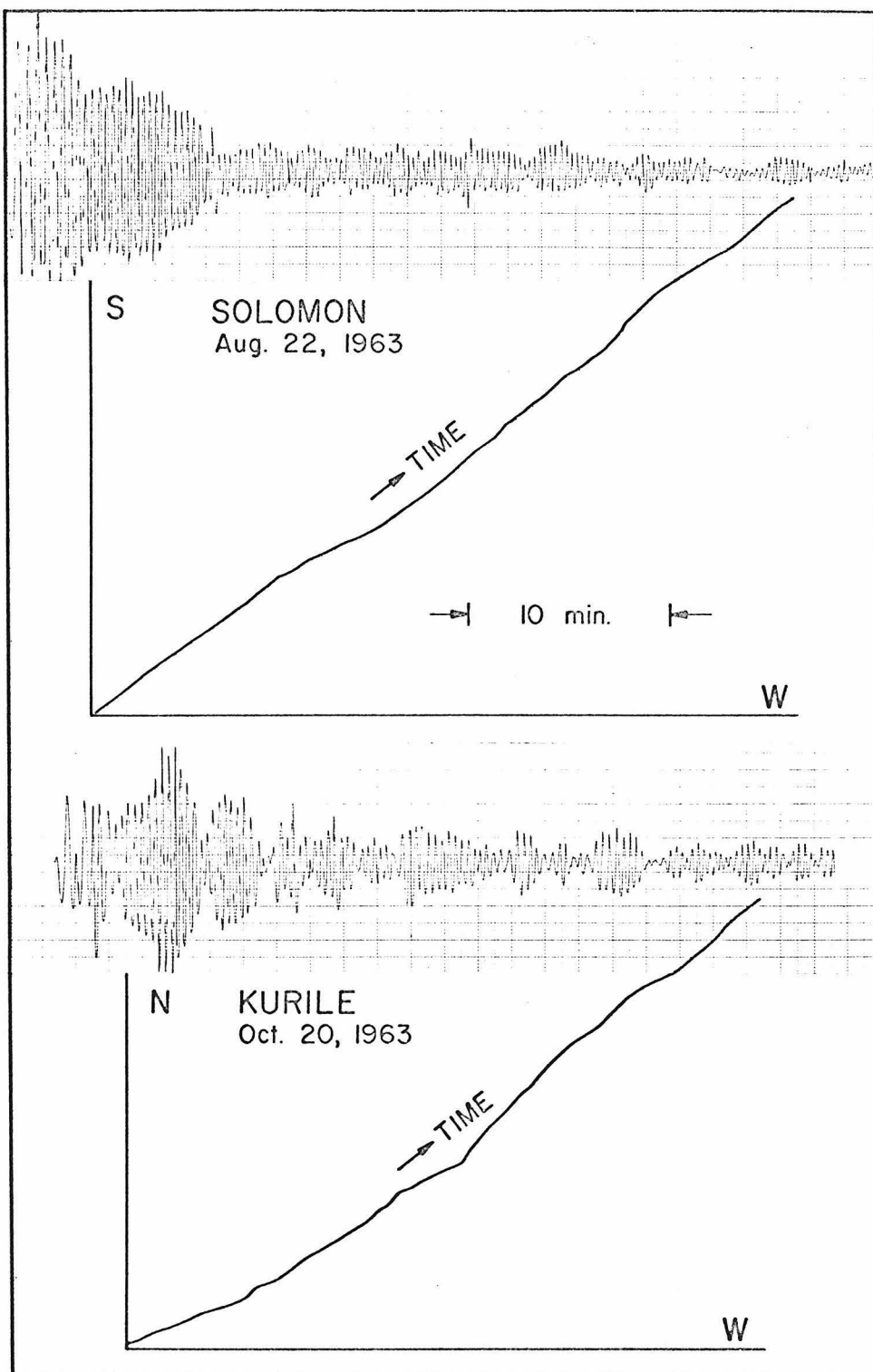


Fig. 19

Appendix I

Attenuation of Body Waves

The surface wave Q has been measured by several authors. Ben-Menahem (1965) compiled his work into a set of curves for Q of Rayleigh and Love wave. Since surface waves sample an average Q over the depth, it is necessary to invert these data to obtain Q (the intrinsic Q) as a function of r. Anderson et al (1964) have developed a technique for inverting Q and presented a few possible Q models, for the shear waves. By assuming a ratio of Q_p/Q_s we can easily have a Q model for P wave.

The total attenuation of a body wave along the ray can be written as

$$e^{-\int \gamma(\omega, s) ds}$$

and the integral can be written as

$$I = \frac{\omega}{2} \int \frac{ds}{Q(r) V(s)}$$

where s is the integration parameter along the ray and V(r) the velocity distribution ray we have the relation $r = r(s)$.

Let

$$\eta = r/v$$

$$\rho = r/v \sin i$$

where i is the angle of incidence, the integral can be written as

$$I = \frac{\omega}{2} \int \frac{F(\eta)}{\eta^2 - \rho^2} d\eta$$

where

$$F(\eta) = \eta/Q(\eta) \left(1 - \eta \frac{dv}{ds}\right)$$

Teng (1965) used MM8Q₂ and MM8Q_β models of Anderson et al (1965) for Q used a polynomial to fit the computed F(η). The integral can then be computed numerically whenever the ray is specified.

Appendix II

Integration of Body Wave Radiation Pattern

Let

$$\alpha_1 = \frac{1}{2} \sin\lambda \sin 2\delta$$

$$\beta_2 = \frac{1}{2} \sin\delta \cos\lambda$$

$$\beta_1 = \sin\lambda \cos 2\delta$$

$$\beta_2 = \cos\lambda \cos\delta$$

$$\text{Then } R_P(\theta, \phi) = 4\alpha_1 \cos\theta + 4(\alpha_2 \sin 2\phi - \alpha_1 \sin^2\phi) \sin^2\theta$$

$$+ (\beta_1 \sin\phi + \beta_2 \cos\phi) \sin 2\theta$$

$$R_{SH}(\theta, \phi) = \left[\alpha_1 \sin\phi + \alpha_2 \cos 2\phi \right] \sin\theta$$

$$+ \left[\beta_1 \cos\phi + \beta_2 \sin\phi \right] \cos\theta$$

$$R_{SV}(\theta, \phi) = \left[\alpha_1 (1 + \sin^2\phi) + \alpha_2 \sin 2\phi \right] \sin 2\theta$$

$$+ \left[\beta_1 \cos\phi + \beta_2 \sin\phi \right] \cos 2\theta$$

The integral we have to compute is

$$I = \int_0^{2\pi} \int_0^{\pi} R^2(\theta, \phi) \sin\theta \, d\theta \, d\phi$$

They are, for the three wave types

$$I_p = \int_0^{2\pi} \int_0^{\pi} \left\{ 16 \alpha_1^2 \cos^4 \theta + 16 (\alpha_2 \sin \phi - \alpha_1 \sin^2 \phi)^2 \sin^4 \theta \right. \\ \left. + (\beta_1 \cos \phi + \beta_2 \sin \phi)^2 \sin^2 2\theta \right. \\ \left. - 32 \alpha_1^2 \sin^2 \phi \cos^2 \theta \sin^2 \theta \right\} \sin \theta \, d\theta \, d\phi$$

$$I_{SH} = \int_0^{2\pi} \int_0^{\pi} \left\{ (\alpha_1^2 \sin^2 2\phi + \alpha_2^2 \cos^2 2\phi) \sin^2 \theta + (\beta_1^2 \cos^2 \phi + \beta_2^2 \sin^2 \phi) \right. \\ \left. \cdot \cos^2 \theta \right\} \sin \theta \, d\theta \, d\phi$$

$$I_{SV} = \int_0^{2\pi} \int_0^{\pi} \left\{ \left[\alpha_1^2 (9/4 + \frac{1}{4} \cos^2 2\phi) + \alpha_2^2 \sin^2 2\phi \right] \sin^2 2\theta \right. \\ \left. + \left[\beta_1^2 \cos^2 \phi + \beta_2^2 \sin^2 \phi \right] \cos^2 2\theta \right\} \sin \theta \, d\theta \, d\phi$$

Note we have already eliminated the terms that vanishes.

The individual definite integrals in these expressions are

$$\int_0^{\pi} \cos^4 \theta \sin \theta \, d\theta = \frac{2}{5}$$

$$\int_0^{\pi} \sin^5 \theta \, d\theta = \frac{16}{15}$$

$$\int_0^{\pi} \sin^2 2\theta \sin \theta \, d\theta = \frac{16}{15}$$

$$\int_0^{\pi} \cos^2 2\theta \sin \theta \, d\theta = \frac{14}{15}$$

$$\int_0^{2\pi} \cos^2 2\phi \, d\phi = \pi$$

$$\int_0^{2\pi} \sin^2 2\phi \, d\phi = \pi$$

$$\int_0^{2\pi} \sin^2 \phi \, d\phi = \pi$$

$$\int_0^{2\pi} \cos^2 \phi \, d\phi = \pi$$

The results are

$$I_p = \frac{4}{15} \pi$$

$$I_{sH} = \frac{4}{3} \pi \left[\alpha_1^2 + 4 \alpha_2^2 \right] + 2/3 \pi \left[\beta_1^2 + \beta_2^2 \right]$$

$$I_{sV} = \frac{\pi}{15} \left[19 \alpha_1^2 + 16 \alpha_2^2 \right] + \frac{14}{15} \pi \left[\beta_1^2 + \beta_2^2 \right]$$

Appendix III

Method of Integration for the Integral (7.4)

We shall use the integral (7.4) of BLK as an example to illustrate the method of integration used.

$$\begin{pmatrix} u \\ v \\ w \end{pmatrix} = \frac{S}{(2\pi)^3} \int_{-\infty}^{\infty} \frac{d\omega}{i\omega} \int_{-\infty}^{\infty} d\xi \int_{-\infty}^{\infty} d\eta \frac{\xi\eta\zeta'}{\mathcal{R}} \begin{pmatrix} \xi \\ \eta \\ \zeta \end{pmatrix} e^{i(\omega t - \xi x - \eta y - \zeta z)} \quad (7.4)$$

Let us consider the integral

$$I = \int_{-\infty}^{\infty} d\xi \int_{-\infty}^{\infty} d\eta \frac{\xi\eta\zeta'}{\mathcal{R}} \begin{pmatrix} \xi \\ \eta \\ \zeta \end{pmatrix} e^{-i(\xi x + \eta y + \zeta z)}$$

Change the variables ξ, η to θ and ϕ via the transformations

$$\begin{aligned} x &= r \sin\theta_0 \cos\psi & \xi &= \rho \sin\theta \cos\phi \\ y &= r \sin\theta_0 \sin\psi & \eta &= \rho \sin\theta \sin\phi \\ z &= r \cos\theta_0 & \zeta &= \rho \cos\theta. \end{aligned} \quad (I.1)$$

The Jacobian of the transformation is

$$\frac{\partial(\xi, \eta)}{\partial(\theta, \phi)} = \rho^2 \cos\theta \sin\theta$$

In order to keep the original integration limits, θ has to be extended to imaginary values. We choose the contour in the complex θ plane such that the wave will be bounded as $z \rightarrow \infty$. Thus, we stipulate the path to be from 0 to $\pi/2$ to $i\infty$. The integration on ϕ will be from 0 to 2π .

Before integration the singularities of the integrand has to be mapped. Substituting (I.1) into the integrand, we obtain, for the θ dependent part

$$V(\theta) = \frac{4 \cos\theta \sin^2\theta \sqrt{n^2 - \sin^2\theta}}{(n^2 - \sin^2\theta)^2 + 4 \cos\phi \sqrt{n^2 - \sin^2\theta} \sin^2\theta} \quad (\text{I.2})$$

where $n^2 = \frac{\alpha^2}{\beta^2}$; notice that $V(\theta) = V(-\theta)$, a fact which will be used later.

As a result of the presence of the radical we have two Riemann sheets jointed along the branch cut $\sqrt{n^2 - \sin^2\theta} = 0$, starting at the branch points $\theta = \pm \sin^{-1} n$. Let $\theta = \theta' + i\theta''$, using the relation

$$\sin\theta = \sin\theta' \cosh\theta'' + i \cos\theta' \sinh\theta'' \quad (\text{I.3})$$

$$\text{and } \cos\theta = \cos\theta' \cosh\theta'' - i \sin\theta' \sinh\theta''$$

and the condition

$$\text{Im } \rho \cos\theta < 0.$$

The branch points will be located at

$$(\pi/2, \sinh^{-1} n)$$

$$(-\pi/2, \sinh^{-1} n)$$

To locate the poles we have to solve the Rayleigh equation

$$(n^2 - 2\sin^2\theta)^2 + 4 \cos\theta \sqrt{n^2 - \sin^2\theta} \sin^2\theta = 0$$

or

$$\left(2 - \frac{n^2}{\sin^2\theta}\right)^2 + 4 \frac{\sqrt{1 - \sin^2\theta}}{\sin^2\theta} - 1 \sqrt{\frac{n^2}{\sin^2\theta} - 1} = 0$$

which is the conventional half-space Rayleigh equation with the substitutions

$$\frac{1}{\sin^2\theta} = c^2/\alpha^2$$

and

$$\frac{n^2}{\sin^2\theta} = c^2/\beta^2$$

(See, e.g., Ewing, Jardetzky and Press, 1957). For Poisson solid the roots we are interested in are given by

$$\frac{n^2}{\sin^2\theta} = 2 - 2/\sqrt{3}$$

or

$$\sin\theta = \pm \frac{\sqrt{3}}{2 - 2/\sqrt{3}} > 1.$$

Again let $\theta = \theta' + i\theta''$, there are four poles

$$\theta' = \pi/2 \qquad \theta'' = \sinh^{-1} \frac{\sqrt{3}}{2 - 2/\sqrt{3}}$$

$$\theta' = -\pi/2 \qquad \theta'' = \sinh^{-1} \frac{\sqrt{3}}{2 - 2\sqrt{3}}$$

$$\theta' = \pi/2 \qquad \theta'' = 0 + \sinh^{-1} \frac{\sqrt{3}}{2 - 2\sqrt{3}}$$

$$\theta' = -\pi/2 \qquad \theta'' = 0 - \sinh^{-1} \frac{\sqrt{3}}{2 - 2\sqrt{3}}$$

The integration sheet will be defined by

$$\text{Im } \cos\theta < 0$$

$$\text{i.e., } \sin\theta' \sinh\theta'' < 0.$$

The poles are

$$\theta' = \frac{\pi}{2} \qquad \theta'' = \sinh^{-1} \frac{\sqrt{3}}{2 - 2\sqrt{3}}$$

$$\theta' = \pi/2 \qquad \theta'' = \sinh^{-1} \frac{\sqrt{3}}{2 - 2\sqrt{3}}$$

The location of poles, branch points, branch cut, path of integration is plotted in figure 18.

We are now ready to deform the path of integration. Before we do that, we shall first write down the integral (7.4) of BLK in its new form under the transformations (I.7):

$$\begin{aligned} \vec{u}_p &= \frac{S\hat{r}}{(2\pi)^3} \int_{-\infty}^{\infty} F(\omega) e^{i\omega t} d\omega \int_0^{\pi/2+i\infty} d\theta \int_0^{2\pi} d\phi \sin\theta V(\theta) \sin\phi \cos\phi \\ &\quad \cdot \rho \sin\theta \sin\theta_0 \cos(\phi - \psi) + \cos\theta \cos\theta_0 \\ &\quad e^{-i\rho r} (\sin\theta \sin\theta_0 \cos(\phi - \psi) + \cos\theta \cos\theta_0) \\ &= \frac{S\hat{r}}{(2\pi)^3} \int_{-\infty}^{\infty} F(\omega) e^{i\omega t} d\omega \int_0^{\pi/2+i\infty} d\theta \int_0^{2\pi} d\phi \sin\theta V(\theta) \sin\phi \cos\phi \\ &\quad \frac{id}{dr} e^{i\rho r} (\sin\theta \sin\theta_0 \cos(\phi - \psi) + \cos\theta \cos\theta_0) \end{aligned}$$

where, as in BLK,

$$\hat{r} = \begin{pmatrix} \sin\theta \cos\phi \\ \sin\theta \sin\phi \\ \cos\theta \end{pmatrix}$$

Now the ϕ integration can be performed first:

$$\int_0^{2\pi} \sin\phi \cos\phi e^{i\rho r \sin\theta \sin\theta_0 \cos(\phi - \psi)} d\phi$$

$$= -2\pi \sin\psi \cos\psi J_2(\rho r \sin\theta \sin\theta_0).$$

Now

$$J_2(z) = \frac{1}{2} \left[-H_2^{(2)}(-z) + H_2^{(2)}(z) \right]$$

Using the relation $V(\theta) = V(-\theta)$, the integral can be written as

$$\vec{u}_p = \frac{-\hat{S}r}{(2\pi)^3} \int_{-\infty}^{\infty} F(\omega) e^{i\omega t} d\omega \frac{d}{dr} \frac{1}{2} \int_{-\pi/2-i\infty}^{+\pi/2+i\infty} \sin\theta V(\theta) H_2^{(2)}(\rho r \sin\theta \sin\theta_0) e^{-i\rho r \cos\theta \cos\theta_0} d\theta$$

Keeping only the first term of the asymptotic expansion of $H_2^{(2)}$ the expression in the parenthesis can be written as

$$\frac{1}{2} \frac{\sqrt{2}}{\pi\rho r} \int_{-\pi/2-i\infty}^{+\pi/2+i\infty} \frac{\sqrt{\sin\theta}}{\sqrt{\sin\theta_0}} V(\theta) e^{-i\rho r \cos(\theta - \theta_0)} d\theta e^{i\pi/4} \quad (I.4)$$

It is immediately clear that the saddle point is at $\theta = \theta_0$, since we require

$$\frac{d}{d\theta} \cos(\theta - \theta_0) = -\sin(\theta - \theta_0) = 0$$

that falls between $-\pi/2$ and $+\pi/2$ and the only solution for this equation is $\theta = \theta_0$. Now we want to deform to a contour such that we can separate the surface wave from the body waves. As depicted in figure 18, the original contour Γ_0 can be reduced to the sum of contours Γ_1, Γ_2 .

Γ_2 can be closed in the manner as shown in figure 18. It is clear from (I.4) that the contribution from Γ_3 tends to 0, due to the exponential. Therefore

$$\int_{\Gamma_1} = \int_B + 2\pi i \text{ Res P.}$$

Now for the integral

$$\int_{\Gamma_1} \frac{\sqrt{\sin\theta}}{\sqrt{\sin\theta_0}} V(\theta) e^{-i\rho r \cos(\theta - \theta_0)} d\theta$$

we see immediately that $\theta' = \theta_0$ is the saddle point, and remembering the identities (I.3) we have the path of constant phase (steepest ascent) in the θ plane (Γ)

$$\cos(\theta' - \theta_0) \cosh\theta'' = 1$$

The path is shown in figure 18; in the plane of integration the process of deformation will not cross any singularity. The results obtained are the same as in BLK.

The residue contribution is

$$\frac{\sqrt{1}}{\sqrt{2\pi\rho r}} \frac{\sqrt{\sin\theta}}{\sqrt{\sin\theta_0}} \frac{4 \cos\theta \sin^2\theta \sqrt{\eta^2 - \sin^2\theta}}{d \frac{d}{d\theta} \left[(\eta^2 - \sin^2\theta) + 4 \cos\theta \sqrt{\eta^2 - \sin^2\theta} \sin^2\theta \right]} e^{-i\rho r \cos(\theta - \theta_0)}$$

evaluated at the Rayleigh Pole.

Appendix IV

Variation of Angle of Incidence of
Oceanic Rayleigh Wave

Because of the high energy content of higher frequency surface wave, it is important to distinguish the waves that are directly from the source, and the waves that have been diffracted at discontinuities on boundaries, although it is possible that surface wave energy is only a minor part in the total energy budget as we have demonstrated both experimentally and theoretically. Such caution is necessary when we want to compare the energy content of Rayleigh wave and Love wave. Both theoretical and experimental group velocity curves show that around a period of 18 seconds the dispersion is the severest for an oceanic path. The group velocity drops from 3.0 km/sec at 17 seconds to about 1.2 km/sec at 15 seconds. Owing to the fact that the relative excitation at this period is very high (Harkrider and Anderson, 1966), the energy associated with this part of the dispersion curve is quite significant compared to the rest of the Rayleigh wave train as can be seen on seismograms, recorded at Pasadena, of South Sea earthquakes with a long oceanic path.

The group velocity curve at these periods is very sensitive to the crustal structure; as the real earth is not homogeneous horizontally, the wave path will deviate from the great circle path. Or rather, at a station, the oceanic wave may arrive via different path at

different time. We have computed the angle of incidence for two oceanic Rayleigh wave trains: they are presented in figure 19. They indicate that the beats could very well be the result of interference of waves traveling by different path. In the figure the Solomon Island earthquake was recorded at Pasadena with a long but almost monotonously decreasing Rayleigh train, the corresponding variation of the angle of incidence is not very pronounced. In contrast the records for Kurile earthquake show a complicated Rayleigh wave with numerous beats; the corresponding angle of incidence plot displays a rather striking variation in the angle. The great circle path from Kurile to Pasadena passes continental margins and complex structures; this may explain the variations.

PART II

REFLECTED WAVES AND CRUSTAL STRUCTURES

Abstract

Haskell's formulation for reflection of the body waves at the base of a solid crust is extended to include overlying liquid layers. Normalized displacement and the phase shift at the base of the crust as a function of angle of incidence and frequency are calculated for two continental models and an oceanic model. Complex reflection coefficients are inverse-Fourier transformed numerically to the time domain to show the change of pulse shape upon reflection. These time traces show that the water layer of the oceanic model causes the main difference between continental and oceanic reflections. Sample seismograms from a deep shock were compared to the theoretical records; they are found to be consistent. PP waves from a deep earthquake recorded at Tonto Forest Seismic Array were processed to display the details of an oceanic PP wave.

TABLE OF CONTENTS

	Page
Introduction.....	1
Method of Computation.....	5
Layer Matrices.....	5
Fourier Synthesis.....	18
Results of Computation.....	20
Crustal Models.....	20
Contour Maps of Reflection Coefficients.....	21
Synthesized Records.....	25
Velocity Structure and Waveform.....	30
Discussion.....	32
Observation of PP Waves.....	37
Conclusion.....	41
References.....	43
List of Tables.....	48
Tables.....	49
Figure Captions.....	51
Figures.....	54
Appendix.....	76
Reflected SH Waves.....	76

Introduction

A fundamental problem in seismology is the determination of elastic wave fields in a realistic spherical earth model; the solution should include not only the direct field but also reflected, and refracted waves, and free oscillations. The solution may contain waves that until now have not been noticed or have been ignored on the seismogram. However, the numerical computation techniques and the time required to obtain a theoretical seismogram are quite formidable. Meanwhile, employing more tractable methods involving far less labor, various aspects of the problem can be individually attacked. Such an approach has been successfully directed toward surface wave studies, using a plane layered system to investigate the dispersion of phase and group velocities.

The present problem is to study the effects of a layered crust, taken as a stack of plane layers, with or without a water layer on top, upon body wave pulses that enter into it and re-emerge after being reflected at the interfaces and free surface. We will study in particular the reflected compressional wave PP, and to a lesser extent, PS, the wave that comes out of the layered system as an S wave. The aim of this work is twofold: first, to clear up the problem of crustal structures and reflected waves, and secondly, to propose a method for world-wide mapping of crustal structures using reflected waves from earthquake sources.

The problem of the surface reflected PP wave has been studied extensively, from a different viewpoint by Gutenberg and Richter (1935),

Byerly et al (1949), and, more recently, Papazachos (1964). Most of the quantitative work in these studies is concerned with the determination of the peak to peak amplitude ratio PP/P , or the variation in the angle of incidence. With the knowledge that the variation of parameters in the mantle is gradual, while that in the crust is most often abrupt, the differences between P and PP are expected to be attributable to the crustal influences. This conclusion has led Gutenberg and Richter (1935) to investigate the difference in crustal structures beneath the Pacific Ocean, the Atlantic Ocean and under the continents, based on the ratio PP/P , but others (Byerly et al, 1949, Ben-Menahem et al, 1965) have indicated or implied that the fluctuation of this ratio could result from the radiation pattern of the source, rather than the crustal structure at the point of reflection. In any event, a great deal of information is lost in investigations using only the maximum amplitude of the time pulses.

The other surface reflected waves, namely, PS , SS , and SP have not received much attention. PS and SP are often superposed either on each other, for shallow earthquakes, or on other body waves for deeper earthquakes; they are occasionally prominent, but have to be used with care. SS waves, on the other hand, often appear as a prominent and well-isolated phase.

In most of the former work the reflection was assumed to occur at the free surface of a half-space or at the interface of two half-spaces in contact; in such cases the reflection coefficients are frequency independent. Calculations using the Haskell-Thomson matrix

formulation show that the dependence becomes accentuated as frequency deviates from 0. The functional relationship between the reflection coefficients and the angle of incidence and frequency is best displayed as a contour map. Both amplitude and phase-shift have been computed for three crustal models, one oceanic and two continental, and plotted as contour maps. These maps enable us to predict the behavior of reflected waves at various epicentral ranges, recorded by instruments with different band-pass characteristics. In order to compare the time pulse on the seismogram with Haskell-Thomson theory we have Fourier-synthesized the complex reflection coefficients for several angles of incidence for the three models mentioned above as well as variations of them. We found that the pulse shapes of the reflected waves indicate the nature of the crust at the point of reflection far more conclusively than do the amplitudes. To show this we have compared the synthesized traces with long-period PP seismograms from the Banda Sea earthquake of March 21, 1964, and we have also attempted to obtain a detailed mid-Pacific structure using seismic array data.

Recent advances in seismic array data processing render it possible to look at small signals that are buried in noise on ordinary seismograms. It is thus possible to use an array to map the crustal structures at points of reflection of reflected P or S waves. This method requires much less labor than conventional refraction profile methods and vast areas can be investigated very expeditiously. Moreover, regions that are inaccessible can be readily investigated. Although surface wave methods have the same advantages, the present

method can yield much finer horizontal and vertical resolutions than can the surface wave method where only the average structure between recording stations can be delineated. However, the present method can be successful only when we have a certain amount of velocity control at the point of reflection.

The same technique can be applied to study the nature of crustal discontinuities by looking at the short-period pulse shapes. And we can also extend the method to detecting possible discontinuities in the upper mantle and to the studying of the influence of upper mantle structure on long-period S waves.

The solution for reflected sound pulses in a perfectly elastic sphere shows that the path for PP reflection is, rather than maximum or minimum, a stationary time path; associated with such a path are the lack of a clear start, and a logarithmic type infinity connected with the amplitude. In a realistic attenuating earth, the latter type of behavior could hardly be expected, although a distortion of pulse shape and a change in amplitude not related to the nature of the reflector may be expected.

Method of Computation

Layer Matrices

If we can represent the incident wave as a plane wave, and the crust as a stack of plane parallel layers, then we can use the Thomson-Haskell matrix method (Haskell, 1953, 1950, 1962; Thomson, 1960). The theory has been discussed in the works of Haskell and Thomson above, and in papers by Dorman (1962) and Harkrider (1964b). Although the discussions of the layered systems including liquid layers are quite general in the works of Dorman and Harkrider, the techniques considered are oriented toward surface waves. On the other hand, Haskell (1960, 1962) formulated the problem of body wave reflection as well as transmission for solid crusts, without extensive discussion, however, for reflections. Since there are some aspects of the matrix formulation which are of particular interest when a model of an oceanic structure is considered, a brief development of the theory for a layered system consisting of liquid layers overlying solid layers will be presented here (Figure 1).

We will use the same notations as Haskell (1953). The dilatation and rotation in the m th layer can be written as

$$\Delta_m = \left[\Delta'_m e^{-ikr_{\alpha m} z} + \Delta''_m e^{ikr_{\alpha m} z} \right] e^{i(\omega t - kx)} \quad (1)$$

and

$$\omega_m = \left[\omega'_m e^{-ikr_{\beta m} z} + \omega''_m e^{ikr_{\beta m} z} \right] e^{i(\omega t - kx)}$$

respectively, where

$k = \omega/c =$ wave number in direction of x

$$r_{\alpha m} = + \left[(c/\alpha_m)^2 - 1 \right]^{1/2} \quad c > \alpha_m$$

$$- i \left[1 - (c/\alpha_m)^2 \right]^{1/2} \quad c < \alpha_m$$

$$r_{\beta m} = + \left[(c/\beta_m)^2 - 1 \right]^{1/2} \quad c > \beta_m$$

$$- i \left[1 - (c/\beta_m)^2 \right]^{1/2} \quad c < \beta_m$$

$$\gamma_m = 2(\beta_m/c)^2$$

with

$\rho_m =$ density

$\lambda_m, \mu_m =$ Lamé elastic constants

$$\alpha_m = \left[(\lambda_m + 2\mu_m)/\rho_m \right]^{1/2} = \text{velocity of propagation of dilatational waves}$$

$$\beta_m = \left[\mu_m/\rho_m \right]^{1/2} = \text{velocity of propagation of rotational waves}$$

In a solid layer both Δ_m and ω_m exist, while in a liquid layer or a layer where the rigidity vanishes, $\omega_m \equiv 0$. The displacements and

stresses corresponding to the above definitions are

$$\begin{aligned}
 u &= - (\alpha_m/\omega)^2 (\partial\Delta_m/\partial x) - 2(\beta_m/\omega)^2 (\partial\omega_m/\partial z) \\
 w &= - (\alpha_m/\omega)^2 (\partial\Delta_m/\partial z) + 2(\beta_m/\omega)^2 (\partial\omega_m/\partial x) \\
 \sigma &= \rho_m \left\{ \alpha_m^2 \Delta_m + 2 \beta_m^2 \left[(\alpha_m/\omega)^2 (\partial^2\Delta_m/\partial x^2) \right. \right. \\
 &\quad \left. \left. + 2(\beta_m/\omega) (\partial^2\omega_m/\partial x\partial z) \right] \right\} \quad (2)
 \end{aligned}$$

$$\begin{aligned}
 \tau &= 2\rho_m \beta_m^2 \left[- (\alpha_m/\omega)^2 (\partial^2\Delta_m/\partial x\partial z) \right. \\
 &\quad \left. + (\beta_m/\omega)^2 \left\{ (\partial^2\omega_m/\partial x^2) - (\partial^2\omega_m/\partial z^2) \right\} \right]
 \end{aligned}$$

The boundary conditions to be satisfied at the interfaces are that these four quantities be continuous.

Inserting (1) into (2) and writing it in matrix form we obtain

$$\begin{bmatrix} \dot{u}_m/c \\ \dot{w}_m/c \\ \sigma_m \\ \tau_m \end{bmatrix} = D_m \begin{bmatrix} \Delta_m' + \Delta_m'' \\ \Delta_m' + \Delta_m'' \\ \omega_m' + \omega_m'' \\ \omega_m' + \omega_m'' \end{bmatrix} \quad (3)$$

where

$$\begin{aligned}
 D_m = & \begin{aligned}
 & -(\alpha_m/c)^2 \cos P_m & i(\alpha_m/c)^2 \sin P_m & -\gamma_m r_{\beta m} \cos Q_m & i\gamma_m r_{\beta m} \sin Q_m \\
 & i(\alpha_m/c)^2 r_{\beta m} \sin P_m & -(\alpha_m/c)^2 r_{\beta m} \cos P_m & -i\gamma_m \sin Q_m & \gamma_m \cos Q_m \\
 & -\rho_m \alpha_m^2 (\gamma_m - 1) \cos P_m & i\rho_m \alpha_m^2 (\gamma_m - 1) \sin P_m & -\rho_m c^2 \gamma_m r_{\beta m} \cos Q_m & i\rho_m c^2 \alpha_m r_{\beta m} \sin Q_m \\
 & -i\rho_m \alpha_m^2 \gamma_m r_{\alpha m} \sin P_m & \rho_m \alpha_m^2 \gamma_m r_{\alpha m} \cos P_m & i\rho_m c^2 \gamma_m (\gamma_m - 1) \sin Q_m & -\rho_m c^2 \gamma_m (\gamma_m - 1) \cos Q_m
 \end{aligned}
 \end{aligned}$$

with d_m = layer thickness and, $Q = k r_{\beta m} d_m$

If we put the origin at $(m - 1)$ th interface, then the velocities and stresses at that interface are related to the dilatation and rotation in that layer by

$$\begin{bmatrix} \dot{u}_m - 1/c \\ \dot{w}_m - 1/c \\ \sigma_m - 1 \\ \tau_m - 1 \end{bmatrix} = E_m \begin{bmatrix} \Delta'_m + \Delta''_m \\ \Delta'_m - \Delta''_m \\ \omega'_m - \omega''_m \\ \omega'_m + \omega''_m \end{bmatrix} \quad (4)$$

Where E_m is obtained by setting $d_m = 0$ in D_m :

$$E_m = \begin{vmatrix} -(\alpha_m/c)^2 & 0 & -\gamma_m r_{\beta m} & 0 \\ 0 & -(\alpha_m/c)^2 r_{\alpha m} & 0 & \gamma_m \\ -\rho_m \alpha_m^2 (\gamma_m - 1) & 0 & -\rho_m c^2 \gamma_m r_{\beta m} & 0 \\ 0 & \rho_m \alpha_m^2 \gamma_m r_{\alpha m} & 0 & -\rho_m c^2 \gamma_m (\gamma_m - 1) \end{vmatrix}$$

From (3) and (4) we may obtain the relation between the displacements and stresses at the m th interface and at the $(m - 1)$ th interface by eliminating $\Delta'_m + \Delta''_m$ etc.:

$$\begin{bmatrix} \dot{u}_m/c \\ \dot{w}_m/c \\ \sigma_m \\ \tau_m \end{bmatrix} = D_m E_m^{-1} \begin{bmatrix} \dot{u}_{m-1}/c \\ \dot{w}_{m-1}/c \\ \sigma_{m-1} \\ \tau_{m-1} \end{bmatrix} \quad (5)$$

where

$$E_m^{-1} \begin{vmatrix} 2(\beta_m/\alpha_m)^2 & 0 & (\rho_m \alpha_m^2)^{-1} & 0 \\ 0 & c^2(\gamma_m - 1)/\alpha_m^2 r_{\alpha m} & 0 & (\rho_m \alpha_m^2 r_{\alpha m})^{-1} \\ (\gamma_m - 1)/\gamma_m r_{\beta m} & 0 & -(\rho_m c^2 \gamma_m r_{\beta m})^{-1} & 0 \\ 0 & 1 & 0 & (\rho_m c^2 \gamma_m)^{-1} \end{vmatrix}$$

Let us define

$$A_m = D_m E_m^{-1}$$

then, evidently, one can write

$$\begin{bmatrix} \dot{u}_{m-1}/c \\ \dot{w}_{m-1}/c \\ \sigma_{m-1} \\ \tau_{m-1} \end{bmatrix} = A_{m-1} A_{m-2} \cdots A_1 \begin{bmatrix} \dot{u}_0/c \\ \dot{w}_0/c \\ \sigma_0 \\ \tau_0 \end{bmatrix} \quad (6)$$

and to relate the dilatations and rotations in the half-space (the nth "layer") we have

$$\begin{bmatrix} \Delta'_m + \Delta''_m \\ \Delta'_m - \Delta''_m \\ \omega'_m - \omega''_m \\ \omega'_m + \omega_m \end{bmatrix} = E_m^{-1} A_{m-1} A_{m-2} \cdots A_1 \begin{bmatrix} \dot{u}_0/c \\ \dot{w}_0/c \\ \sigma_0 \\ \tau_0 \end{bmatrix} \quad (7)$$

The formulation just outlined is for solid layers. If we have two liquid layers or a liquid layer and a solid layer in contact, then the boundary conditions would require w/c and σ to be continuous at the boundary instead of all four quantities. Namely,

$$\begin{bmatrix} \dot{w}_m/c \\ \sigma_m \end{bmatrix} = L_m \begin{bmatrix} \dot{w}_{m-1}/c \\ \sigma_{m-1} \end{bmatrix} \quad (8)$$

where

$$L_m = \begin{vmatrix} \cos P_m & i r_{\alpha m} (\rho_m c^2)^{-1} \sin P_m \\ i \rho_m c^2 r_{\alpha m}^{-1} \sin P_m & \cos P_m \end{vmatrix}$$

This can be obtained from $D_m E_m^{-1}$ by setting $\beta_m = 0$ and take the four central elements.

In a system of n layers (figure 7) let the upper ℓ ($\ell < n$) layers be liquid and the remaining layers be solid. Then the relations among the horizontal particle velocity at the liquid-solid interface, the vertical particle velocity at the free surface and the amplitude of the dilatational and rotational waves in the half space may be expressed as

$$\begin{bmatrix} \Delta_n' + \Delta_n'' \\ \Delta_n' - \Delta_n'' \\ \omega_n' - \omega_n'' \\ \omega_n' + \omega_n'' \end{bmatrix} = E_n^{-1} A_{n-1} A_{n-2} \cdots A_{\ell+1} F_\ell \cdots F_1 \begin{bmatrix} \dot{u}_\ell/c \\ \dot{w}_0/c \\ 0 \\ 0 \end{bmatrix} \quad (9)$$

where:

- 1) E_n^{-1} and A_i ($i = \ell + 1, n - 1$) are the standard 4×4 layer matrices for the solid layers
- 2) \dot{u}_ℓ is the horizontal component of the particle velocity at the top of the $\ell + 1$ layer (that is the top of the solid section)
- 3) \dot{w}_0 is the vertical component of the particle velocity at the free surface.
- 4) F_j ($j = 1, \ell$) is a 4×4 matrix of the form

$$\begin{vmatrix} 1 & 0 & 0 & 0 \\ 0 & \cos P_m & i r_{\alpha m} (\rho c^2)^{-1} \sin P_m & 0 \\ 0 & i r_{\alpha m}^{-1} (\rho c^2) \sin P_m & \cos P_m & 0 \\ 0 & 0 & 0 & 1 \end{vmatrix}$$

5) c is the phase velocity

If we let

$$E_n^{-1} A_{n-1} A_{n-2} \cdots A_{\ell+1} F_\ell \cdots F_1 = J$$

which is dependent on the layer parameters, the compressional velocity, the shear velocity, the thickness and the density, we then have from (1) a set of four simultaneous linear equations containing the unknowns Δ'_n , Δ''_n , ω'_n , ω''_n , \dot{u}_r/c and \dot{w}_o/c :

$$\begin{aligned} \Delta'_n + \Delta''_n &= J_{11} \dot{u}_\ell/c + J_{12} \dot{w}_o/c \\ \Delta'_n - \Delta''_n &= J_{21} \dot{u}_\ell/c + J_{22} \dot{w}_o/c \\ \omega'_n - \omega''_n &= J_{31} \dot{u}_\ell/c + J_{32} \dot{w}_o/c \\ \omega'_n - \omega''_n &= J_{41} \dot{u}_\ell/c + J_{42} \dot{w}_o/c \end{aligned} \tag{10}$$

Since we are interested in the displacement at the free surface (or interface) the reflected waves for dilatational waves or rotational waves we can set either $\Delta''_n = 1$, $\omega''_n = 0$ or $\Delta''_n = 0$, $\omega''_n = 1$; these correspond to incident P wave and incident S waves respectively.

In the case of an incident P wave with unit dilatational amplitude: $\Delta''_n = 1$ and $\omega''_n = 0$, the four remaining quantities can be solved as

$$\Delta'_{np} = D^{-1} (J_{11} + J_{12}) (J_{32} - J_{42}) - (J_{12} + J_{22}) (J_{31} - J_{41})$$

$$\omega'_{np} = 2D^{-1} J_{32} J_{41} - J_{31} J_{42}$$

$$\dot{u}'_{lp}/c = 2D^{-1} J_{32} - J_{42} \quad (11)$$

$$\dot{w}'_{op}/c = 2D^{-1} J_{41} - J_{31}$$

Similarly in the case of an incident S wave of unit rotational amplitude, $\Delta''_n = 0$ and $\omega''_n = 1$, we have

$$\Delta'_{ns} = 2D^{-1} J_{12} J_{21} - J_{11} J_{22}$$

$$\omega'_{ns} = D^{-1} (J_{12} - J_{22}) (J_{31} + J_{41}) - (J_{11} - J_{21}) (J_{32} + J_{42})$$

$$\dot{u}'_{ls}/c = 2D^{-1} J_{12} - J_{22} \quad (12)$$

$$\dot{w}'_{os}/c = 2D^{-1} J_{21} - J_{11}$$

where

$$D = (J_{11} - J_{21}) (J_{32} - J_{42}) - (J_{12} - J_{22}) (J_{31} - J_{41})$$

using the following relations which have been proven by Haskell (1962):

$$E_{pp} + E_{ps} = 1$$

then the equations derived from (13) may be written as

$$\begin{aligned}\dot{u}_r/c &= S_{11} \dot{u}_r/c + S_{12} \dot{w}_o/c \\ \dot{w}_r/c &= S_{21} \dot{u}_r/c + S_{22} \dot{w}_o/c \\ \sigma_r &= S_{31} \dot{u}_r/c + S_{32} \dot{w}_o/c \\ \tau_r &= S_{41} \dot{u}_r/c + S_{42} \dot{w}_o/c\end{aligned}\tag{14}$$

From the properties of the matrices F_j described above and in Haskell (1953), it is easily seen that

$$S_{1j} = S_{j1} = 0 \quad j = 2,3,4$$

$$S_{11} = 1$$

Thus, equations (13)-(14) may be written as

$$\begin{aligned}\dot{u}_r/c &= \dot{u}_r/c \\ \dot{w}_o/c &= S_{22} \dot{w}_o/c \\ \sigma_r &= S_{32} \dot{w}_o/c \\ \tau_r &= 0.\end{aligned}$$

and

$$E_{ss} + E_{sp} = 1$$

we can, from the value of Δ'/Δ'' , have an estimate of the value of ω'_n/Δ'' and vice versa. Since Δ'_n and ω'_n , for a certain crustal structure model, are functions of frequency and angle of incidence, we can draw contour maps giving the variations of amplitude or phase of Δ'_n and ω'_n as a function of the two above-mentioned variables. Using the relations 15 and 16, one can expect how the contour of the other would behave.

There are two other cases where we can readily apply the matrix technique: Namely, 1) Oceanic bottom seismometry and 2) ocean with ice as the top layer.

1) Ocean bottom seismometry. We have implied in the equations (9) that

$$\begin{bmatrix} \dot{u}_r/c \\ \dot{w}_r/c \\ \sigma_r \\ \tau_r \end{bmatrix} = F_r \cdots \cdots F_1 \begin{bmatrix} \dot{u}_r/c \\ \dot{w}_o/c \\ 0 \\ 0 \end{bmatrix} \quad (13)$$

If we let

$$F_r \cdots \cdots F_1 = S$$

2) Ocean with ice on top. Such configuration has been considered in detail by Dorman (1962) in connection with Rayleigh wave propagation in a layered system with alternating solid and liquid layers. To be more specific we shall assume that our system consists of a solid layer (ice) overlying a liquid layer (ocean), which in turn overlies a stack of solid layers (the crust); in this case, using the same development as before, we arrive at the relation

$$\begin{bmatrix} \Delta'_n + \Delta''_n \\ \Delta'_n - \Delta''_n \\ \omega'_n - \omega''_n \\ \omega'_n + \omega''_n \end{bmatrix} = E_n^{-1} A_{n-1} \cdots A_3 F_2 A_1 \begin{bmatrix} \dot{u}_2/c \\ \dot{w}_o/c \\ 0 \\ 0 \end{bmatrix}$$

with notations having the meaning as elsewhere.

Fourier Synthesis

In order to show the effect of crust on reflected pulses at the bottom of the crust we have synthesized the complex Fourier spectrums for several models and angles of incidence using the following formula which was first discussed by Aki (1960) and subsequently extended by Harkrider (1964 a):

$$\begin{aligned}
 h(t) &= \sum_i \int_{\omega_i - \frac{\Delta\omega_i}{2}}^{\omega_i + \frac{\Delta\omega_i}{2}} \bar{A}(\omega) \cos\phi(\omega) \, d\omega \\
 &= 2 \sum_i \left\{ \bar{A}_i \Delta\omega_i \cos \omega_i (t - \tau_i) \frac{\sin \left[\frac{\Delta\omega_i}{2} (t - t_{gi}) \right]}{\left[\frac{\Delta\omega_i}{2} (t - t_{gi}) \right]} \right. \\
 &\quad - \left(\frac{\partial \bar{A}}{\partial \omega} \right)_i \Delta\omega_i \frac{\sin \omega_i (t - \tau_i)}{(t - t_{gi})} \left[\frac{\sin \left[\frac{\Delta\omega_i}{2} (t - t_{gi}) \right]}{\left[\frac{\Delta\omega_i}{2} (t - t_{gi}) \right]} \right. \\
 &\quad \left. \left. - \cos \frac{\Delta\omega_i}{2} (t - t_{gi}) \right] \right\}
 \end{aligned}$$

$h(t)$ - the synthesized waveform

$\bar{A}(\omega)$ = amplitude spectrum

$\phi(\omega)$ = phase spectrum

τ_i = phase delay

t_{gi} = group delay

ω_i = frequency

$\Delta\omega_i$ = frequency increment.

Results of Computation

Crustal Models

Three crustal models were chosen to show the effects of crustal structures on the variations of reflection coefficients as a function of angle of incidence and frequency. The three models are: (1) average oceanic structure (Raitt, 1963), (2) Peru-Altiplano, (Steinhart and Meyer, 1951), and (3) Central U.S. average crust (McEvelly, 1964). They are listed in Table 1.

The oceanic model is an average of many profiles in the Pacific and Atlantic; no attempt was made to differentiate Atlantic and Pacific crusts since they are probably not significantly different from each other (Raitt, 1963). The depth of the water layer for the oceanic model is taken as 4.5 km. As we shall see later, this depth affects the reflected pulse in a rather interesting way; we have changed the depth to 3 km and 2 km to demonstrate its effect on the synthesized waveform.

The two continental models were chosen to demonstrate the influence of different crustal thickness on reflected waves as well as the differences between the oceanic and continental crusts.

The shear velocities and densities of the Peru-Altiplano and oceanic models are not given in the literature. The shear velocities are calculated from the compressional velocities by assuming various Poisson ratios, while the densities are those deduced from gravity measurements.

Contour Maps of Reflection Coefficients

For each of these models the quantities Δ'_n/Δ''_n and ω'_n/ω''_n at the bottom of the crust are calculated for angles of incidence ranging from 0 to 90 degrees, at $\frac{1}{2}$ degree intervals, and for frequencies from 0 to 0.45 cps, at 0.003 cps intervals. These quantities are reflection coefficients at the bottom of a crust; they include all the multiple reflections between interfaces in the layers above the half-space, since the boundary conditions are properly taken care of at each interface. The reflection coefficients also include the complex conversion of energy between P and S at each interface. The numbers are on-line contoured on IBM 7094 computer.

Figures 2 - 4 contain the reflected P wave amplitude response for the three models just mentioned. Figures 5 and 6 contain the phase shift contours for Central U.S. Crust and average oceanic crust respectively. In figures 7 and 8 we present the PS conversion response for the average oceanic crust and Peru-Altiplano crust and figures 9 and 10 are the corresponding phase shift contours. The correspondence between the angle of incidence and epicentral distance is indicated in figure 11; it was calculated by Ritzema (1958) based on Jeffrey's travel time data.

Looking at the two pairs of contours, figures 2 and 7 and figures 4 and 8, it is clear that where the reflected P amplitude is large, the reflected S is small and vice versa. This of course is what we expected because of the relation

$$E_{pp} + E_{ps} = 1,$$

where the energies are normalized to the incident energy, (Haskell, 1962).

It is clear that for very low frequency the reflection coefficients approach those calculated by Gutenberg (1944) and Brekhovskikh (1960) for a homogeneous half-space. As frequency increases the behavior of the coefficients begins to have significant differences from those of a homogeneous half-space, which are independent of frequency. We have stated above that different angles of incidence corresponds to different epicentral distances from the source; the frequency dependence of reflection coefficients implies therefore that interpreting amplitude ratios PP/P which have been observed with different instruments or at different distances under the assumption of a homogeneous half-space at the reflection point may yield results that are devoid of meaning.

It might be proper to point out here that evidences from both body waves and surface waves show a frequency dependence of amplitude attenuation (Ben-Menahem, 1965; Anderson and Julian, 1965; Teng, 1965); the high frequency waves, say, 1 second waves, suffer a much higher attenuation than 20 second waves. Because of this phenomenon, and the high attenuation in the upper mantle (Kovach and Anderson, 1964; Anderson, 1966), the short period data, at distances for which a large portion of the ray path is within the upper mantle, may have amplitudes much smaller

(after being corrected for geometrical spreading) than at distances for which passage through the upper mantle is shorter. As attenuation for S waves is generally much higher than for P waves, the effect would be more pronounced for S than for P. In our present study the attenuation will not be considered; we will concentrate our attention on the longer waves (around 20 seconds) and on those crustal effects which would not be marred by attenuation.

For PP waves the middle portion of the contour map with angle of incidence between 25° and 50° is of interest, while for pP the smaller angles of incidence are pertinent. However, in dealing with pP, consideration has to be given to the curvature of the wave front, as the distance between the source and the reflector is often small for the wave length concerned, and the assumption of a plane wave incident at the base of the crust may not be valid. This is born out by the fact that curvature of the wave front is responsible for the generation of Rayleigh type of surface waves - a plane wave when incidental on a plane layered media will not generate such a wave; evidently a part of the energy will be lost upon reflection as far as the P and S body waves are concerned. Nevertheless, if the condition $kR \gg 1$, where k , as usual, denotes wave number, and R , the distance between source and receiver is satisfied, geometrical optics is applicable, and the Haskell-Thomson matrix formulation is a first order approximation to the problem (Brekhovskikh, 1960; Fuchs, 1965).

For PS waves, the range of the angle of incidence on the contour map that is of interest is between 38° and 70° . As in the case of pP the smaller angle of incidence would correspond to PS. But as indicated by the contours in figures 7 and 8, the conversion from P and S at those angles is extremely small; this is the reason why pS has very seldom been positively identified on the seismogram.

The reflected P contours of all three models are rather similar in their general features. For angles of incidence below 15° the values are high (≥ 0.9). They decrease as the angle increases; their minimum is around 70° and they increase to 1 near 90° , with bands of highs across the contour map. The variation with frequency has a very obvious scaling phenomenon. For example, figures 3 and 4 have quite a lot in common regarding the distribution of local minimums and maximums, however, figure 4, the contour for the thick Peru-Altiplano structure, has a much faster variation than figure 3, for the Central U.S. structure. This is expected from the fact that the reflection coefficient from a layered crust is actually scaled by a dimensionless parameter formed by a combination of k , H_j and $\sin i$ where k is the wave number, H_j the thickness of the layers and i the angle of incidence (Fernandez, 1965). The details of variations, nevertheless, do depend on the distribution of the elastic properties in each layer.

The phase shift contours (figures 4,5,9 and 10) have the same scaling phenomena.

From the contour map it is easy to see at what angle of incidence we would expect the amplitude to be small, variations rapid or phase shift turning complicated. For PP waves, such phenomena occur near an angle of incidence of 50° , which corresponds to an epicentral distance of 40° , and the situation becomes worse beyond 50° . This can perhaps explain (Gutenberg and Richter, 1935) that PP waves are not very prominent for epicentral distances smaller than 40° .

Synthesized Records

Numerical Fourier synthesis scheme discussed in the previous section was used to transform to time domain the frequency dependent, complex Fourier spectrum computed by employing the Haskell-Thomson matrix method for several angles of incidence for a flat frequency spectrum (Fourier transform of $\delta(t)$) input. Synthesized records enable us to gain some insight as to what happens to the wave after its impingement on the bottom of the crust. Although the amplitude response contour together with the phase-shift contour for one crustal model contain all the information concerning the reflection, yet it is from the synthesized records that we can see the relative magnitude of reflections from interfaces and their temporal behaviors. The complex spectrums were multiplied by the response of a simulated 30 - 100 pendulum-galvanometer system, critically damped, to suppress ultra long-period components for better synthesis and for comparison

with the seismograms recorded by long-period WWNSS stations. The operations involved can be summed up as

$$\bar{f}(t) = \int_{-\omega_0}^{\omega_0} F(\omega) H(\omega) e^{-i\omega t} d\omega = \int_{-T_1}^{T_2} f(\tau) h(t-\tau) d\tau$$

where

$\bar{f}(t)$ = synthesized trace

$F(\omega)$ = the complex frequency response of the crust

$H(\omega)$ = the complex frequency response of the 30-100
instrument

$f(t)$ = impulse time response of the crust

$h(t)$ = impulse time response of the 30-100 instrument

The synthesized records for reflected P waves at angles of incidence equal to 30, 45 and 60 degrees for the three crustal models are presented in figures 12, 13, 14. The bottom two traces in figures 12 and 14 are what the seismograms would appear to be for an instrument located on a continent having the average Central U.S. structure. (Namely, the crustal transmission response at the recording station was multiplied to the spectrum described above before synthesizing). The others illustrate the crustal effects at the point of reflection for different models. Comparing boxes A and C of

figure 12 and boxes A and B of figure 14, it is evident that the salient features of the incident wave at the bottom of the crust under the receiver are preserved; oscillations corresponding to reflections at interfaces during transmission through the crust are added to the incident wave.

The reflected P waves from an oceanic crust (figure 12) are rather complicated owing to the presence of two major acoustic impedance mismatches; one at the solid-liquid interface and the other at the free surface. Thus we expect to see two main reflections at an interval depending on the depth of the ocean. Further, the water layer on top of the solid is an efficient energy trap; for a P wave incident in water against a solid, about 65% of the energy is reflected, only 35% (See Ergin, 1952) refracted. This is the reason why we can see so many multiply reflected waves on the synthesized trace. The arrivals on each trace can be identified quite easily. The first signal, small, and often preceded by a low frequency hump, which is due to the imperfection of our Fourier synthesis procedure, is the reflection of the bottom of the crust. Then comes the reflection from the interface, and following it, at regular intervals, are the multiply reflected waves. The time interval between two successive reflections is approximately equal to the two-way travel time for a P wave in the water layer. This results from the fact that the contrast between the P wave velocity in the half-space and that in the water is so great, for the angle of incidence

considered the ray path is close to the normal in the water layer, and hence, the travel time approaches that for a vertical transit. Notice also the polarity is changed for every successive arrival, due to the phase change occurring at the free surface upon each reflection. The amplitude of these waves decreases as time goes on as a result of the energy being transmitted or converted to the S wave energy at each reflection from the bottom of the ocean. As the ocean depth decreases the interval between the multiply reflected waves decreases; for a two-thousand meter deep ocean they are no longer very distinct. This is demonstrated in box B of figure 12. The water depth was decreased from 4.5 km to 3 km for the upper trace and to 2 km for the lower trace.

Much the same description can be applied to the PS waves (figure 15). Although only a small portion of the energy is converted to SV waves for a P wave incident in water against the solid, the amplitudes of the later arrivals are not as distinctive as in the case of PP waves. The PS wave may consequently appear to be "cleaner" than the PP wave, and we shall see later the difference between a PS wave reflected under oceanic crust would not be very much different from a PS wave reflected under the continent. (cf. figures 15 and 16).

The continental reflections (figures 13 and 14) are quite different from their oceanic counterparts. There is only one surface that will give large reflection; that is the free surface. On each trace the clearly isolated first arrival, which appears immediately

after the wave hits the bottom of the crust, is the reflection from the base of the crust. Following it is another arrival of smaller amplitude reflected off the interfaces, and then comes the free-surface reflection, which is much larger than the preceding ones. Immediately following is another arrival which only shows a trace for $i_0 = 30^\circ$, but increases in size as the angle of incidence increases. The travel time of this wave corresponds to PSP wave, i.e. a P wave is converted an S wave upon impinging the crust and travels in the crust as an S wave, until it hits the free surface whereupon it is converted back to a P wave and comes out of the layered system as a P wave. The increase in amplitude as the angle of incidence is increased agrees well with this interpretation based on the contour map.

For all these arrivals, the interval between two successive waves and their amplitude relations are determined by the distribution of elastic parameters and the thickness of the crust. This is born out by the otherwise rather similar synthesized records for the Central U.S. crust and the Peru-Altiplano crust. In contrast to oceanic reflections, very little energy is trapped in the layered system; the records for continental models are therefore relatively clean compared to records for oceanic models.

The PS waves (figure 16) show features very similar to those of figure 14, although there is a very obvious polarity change. The arrival we identified as PSP in figure 14 has the same travel time

as the free surface reflection in figure 16.

In the Appendix we shall give a discussion on reflected SH-SH waves.

Velocity Structure and the Waveform

Crustal structures are often viewed as a stack of layers with sharp discontinuities. However, some parts of North America, central Wisconsin, for example, are thought to have a crust with a linear gradient. The actual configuration will, of course, affect the wave form, since the reflection coefficients are a function of frequency (see Brekovskikh, 1960). Since our method cannot handle a continuous variation of layer parameters, we have approximated the gradient by dividing the crust into finer layers. To show the frequency dependence, we have simulated both long (30-100) and short period (1-0.75) seismometers in our synthesis.

The appearance of pulses recorded by a short period instrument is considerably different from that recorded by a long period instrument because of more severe phase distortion. Figure 17 is a short period record for a Central U.S. model. This is to be compared to the middle trace of figure 13. The arrival time of the free surface reflection in figure 17 coincides with that in figure 13; however, the pulse is much shorter as it should be (note the difference in time scale), and has more swings. The arrivals after the main pulse can readily be identified in this case.

We have first divided both the bottom two kilometers and the top two

kilometers of the crust into five layers of 0.4 km each with parameters increasing slowly downward (see figure 18). The synthesized long period record (top trace) is almost identical to the middle trace of figure 13 (at the same angle of incidence for a regular central U.S. crust). The short period record, on the other hand, shows a very different pulse shape (cf. figure 17). The difference seems to be due to the reverberations set up in the top layer.

When the whole crust is divided into 10 layers of 2 km each with parameters increasing linearly downward (see figure 19), the reflection from the bottom, which shows up clearly in figure 13, becomes very small; the long period record (top trace) has a much smoother appearance than that for models with only four layers; the short period record (bottom trace) shows faint interface reflections, and the free surface reflection resembles that of the bottom trace of fig. 18.

Based on these observations, it appears that for the purpose of determining crustal structure at the point of reflection for PP or PS, the pulse shapes of these waves will yield the necessary information if we have some control of the velocity at the point of reflection.

Discussion

We concluded in the last section that pulse shape of PP or PS could be employed to determine the nature of the crust at the point of reflection. This is assuming, in the first place, that the source time function is relatively simple - a fact which we can infer from the shape of P wave, and secondly, that the noise level on the seismogram is sufficiently low for us to discern those reflected arrivals with certainty. The first requirement can usually be met by a deep earthquake, with magnitude 7 or less. The second requirement is, on ordinary seismograms, hard to fulfill; microseisms as well as crustal reverberations set up by preceding signals will mar the shape of PP; the interface reflections will be buried in the noise. Under these conditions, the pulse shape can only reveal whether the crust is oceanic or continental. Detailed structure can be obtained only if we process these signals to filter out the noise, and recover the small interface reflections. We must remember, however, that the submarine topography in the case of oceanic reflections and the land topography in the case of continental reflections can modify the pulse shape considerably when the wave length we are observing is commensurate with the dimension of the topographical features. Further examples, mostly recorded by short-period instruments, can be found in the work by Gutenberg and Richter (1935).

Recent advances in seismometer array data processing show

promise that the signal-noise ratio enhancement can be effectively achieved for our purpose (figure 21; Johnson, 1966). It seems possible now to use an array of seismometers monitoring earthquakes and apply the method we described to map the crustal structures of a large part of the world. However, in order to obtain the impulse response of the crust, the effects of source time function, radiation patterns, attenuation and crustal transfer function at the receiver have to be taken into consideration. We shall describe briefly the approach to this problem.

The complex frequency spectrum $PP(\omega)$ can be written as

$$PP(\omega) = F(\omega) R(\omega) T(\omega, i_{pp}) e^{-\int_{C_2} \gamma(\omega, s) ds / G_{pp}}$$

Here,

$F(\omega)$ = the source spectrum,

G_{pp} = frequency independent geometric spreading factor

$R(\omega)$ = reflection transfer function at the point of reflection

$T(\omega, i_{pp})$ = transmission transfer function at the recording station for PP.

$\gamma(\omega)$ = attenuation coefficient
 $e^{-\int_{C_2} \gamma(\omega, s) ds}$ = the total attenuation of the wave along the PP ray path C_2 , and similarly, the P wave

spectrum can be written as

$$P(\omega) = \beta \frac{F(\omega)}{G_p} T(\omega, i_p) e^{-\int_{C_1} \gamma(\omega, s) ds}$$

where

β = the amplitude ratio at the source of the waves
that later reach the station as PP and P.

$T(\omega, i_p)$ = transmission transfer function of the crust
at the receiving station for P.

$e^{-\int_{C_1} \gamma(\omega, s) ds}$ = total attenuation of P along the ray path C_1 .

then

$$R(\omega) = \frac{PP(\omega)}{P(\omega) A(\omega)}$$

where

$$A(\omega) = e^{-\int_{C_2} \gamma(\omega, s) ds - \int_{C_1} \gamma(\omega, s) ds} \frac{T(\omega, i_{PP}) G_p}{T(\omega, i_p) G_{PP}}$$

In these expressions $T(\omega, i)$ can be calculated by the Haskell-Thomson matrix method, and $\gamma(\omega, s)$ was determined by Anderson and Julian (1965) and Teng (1965). As PP travels through the upper mantle and crust, where the attenuation is high, two more times than P does, so the high frequency components will be more severely

suppressed for PP than for P; to compensate for this effect is therefore very important in order to obtain the correct $R(\omega)$. The factor β can be obtained if we know the source radiation pattern (Ben-Menahem et al, 1965; Teng and Ben-Menahem, 1965).

After we obtain $R(\omega)$ we can Fourier-synthesize it to obtain the impulse response of the crust at point of reflection and then modify the crustal models pertinent to the specific area to fit the observed impulse response. It is desirable to use broad-band instruments for recording, to recover more information; however, short period data will enable us to determine the sharpness of discontinuities. Theoretically we can easily approximate a gradual change by using a stack of thin layers with gradual elastic parameter variation through the stack. (cf. figure 19).

It should be noted that the computations in this paper did not take into account either the curvature of the earth or the curvature of the wave front. The problem of reflected waves in a liquid sphere was treated by Jeffreys and Lapwood (1957), Burridge (1962) and Alterman and Kornfeld (1965) and in a solid sphere by Burridge (1963). One of the conclusions they reached is that for PP waves that correspond to stationary time paths the pulse shape is related to the P pulse as the Fourier integral is related to the Allied-Fourier integral. Thus if the source function is $\delta(t)$ the PP pulse will appear as $\delta'(t)$. Detailed discussion is given in Burridge (1963). The spherical effect can be incorporated into the results obtained in the

present work if the phenomenon should become salient in the frequency range under observation.

Observation of PP Waves

A number of observations was made of PP on actual seismograms. Good PP pulses could usually be found on the records for very shallow or deep earthquakes at distances such that PP is well isolated from phases such as P'', SKP, pPcP, etc. Then the main features of PP can be clearly discerned. While, in general, the long period seismograms have a higher signal to noise ratio than the short period seismograms, the time difference between the reflected arrivals is often smaller than the duration of the input pulse - as revealed by the duration of the direct P wave (figure 20). The interface and free surface reflection arrivals tend to merge into each other and it is quite impossible to distinguish the individual pulses. The difference between oceanic and continental reflections is, however, pronounced enough on long period records to be used to distinguish these two categories of crustal structures. In figure 20 selected PP waves from March 21, 1963 Banda Sea shock are presented to demonstrate this conclusion. The earthquake occurred at a depth of 350 km and has a magnitude of $6\frac{1}{2}$. Perusal of the travel time curves by Gutenberg and Richter (1936) shows that between epicentral distances of 70 and 125 degrees, PP waves would be separated from other arrivals by at least one minute. In the figure we have given the station abbreviations for each long period and short period WWNSS record; epicentral distances and the geographical locations of the points of reflection are listed in Table 2. The oceanic PP's at

ALQ, COL, LON and TUC are apparently quite distinctive compared to the continental PP at ATU and STU. The former group of records shows a number of arrivals following the incipient rise. On the COL trace we are able to detect arrivals that appear at 10 second intervals: at 18, 28, 38, and 48 seconds counting from the arrow. Taking into account of the angle of incidence in the water layer ($\sim 6.4^\circ$) and assuming a velocity of 1.5 km/sec, the water depth is found to be 7 kilometers approximately. The map indicates a water depth of over 3500 fathoms (~ 6.4 km) near the point of reflection. These arrivals could therefore be the multiple reflections in the water layer. The other three oceanic PP waves show the same type of behavior though with less distinctive later arrivals. At ATU and STU the PP waves have a very simple structure, conforming to our theoretical prediction. The reflection from the bottom of the crust (if there is one) can not be clearly discerned. The data cannot be used to obtain the crustal thickness at the point of reflection.

The short-period records are often cluttered with pulses generated by the incident wave in the crust at the receiver, possibly when passing other diffractive objects. Nevertheless, the difference between oceanic reflection and continental reflection is still quite clear. This is shown in figure 20, with two short-period traces for the same earthquake, COL and STU. On the COL trace, it is noticeable that the higher frequency content in PP waves is much less than that in the direct P at the same stations.

This effect, as we have asserted before, could be due to the relatively more severe attenuation for PP since it has travelled through the upper mantle two more times than P has, where the attenuation is high, and also to the band-pass nature of the reflector.

To further show the feasibility of using PP to map the world-wide crustal structure we have processed data from the Tonto Forest extended array. As the detail of the set-up of the array and the data processing has been described by Johnson (1966), we will not go into detailed discussion here. The PP wave we used is from another Banda Sea-deep earthquake (August 20, 1965). The results of processing eight channels of data is presented in figure 21. The processing is essentially a correlation filtering in the wave number-frequency plane, whereby only signals with a certain phase velocity can pass through the filter. The effectiveness of this method for signal-noise ratio enhancement is demonstrated by the difference between the unprocessed record and the final result (figure 21).

Based on our theoretical seismograms we have made the following interpretation (cf. figure 21): (1) is the reflection from the bottom of the crust, (2) is the reflection from the water-solid interface or possibly sediment-solid interface, (3) is the reflection from free surface and (4) is the wave that has made one more bounce in the water layer.

Judging from the amplitude ratio of (4) to (3), the next expected multiple reflection would be buried in the noise. In order to see the

later multiples we have to use longer period instruments and use the procedure described in the last section.

Conclusion

From the preceding discussion we see that PP/P is a function of frequency, depending not only on the structure at the point of reflection but also on the radiation pattern of the source, the structure under the receiver, and the absorption of wave energy while propagating along specific paths. Only after these factors are removed can we recover the spectral properties of the crust at the point of reflection.

The general characteristics of a PP pulse itself also indicate the gross nature of the crust, whether it is oceanic or continental at the point of reflection. However, to study the detailed structure we have to be able to read relatively small arrivals from discontinuities, and in order to have a measure of the sharpness of the discontinuity we have to use the amplitude data; for all these we are bound to resort to more effective signal-noise ratio enhancement methods.

We have mentioned before that in addition to PP and PS, the method used in the present work could easily be applied to SS and SP, and, if the condition $kR \gg 1$ is satisfied, to pP, pS, and sS. The short period data might be used to approach the last requirement. Thus, with the advancement in seismometer array data processing, we will be able to use the data from one array to study crustal structures in many areas of the Earth; we can employ pP, sS, sP for the region near the source and PP, PS, SS, and SP for regions between the

source and the recording station, to map the crusts in those areas. This method would require only very limited facilities and would yield results for vast areas on the earth, some parts of which are not easily accessible with conventional explosion equipment. The results would also be much more detailed than can be obtained by using surface wave data.

References

Aki, K.

1960. "Study of earthquake mechanism by a method of phase equalization applied to Rayleigh and Love Waves," J. Geophys. Res., 64: 729-740.

Alterman, Z., and P. Kornfeld

- 1965 "Shallow focus explosion in a liquid sphere," J. Royal Astron. Soc., 9: 121-152.

Anderson, D.L., and B.R. Julian

- 1965 "Travel times, velocities and amplitudes of body phases," Abstract of papers submitted to the annual meeting of the Seismol. Soc. Am., 1965.

Anderson, D. L.

- "Latest information from seismic observations", Ch. II, The Earth's Mantle. To be published.

Ben-Menahem, Ari, S. Smith, and Leon Teng

- 1965 "A procedure for source studies from spectrum of long-period seismic body waves," Bull. Seismol. Soc. Am., 55: 203-236.

Brekhovskikh, L. M.

- 1960 "Waves in layered media," Academic Press, New York.

Burridge, R.

- 1962 "The reflexion of high-frequency sound in a liquid sphere," Proc. Roy. Soc. London, A, 270: 144-154.

Burridge, R.

- 1963 "The reflexion of a pulse in a solid sphere," Proc. Roy. Soc. London, A, 276: 367-400.

Byerly, Perry, Alexis I. Mei, S.J., and Carl Romney

- 1949 "Dependence on azimuth of the amplitudes of P and PP," Bull. Seismol. Soc. Am., 39: 269-284.

Dorman, J.

- 1962 "Period equation for waves of Rayleigh type on a layered, liquid solid half-space," Bull. Seismol. Soc. Am., 52: 389-397.

Ergin, K.

- 1952 "Energy ratio of the seismic waves reflected and refracted at a rock-water boundary," Bull. Seismol. Soc. Am., 42: 349-372.

Fernandez, L. M.

- 1965 "The determination of crustal thickness from the spectrum of the P wave," Doctoral Dissertation, St. Louis University.

Fuch, K.

- 1966 "The transfer function for P-waves for a system consisting of a point source in a layered medium," Bull. Seismol. Soc. Am., 56: 75-108.

Gutenberg, B., and C. F. Richter

- 1935 "On seismic waves," (2nd paper), Gerlands Beitr. Geophys., 45: 280-360.

Gutenberg, B., and C. F. Richter

- 1936 Unpublished charts with data taken from "Materials for the studies of deep-focus earthquakes," Bull. Seismol. Soc. Am., 26: 341-390.

Gutenberg, B.

- 1944 "Energy ratio of reflected and refracted seismic waves," Bull. Seismol. Soc. Am., 34: 85-102.

Gutenberg, B., and C. F. Richter

- 1956 "Earthquake magnitude, intensity, energy and acceleration," (second paper), Bull. Seismol. Soc. Am., 46: 105-145.

Harkrider, D. G.

- 1964a "Propagation of acoustical gravity waves from an explosive source in the atmosphere," Part I. of Thesis, California Institute of Technology.

Harkrider, D. G.

- 1964b "Surface waves in multilayered elastic media, 1. Rayleigh and Love waves from buried sources in a multilayered elastic half-space," Bull. Seismol. Soc. Am., 54: 627-679.

Haskell, N. A.

- 1953 "The dispersion of surface waves on multilayered media," Bull. Seismol. Soc. Am., 43: 17-34.

Haskell, N. A.

- 1960 "Crustal reflection of plane SH waves," J. Geophys. Res., 65: 4147-4150.

Haskell, N. A.

- 1962 "Crustal reflection of P and SV waves," J. Geophys. Res.,
67: 4751-4767.

Jeffereys, H. and E. R. Lapwood

- 1957 "The reflexion of a pulse within a sphere," Proc. Roy. Soc.
London, A, 241: 455-479.

Johnson, L. R.

- 1966 "Measurement of mantle velocities of P waves with a large
array," Thesis, California Institute of Technology.

Kovach, R. L., and D. L. Anderson

- 1964 "Attenuation of shear waves in the upper and lower mantle,"
Bull. Seismol. Soc. Am., 54: 1855-1864.

McEvelly, T. V.

- 1964 "Central U.S. crust - upper mantle structure from Love
and Rayleigh wave phase velocity inversion," Bull. Seismol.
Soc. Am., 54: 1997-2015.

Mei, A.I., S. J.

- 1964 "The amplitude ratio PP/P as recorded by Galizin seismographs,"
Bull. Seismol. Soc. Am., 33: 149-196.

Papazachos, B.

- 1964 "Angle of incidence and amplitude ratio of P and PP waves,"
Bull. Seismol. Soc. Am., 54: 105-121.

Raitt, R. W.

- 1963 The Crustal Rocks, in "The Sea", edited by M.N. Hill,
Interscience Publishers, pp. 85-102.

Steinhart, J. S., and R. P. Meyer

1961 "Explosion studies of continental structure," Carnegie Inst.
Wash., Publication 622.

Teng, T. L., and A. Ben-Menahem

1965 "Mechanism of deep earthquakes from spectrums of isolated
body-wave signals, 1. The Banda Sea Earthquake of March 21,
1964," J. Geophys. Res., 70: 5157-5170.

Teng, T. L.

1965 "Amplitudes of body waves," Technical Report Contract
AF-49(638)-1337.

List of Tables

	Page
Table I. Crustal Models used in the Computations.....	49
Table II. Locations, epicentral distances of the stations and the geographical points of reflection for PP pertaining to Figure 10.....	50

Table I.

	Average Oceanic			Peru-Altiplano			Central U.S.			
	d	α	β	d	α	β	d	α	β	ρ
Top layer	4.50	1.50	0	4.1	5.3	3.0	11.0	5.10	3.50	2.70
2nd layer	0.45	2.0	1.0	21.2	6.2	3.59	9.0	6.40	3.68	2.90
3rd layer	1.75	5.0	2.88	39.6	6.70	3.94	18.0	6.70	3.94	2.90
4th layer	4.70	6.71	3.86							
Half-Space	∞	8.09	4.65	∞	8.0	4.70	∞	8.15	4.75	3.30

d = layer thickness α = P wave vel. β = S wave vel. ρ = density

Table II

	LOCATION	$\Delta(^{\circ})$	POINT OF REFLECTION
ALQ	Albuquerque, New Mexico, U.S.A.	122.6	Pacific Ocean
ATU	Athens, Greece	105.1	Northern India
COL	College, Alaska, U.S.A.	93.3	Pacific Ocean
LON	Longmire, Washington, U.S.A.	108.5	Pacific Ocean
STU	Stuttgart, Germany	113.5	Western China
TUC	Tucson, Arizona, U.S.A.	119.8	Pacific Ocean

Figure Captions

	Page
Figure 1. Geometry of the problem and numbering of layers and interfaces.....	54
Figure 2. Normalized P wave displacement at the base of the crust, $ \Delta'/\Delta'' $, for the average oceanic structure..	55
Figure 3. Normalized P wave displacement at the base of the crust, $ \Delta'/\Delta'' $, for the average Central U.S. Structure.....	56
Figure 4. Normalized P wave displacement at the base of the crust $ \Delta'/\Delta'' $, for the Peru-Altiplano structure....	57
Figure 5. Phase shift (fractions of a circle) for the reflected P wave at the base of the crust for the Central U.S. structure.....	58
Figure 6. Phase shift (fractions of a circle) for the reflected P wave at the base of the crust for the average oceanic structure.....	59
Figure 7. Normalized S wave displacement at the base of the crust, $ \omega'/\Delta'' $, for the Peru-Altiplano structure....	60
Figure 8. Normalized S wave displacement at the base of the crust, $ \omega'/\Delta'' $, for the average oceanic structure..	61
Figure 9. Phase shift (fraction of a circle) for the reflected S wave at the base of the crust for the Peru-Altiplano structure.....	62

Figure 10.	Phase shift (fraction of a circle) for the reflected S wave at the base of the crust for the average oceanic structure.....	63
Figure 11.	(i - Δ) curve for PP and PS (Ritzema, 1958).....	64
Figure 12.	Synthesized P reflections for average oceanic structure. (A) At the base of the crust. (B) At the base of the crust with water layer thickness decreased to 3 km for upper trace and to 2 km for lower trace. (C) Reflected wave transmitted through an average Central U.S. structure.....	65
Figure 13.	Synthesized P reflections for Central U.S. structure.....	66
Figure 14.	Synthesized P reflections for Peru-Altiplano structure. (A) At the base of the crust. (B) Reflected wave transmitted through an average Central U.S. Structure.....	67
Figure 15.	Synthesized S reflection (with P incident) for the Peru-Altiplano structure.....	68
Figure 16.	Synthesized S reflection (with P incident) for the average oceanic structure.....	69
Figure 17.	Synthesized short-period (simulated 1 - 0.75 seismometer) record of reflected P from the Central U.S. crust.....	70
Figure 18.	Synthesized long-period and short period records of the reflected P wave from a Central U.S. crust with modified top and bottom layers (see text).....	71

	Page
Figure 19. Synthesized long-period and short period records of the reflected P wave from a modified Central U.S. structure (see text).....	72
Figure 20. P and PP waves from March 21, 1964 Banda Sea earthquake recorded by long-period and short-period WWNSS.....	73
Figure 21. Processed TFO seismic array data and interpretation	74
Figure 22. Synthesized SH reflection from different crusts. In boxes B and C the two layered structures have a 10 km crust overlying the half-space.....	75

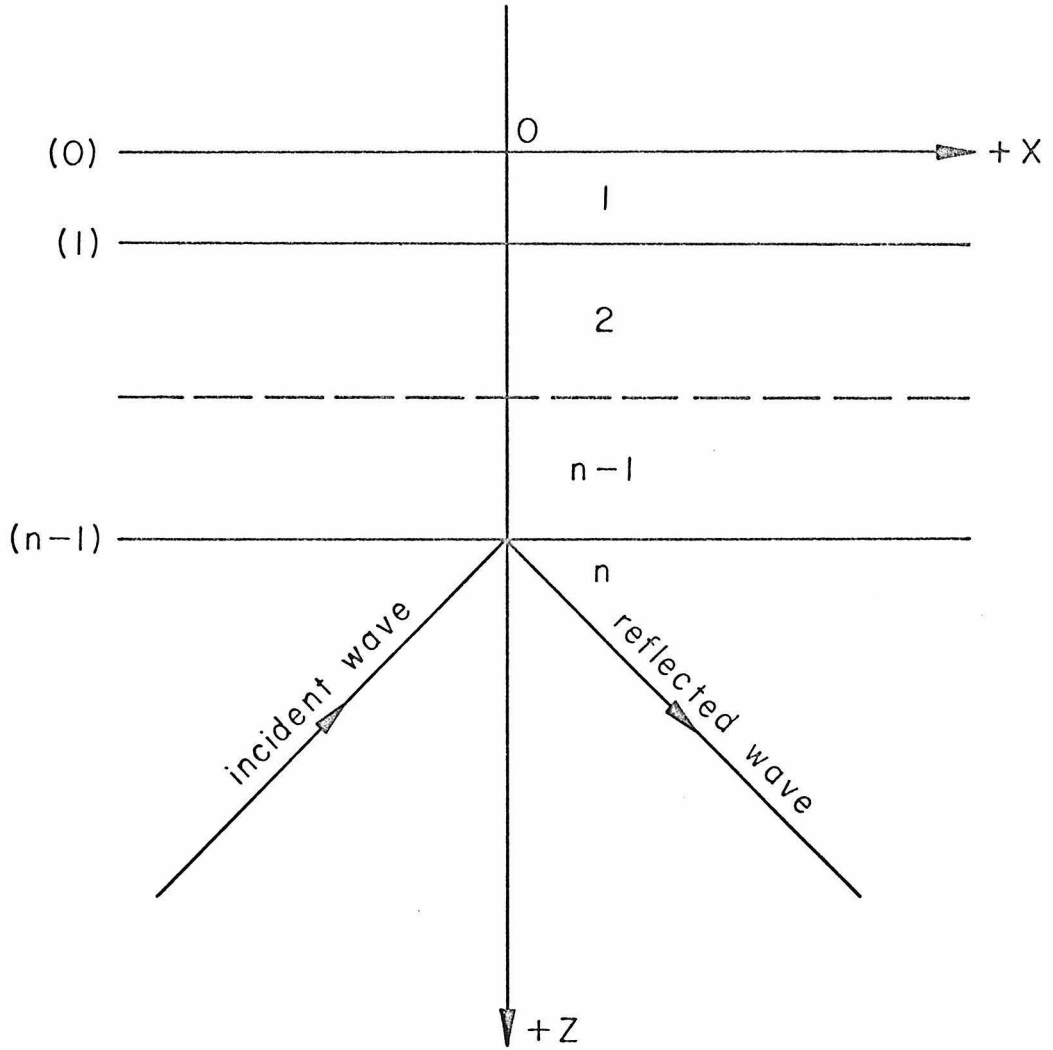


Fig. 1



Fig. 2

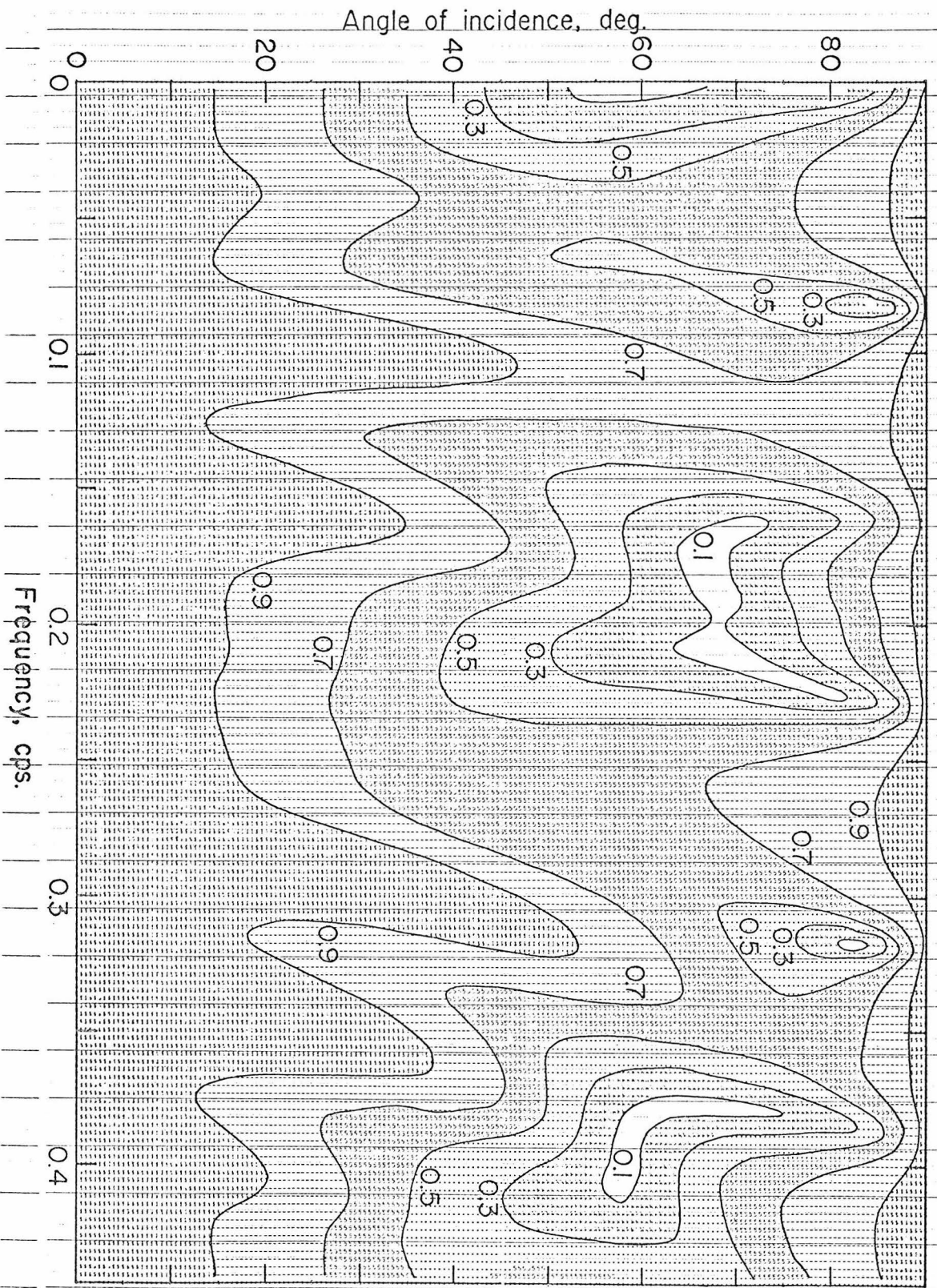


Fig. 3

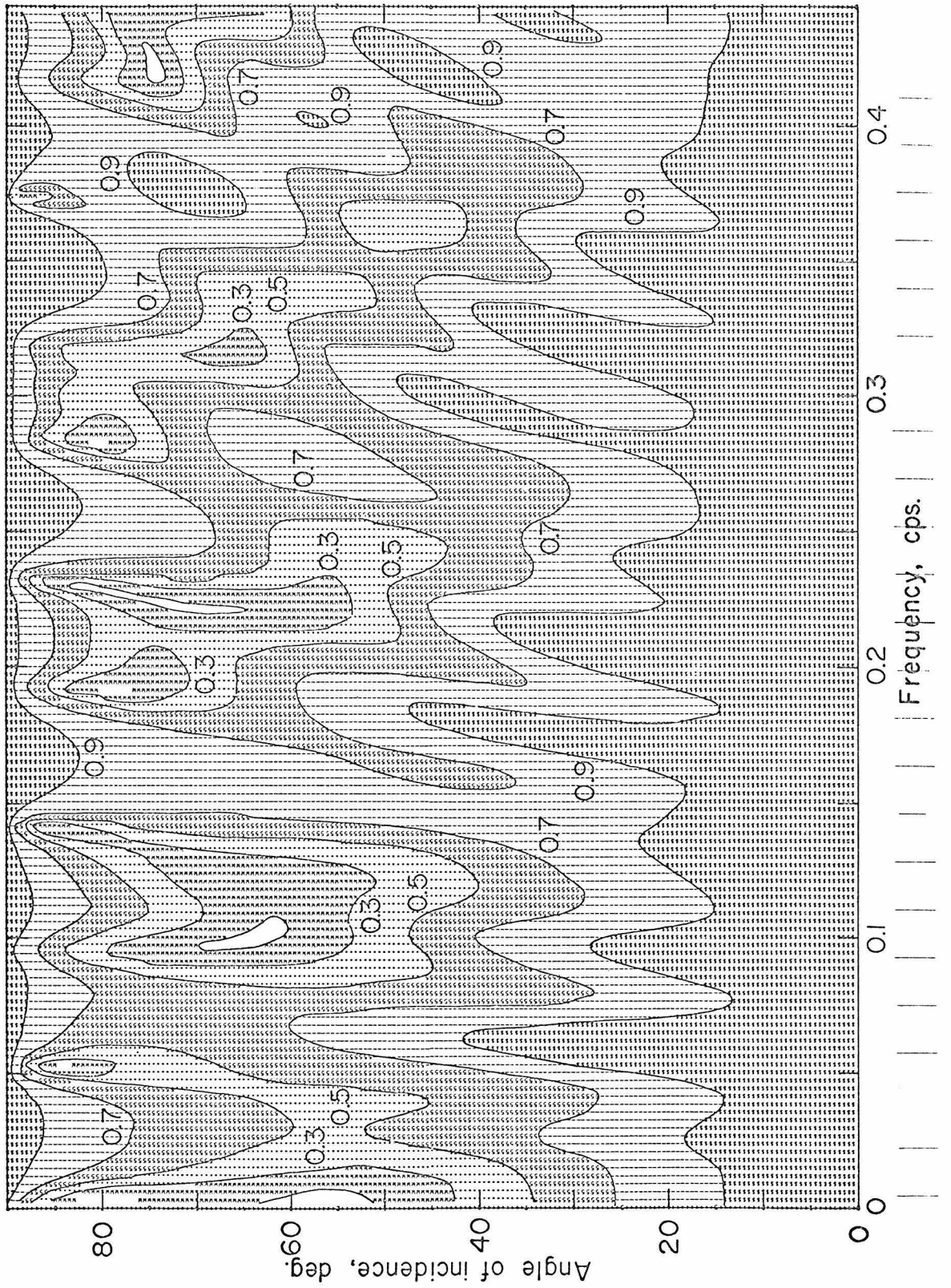


Fig. 4

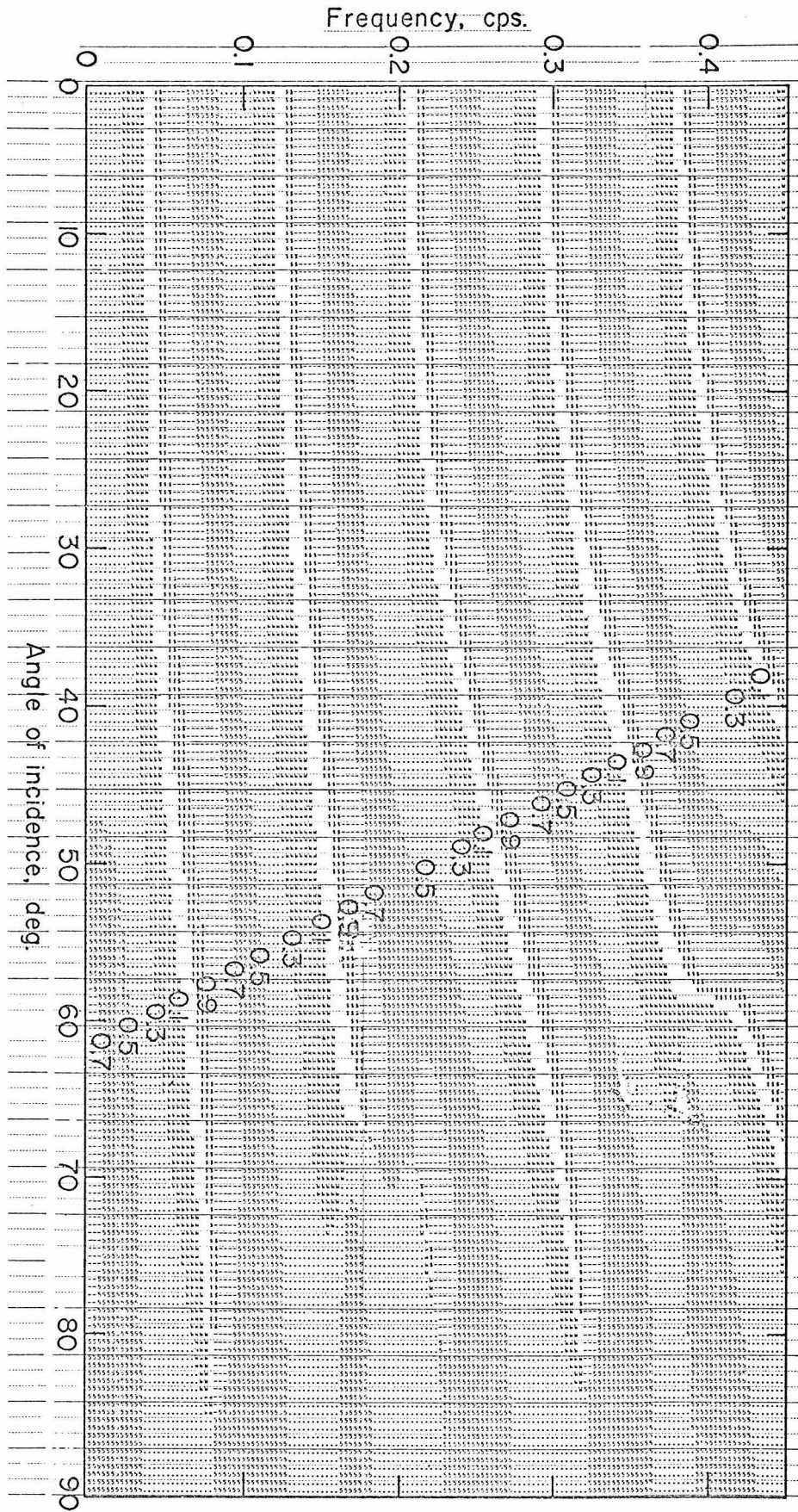


Fig. 5

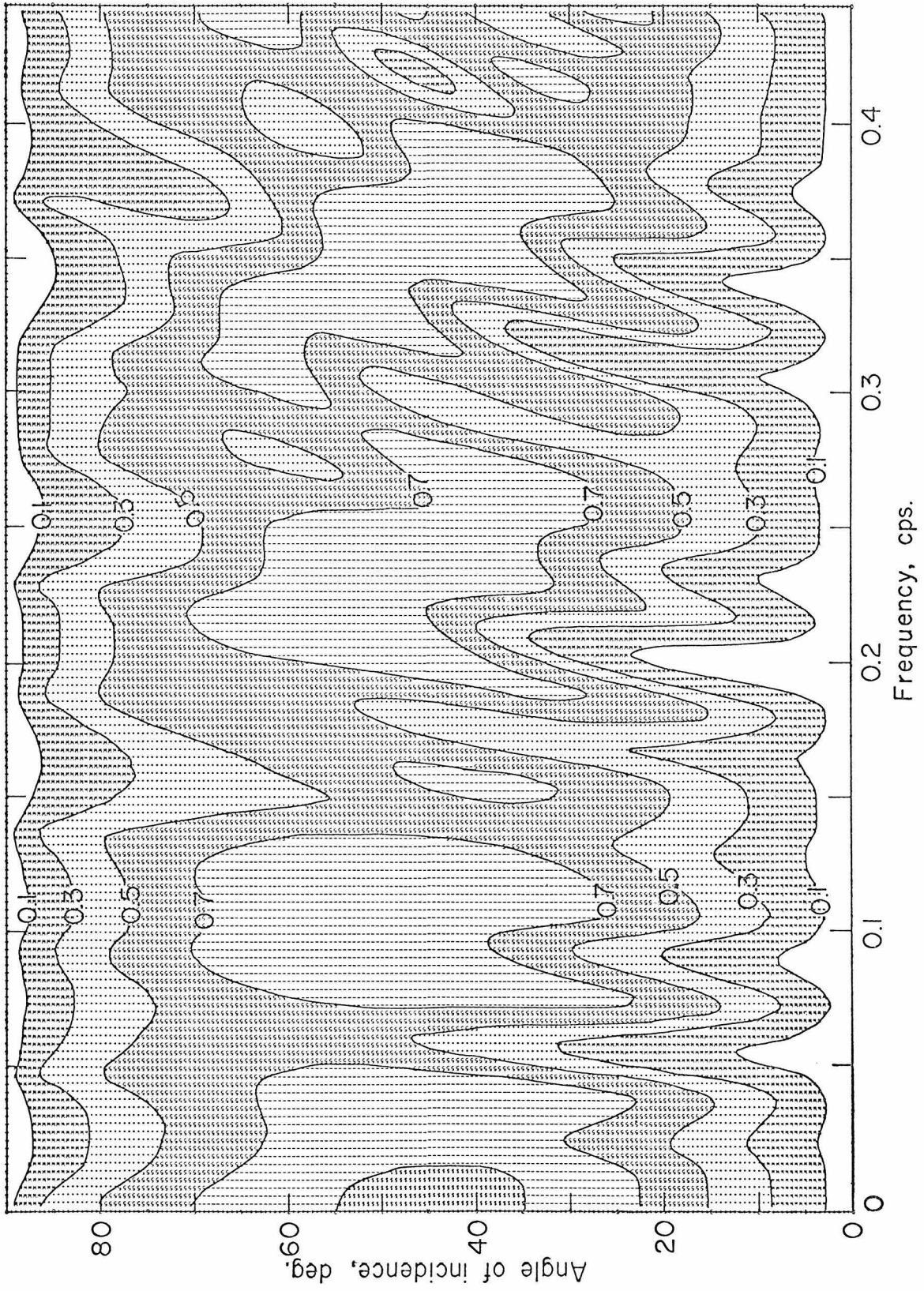


Fig. 7

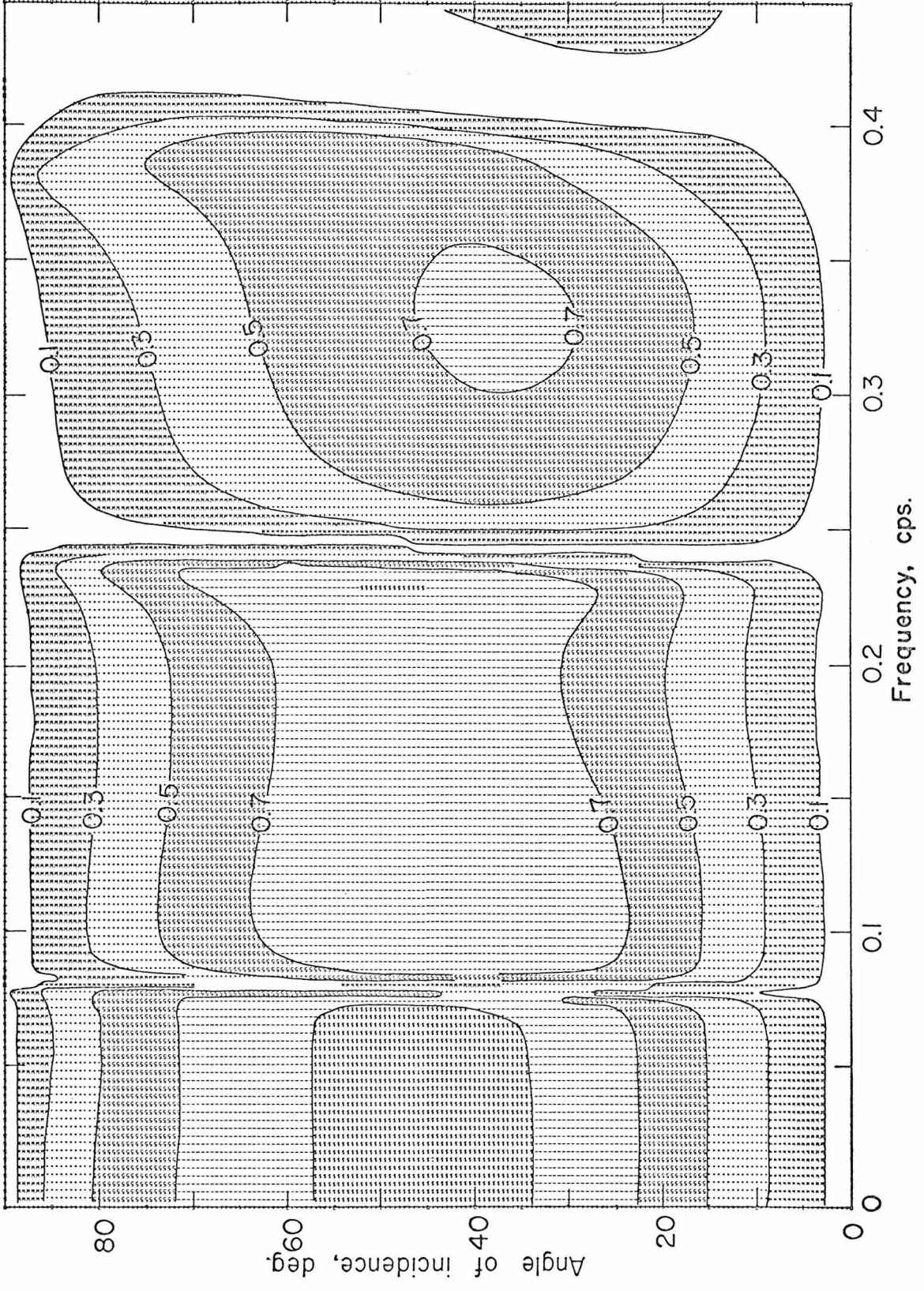


Fig. 8

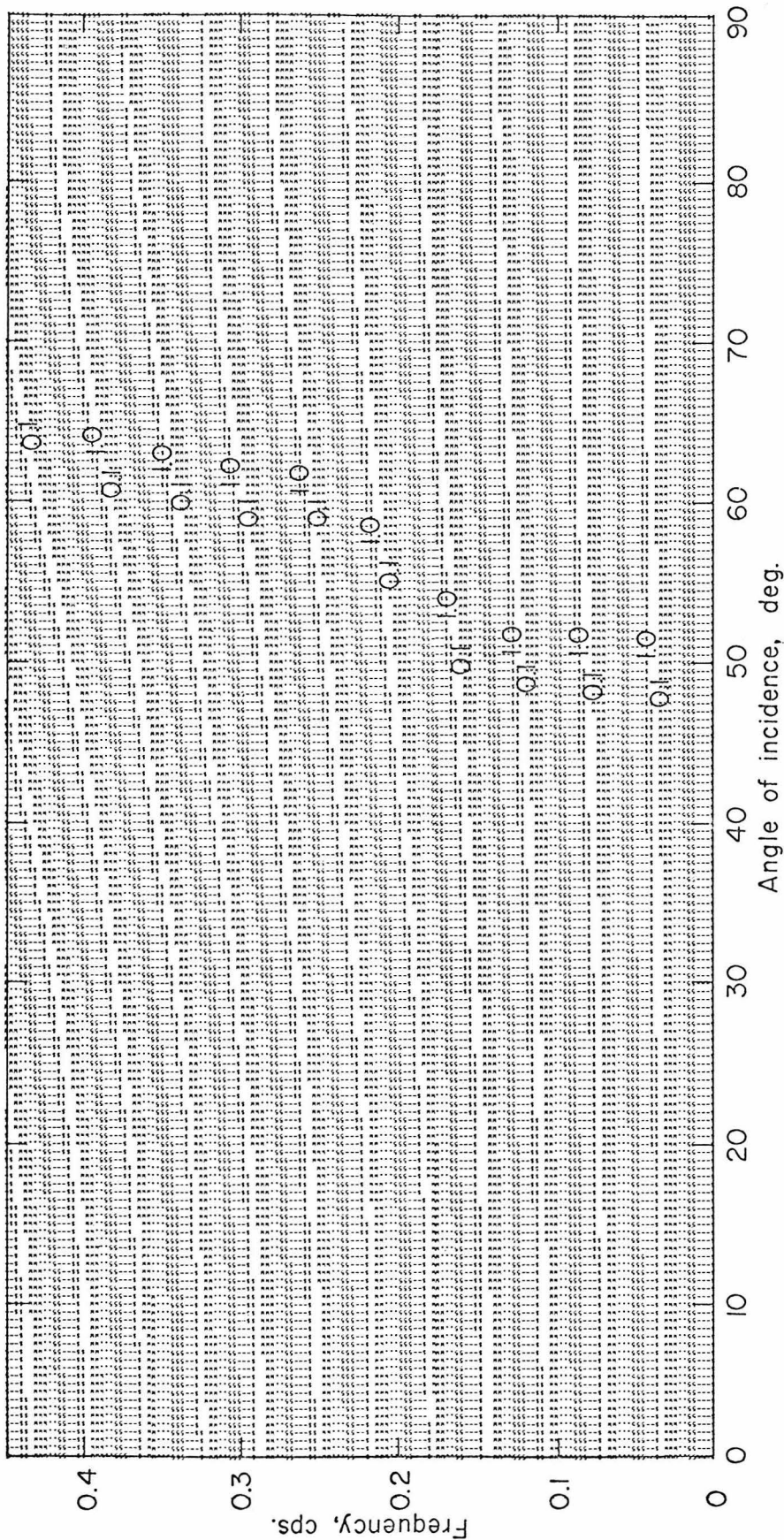


Fig. 9

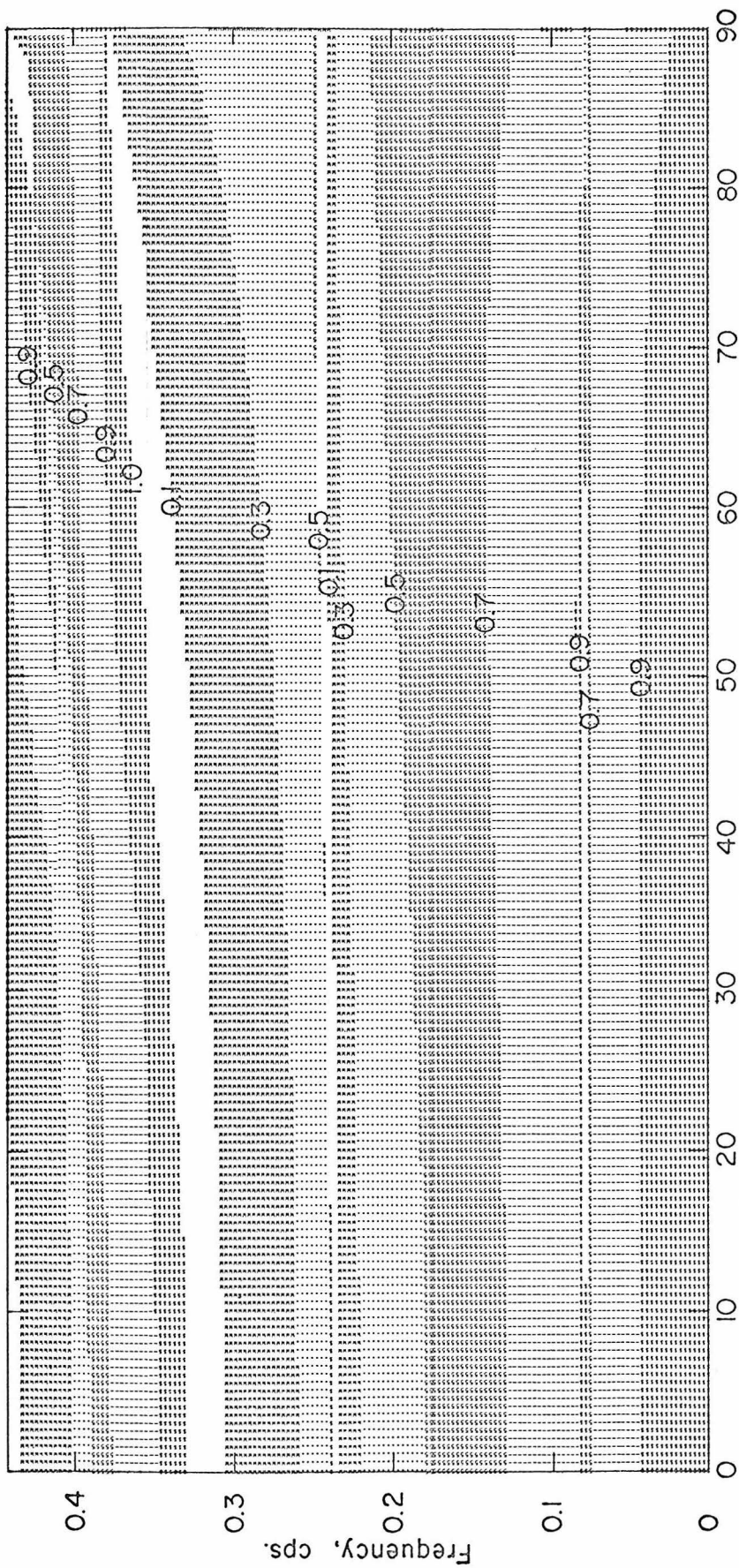


Fig. 10

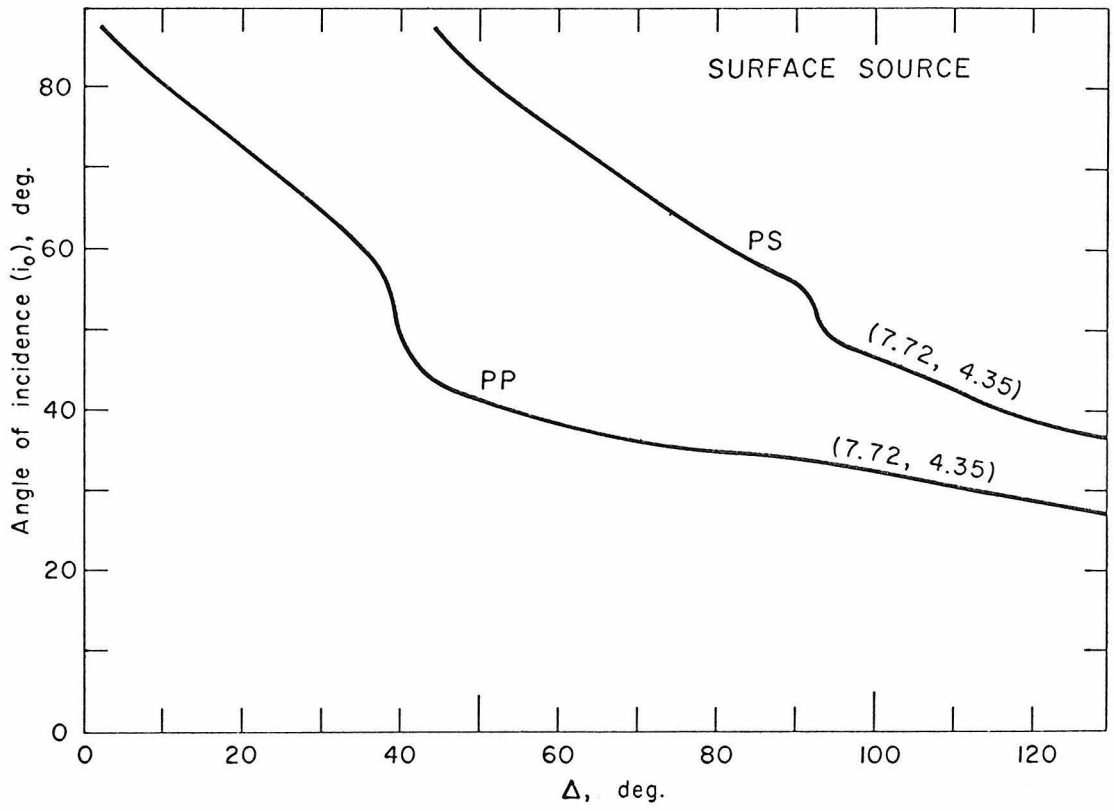


Fig. II

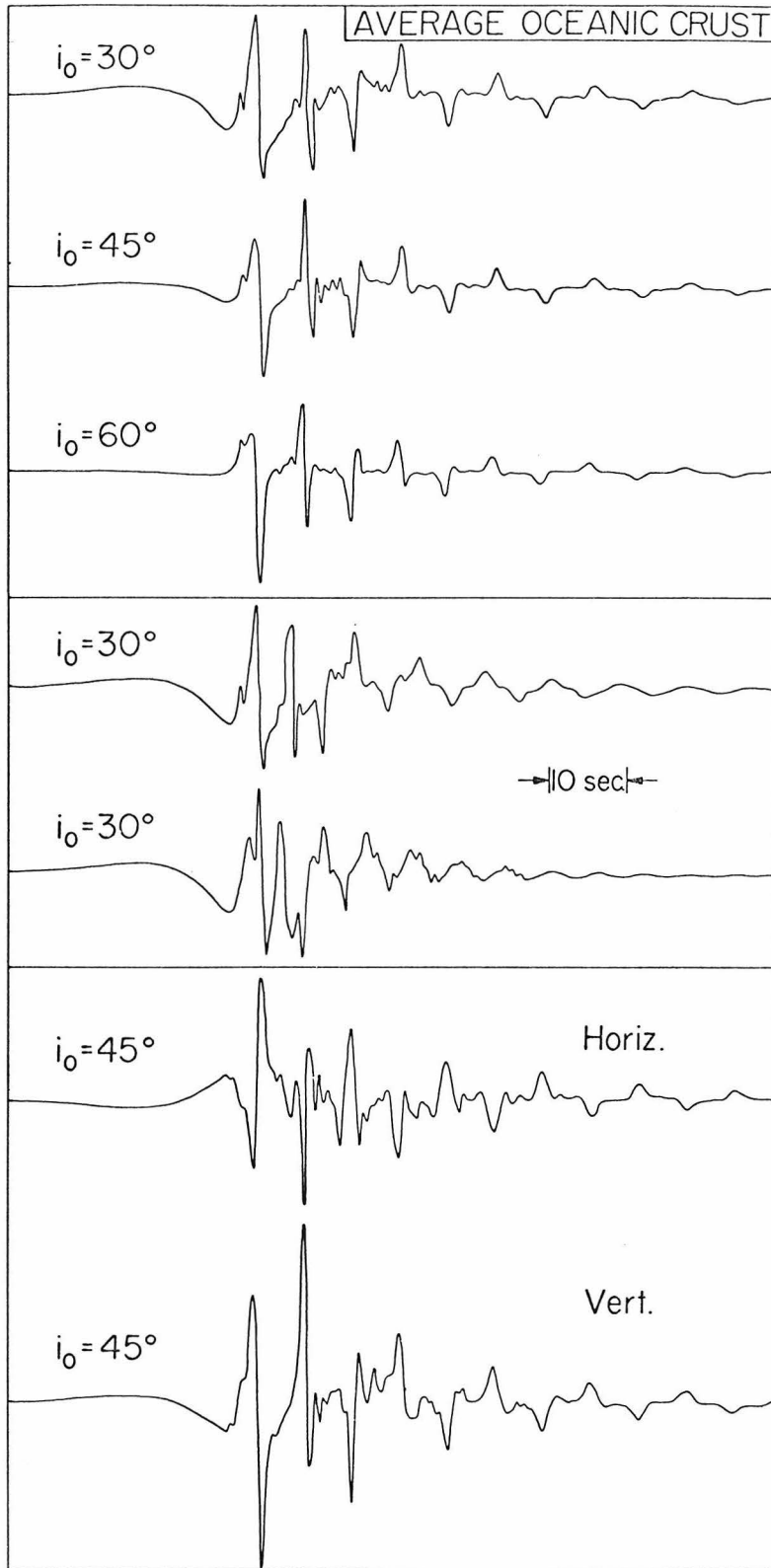


Fig. 12

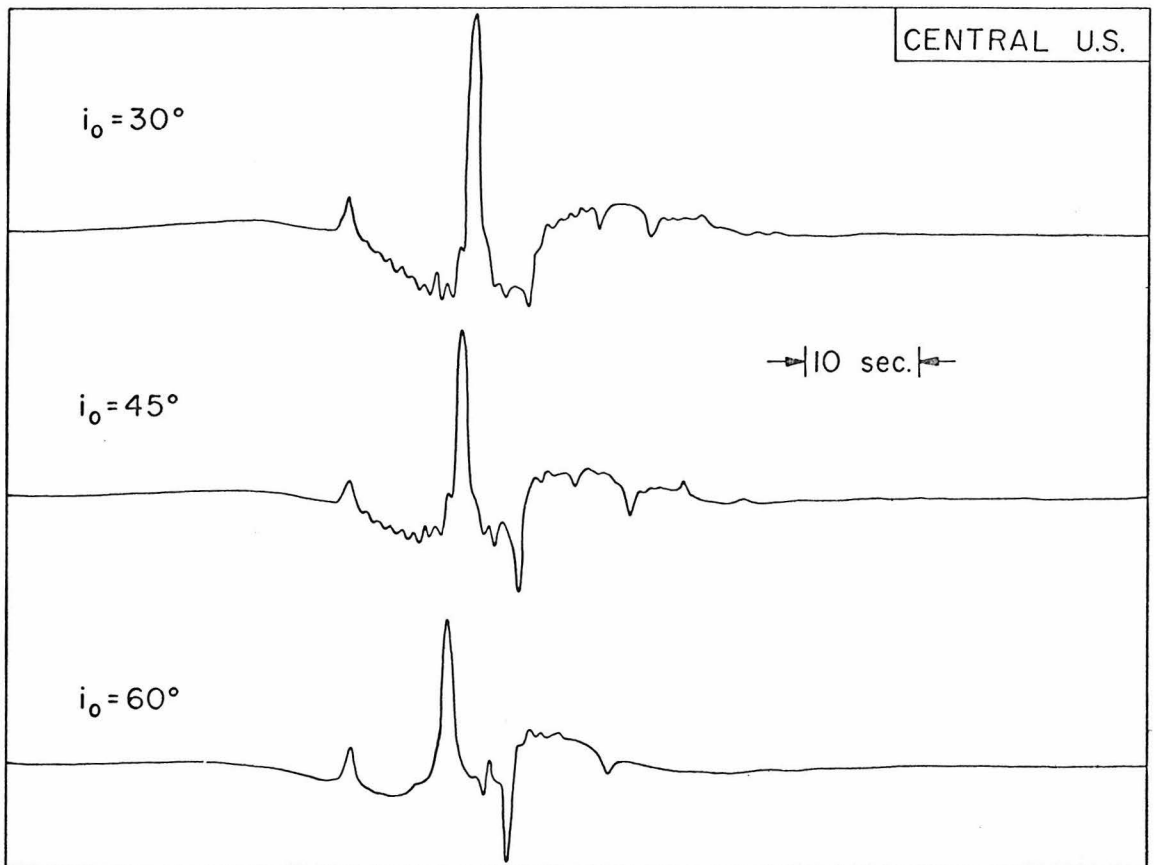


Fig. 13

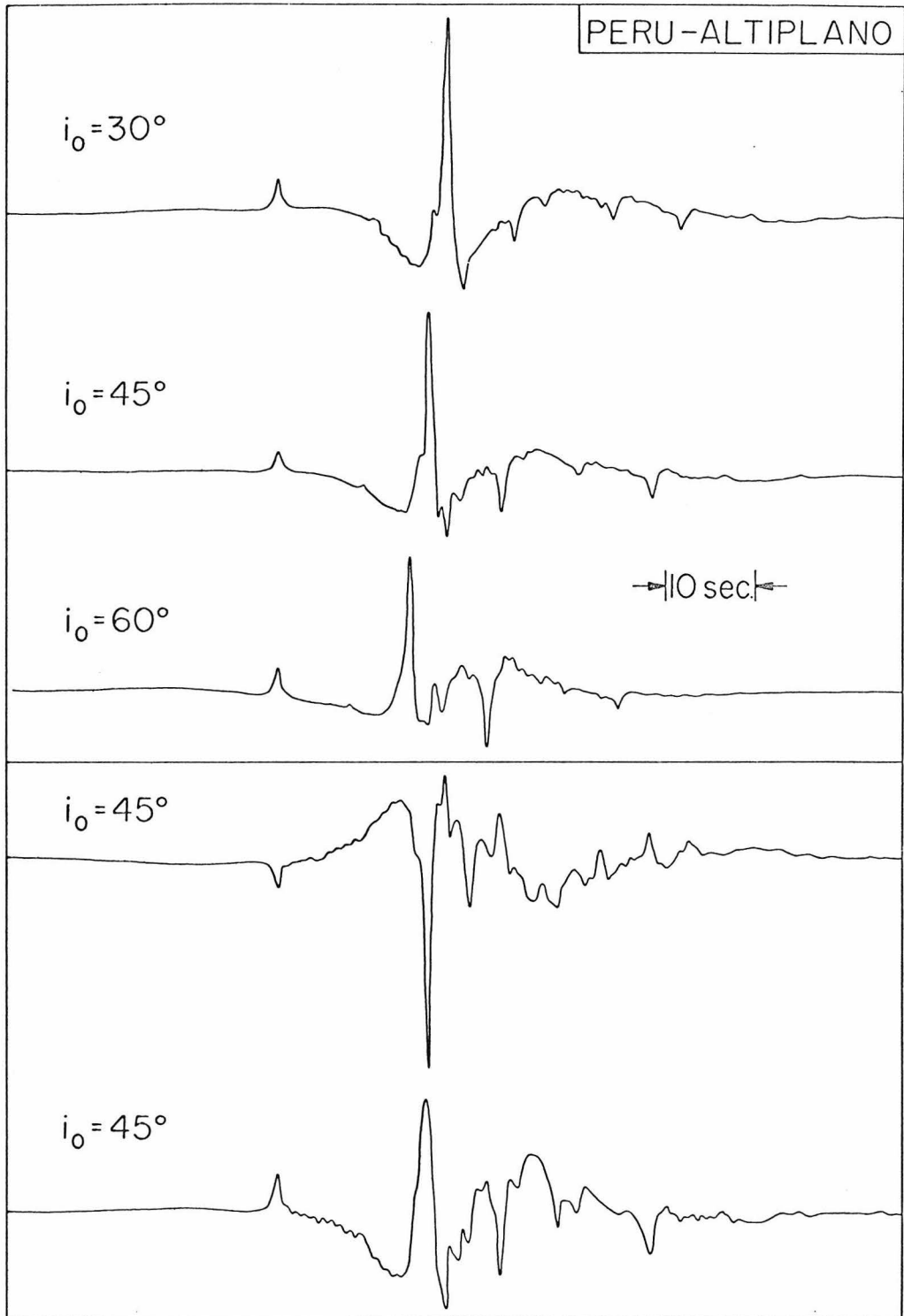


Fig. 14

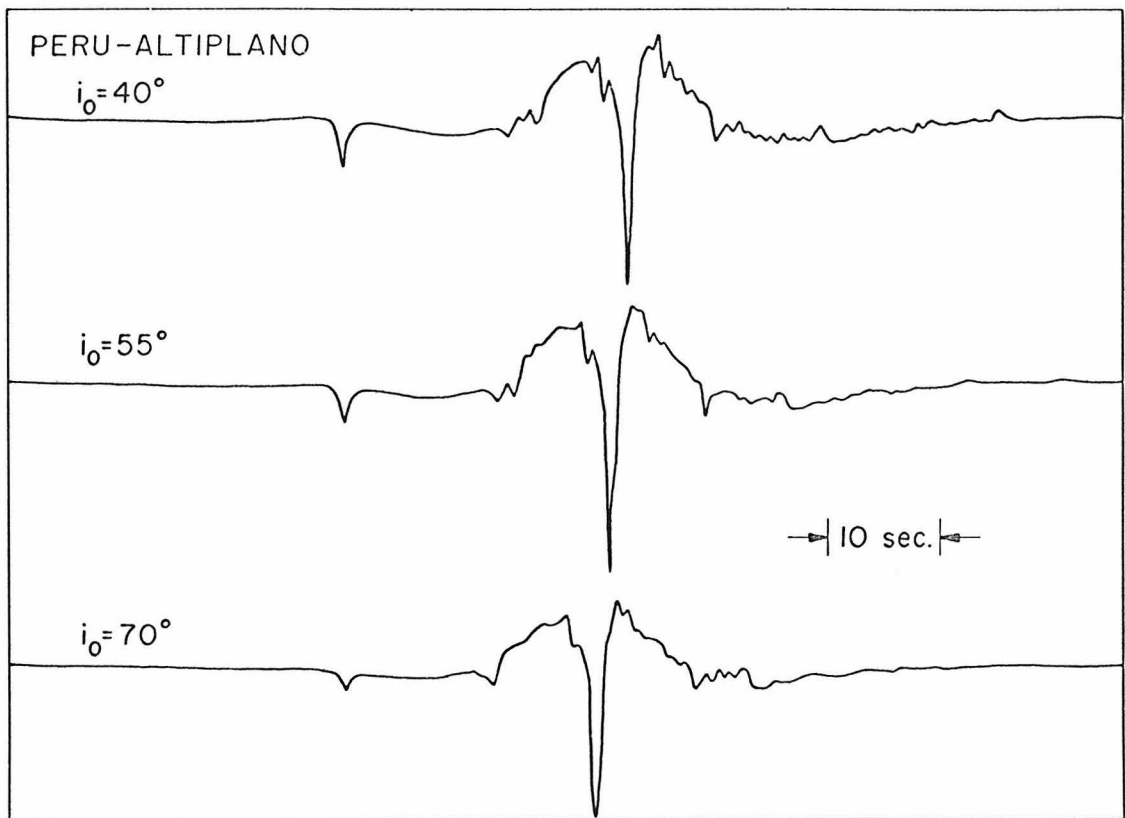


Fig. 15

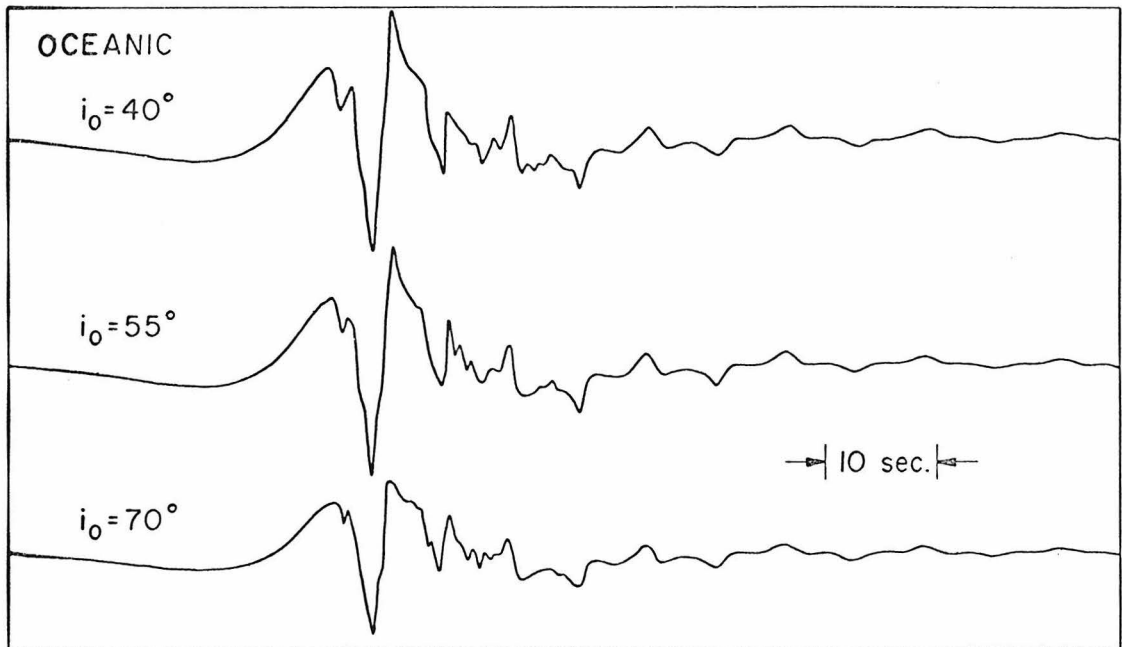


Fig. 16

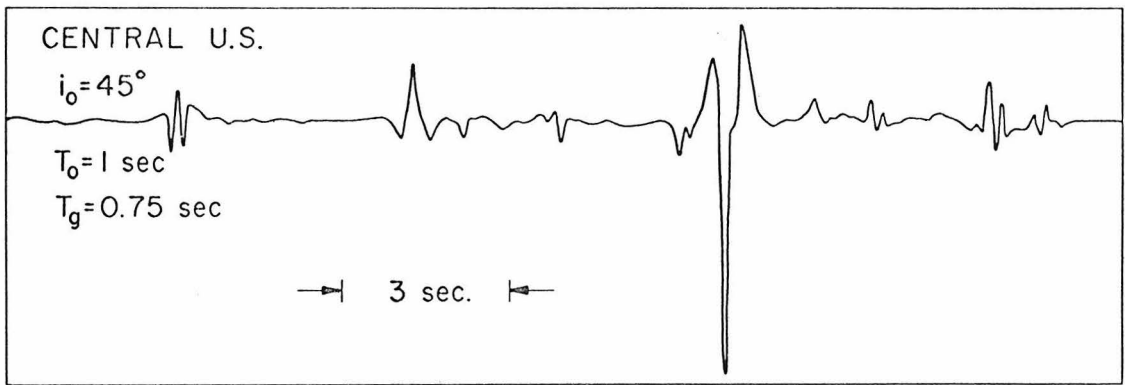


Fig. 17

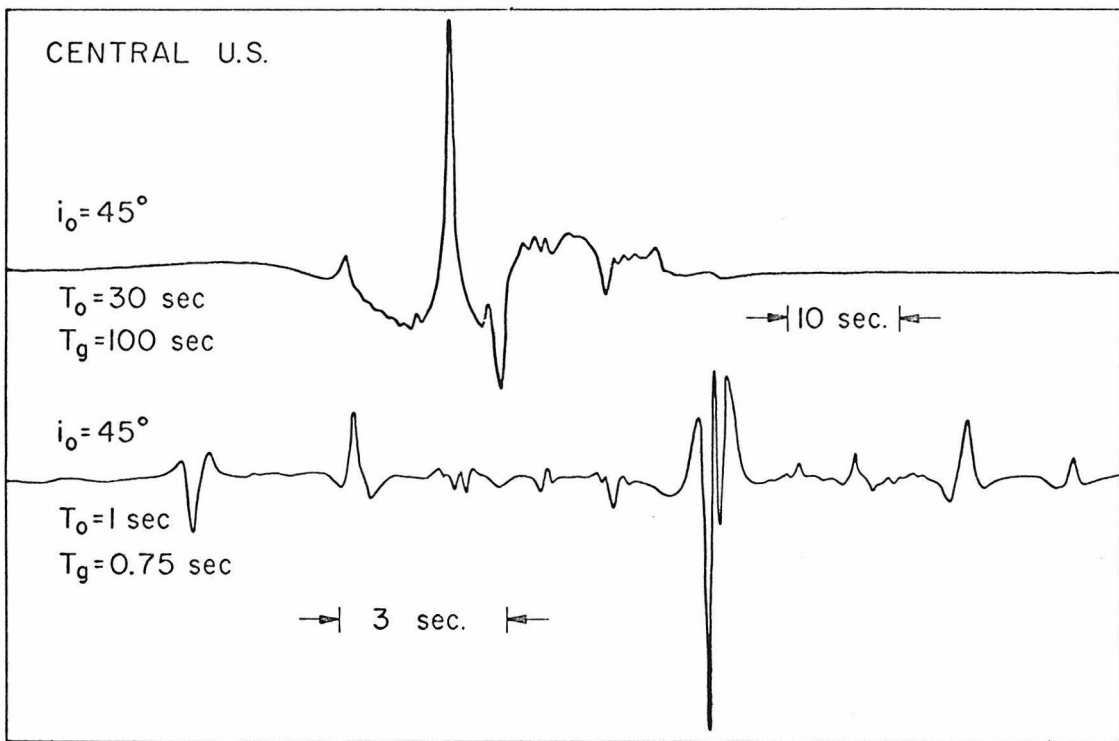


Fig. 18

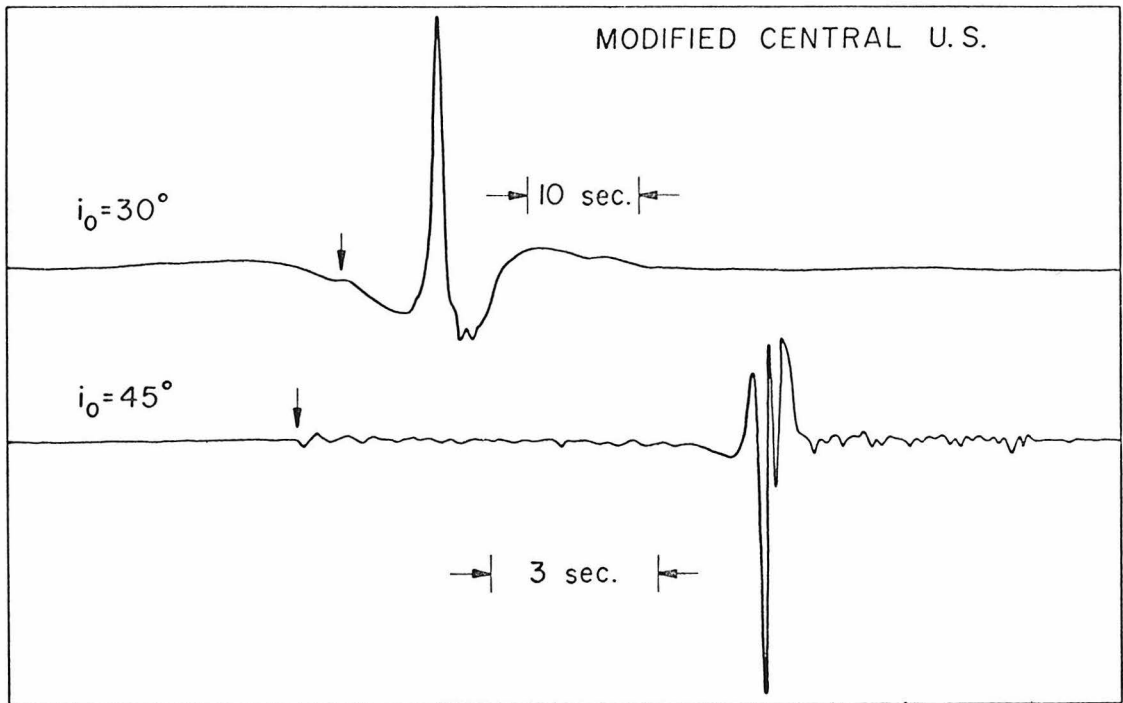


Fig. 19

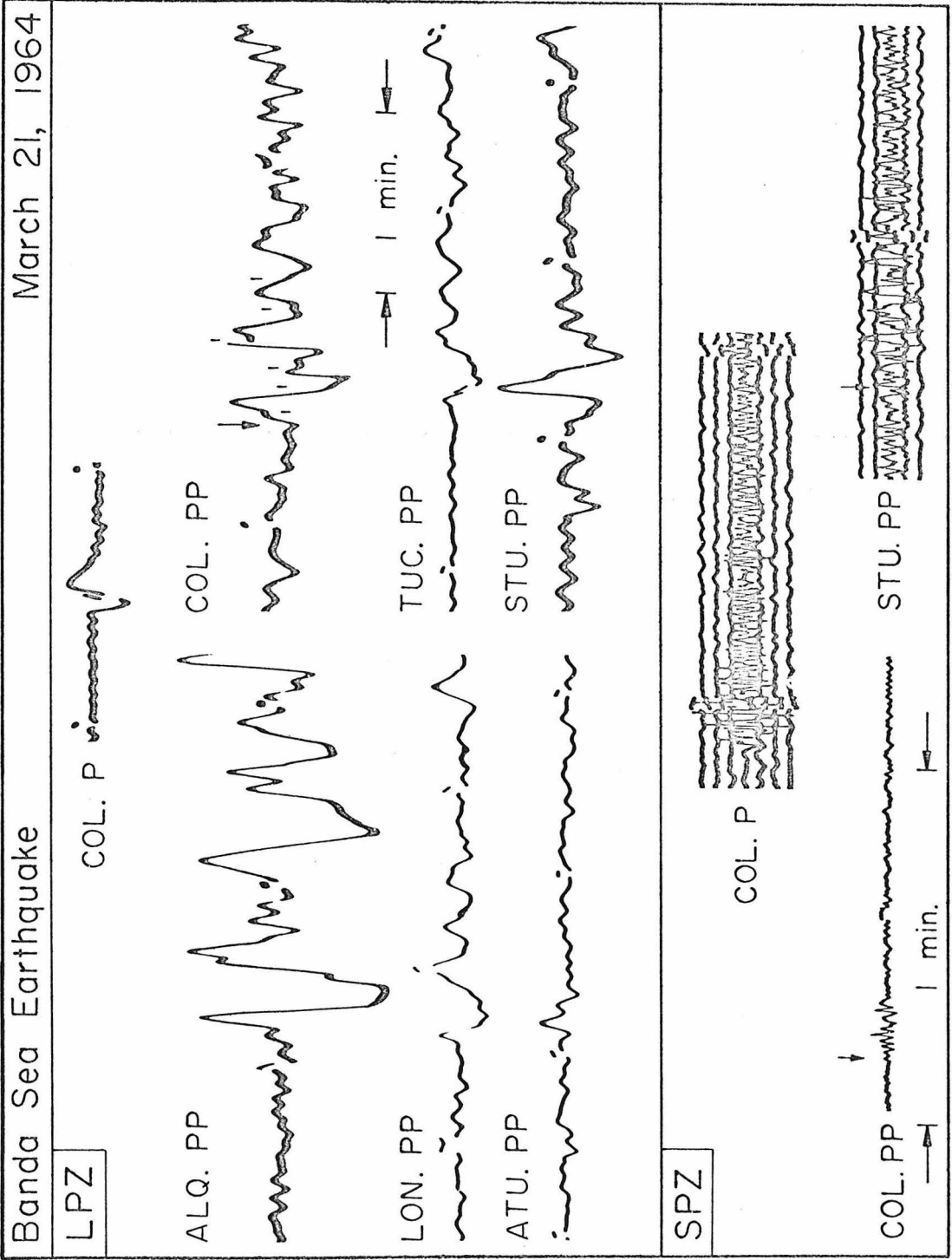


Fig. 20

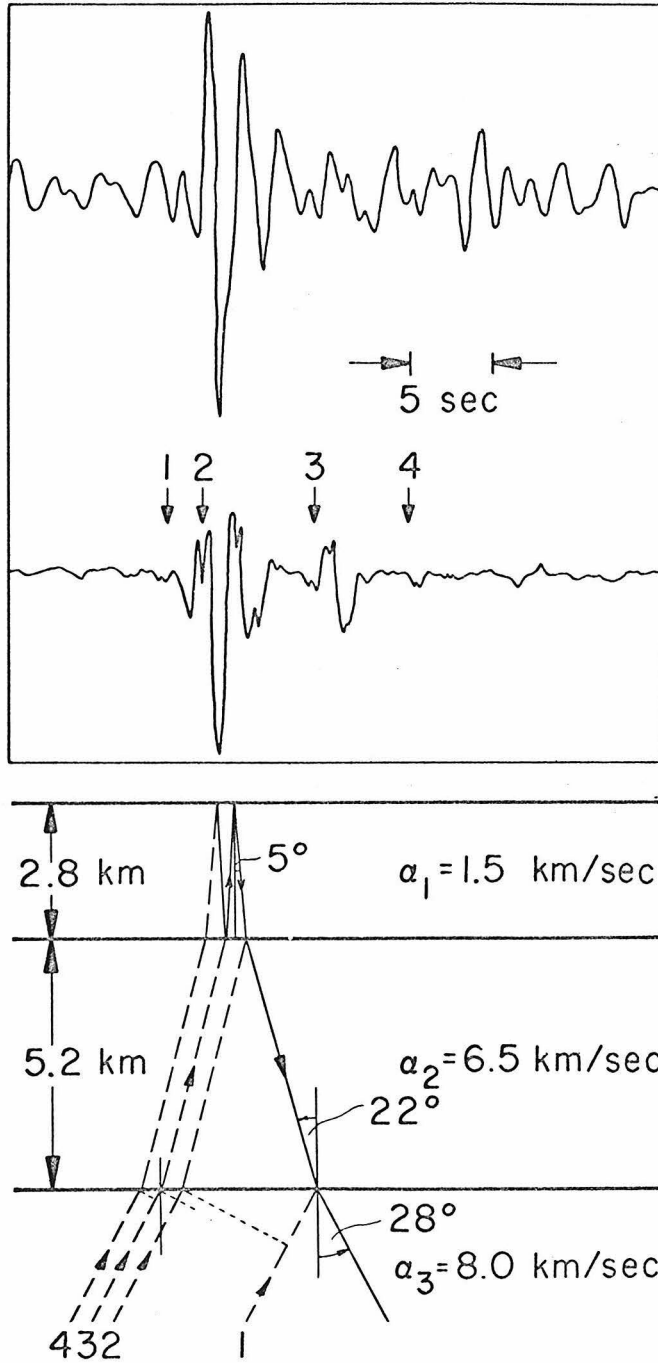


Fig. 21

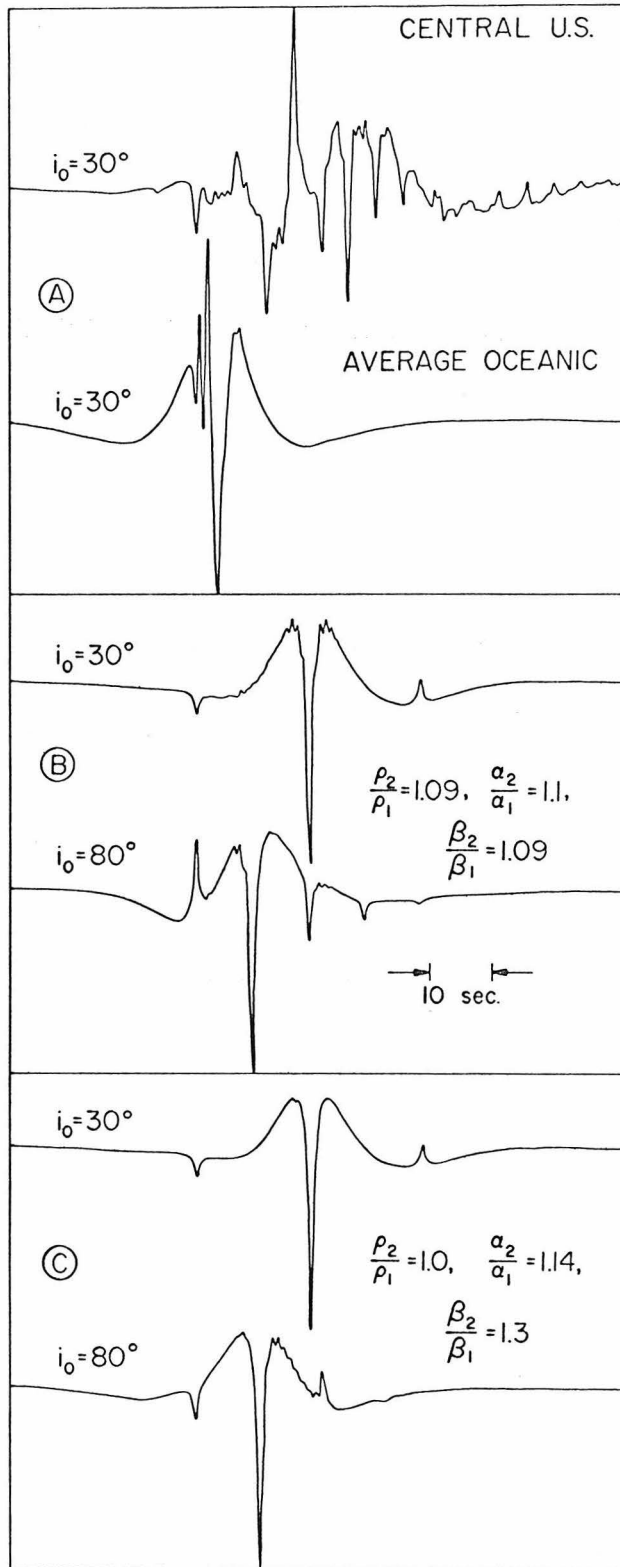


Fig. 22

Appendix

Reflected SH Waves

The SH wave is often a good wave to study because of its large amplitude on the seismogram and the fact that there is no conversion of SH waves to other types of waves at the interface. It is both experimentally and theoretically simpler to treat the SH wave than the P or SV wave. In the presence of a low velocity layer in an elastic system, the SH wave may be trapped and become a guided wave -- the G wave, but that happens only for waves within a certain range of angles of incidence.

The reflection of the SH wave will not be affected by the presence of a water layer on top of the solid crust, since the boundary condition for this case and for the case where the solid is terminated by a free surface will be the same, namely, the vanishing of the shear stress. Nevertheless, a thinner crust, with associated higher velocities, of an oceanic structure, as compared to a normal continental one, would cause the pulse shapes of reflected SH waves to be different under these two circumstances.

We did not present any contour maps for the SH wave because the amplitude of the reflection coefficient is always 1; all the information is contained in the phase shifts, which are difficult to interpret. When the complex reflection coefficients are Fourier synthesized, the influences of the layering reveal themselves very clearly.

In figure 22 the top trace is a reflected SH wave off the central U.S. crustal model, and the next trace is one of an average oceanic structure. The reflected wave from the continental model shows simple and multiple reflections as we would expect from a system of elastic layers with sharp discontinuities, separated so far from each other that individual waves can be discerned. The amplitudes of the multiple reflected waves behave in very much the same way as do the P waves which we discussed before. The appearance of the oceanic reflection is much less complicated than that of the continental one. The reflections from the bottom of the crust and the solid-solid interfaces form the first few swings; the main reflection is from the liquid-solid interface. We can hardly distinguish any later arrivals.

In connection with a phenomenon observed on seismograms for SH-SH waves at various distances we have investigated reflections from two two-layered crusts with velocity and density contrasts used by Gutenberg (1944) to study the reflection and transmission at the interface between two half-spaces. The phenomenon in question (Brune, J.N., personal communication, April 14, 1966) is that the SH waves observed for epicentral distances less than about 40° have precursors appearing on the seismogram 4 or 5 minutes in advance of the proper arrival time of the main SH waves, and in those cases the main SH wave is smeared out. Beyond 40° SH waves usually have a clear start and a well defined pulse form. The transmission and reflection amplitudes at the boundary between two semi-infinite media

calculated by Gutenberg (1944) show that when the wave approaches the boundary from the high velocity side, the reflection is, in general, small. For angles of incidence below 50° , the energy is mostly transmitted. But for angles of incidence greater than 50° there is a sharp increase of reflection coefficient; it goes to 1 at 90° . The angle 50° corresponds, for shallow and intermediate earthquakes, to an epicentral distance of 35-40 degrees. In figure 22 we have shown the possibility for SH to have a reversal in phase and, a relatively large reflected wave amplitude for some structure at two different angles of incidence. It seems plausible that the phenomenon mentioned above can be explained by the discontinuities in the upper mantle.